Fall 12-17-2011

Validation of Seaplane Impact Load Theory and Structural Analysis of the Martin 270

Carrie Sell
csell@uno.edu

Validation of Seaplane Impact Load Theory and Structural Analysis of the Martin 270

A Thesis

Submitted to the Graduate Faculty of the
University of New Orleans
in partial fulfillment of the
requirements for the degree of

Masters of Science
in
Engineering
Naval Architecture and Marine Engineering

by

Carrie Sell

B.S., University of New Orleans, 2010

December 2011

ACKNOWLEDGEMENTS

Seaplanes have been a passion of mine ever since I read “Where is Joe Merchant?” by Jimmy Buffett. Throughout the research process of my thesis, I have learned that there is still a small niche in the marine community that shares a great passion for flying boats. These individuals were the fuel for my study and their desire to help only aided in my desire to work.

I would like to first thank those who inspired me with their passion for seaplanes. Dr. William Vorus introduced me to the importance of seaplanes in Naval Architecture. His enthusiasm and encouragement gave me the stepping stones to take on this project. Dr. Colen Kennell taught me a tremendous amount about seaplanes and even after my research stage with the Navy, he continued to support my research. Bruce Barth reached out to me with his knowledge and friendship. His expertise and stories about Martin seaplanes gave me an appreciation for the men, including Barth, who served in the Navy on these amazing planes.

The Navy was a key contributor to my project, and without its support, this project would not have been possible. Steve Ouimette was the first person to actually support my research and through the Center for Innovation in Ship Design, supplied me with numerous contacts and resources. Ed Devine also supported my work, gave me direction on how to start my project and was always there to help me. The most important gesture I received from all of the Naval Surface Warfare Center Carderock Division employees I worked with was their continued support long after I had officially ended my summer internship.

Equally important is the support I received from the professors in the School of Naval Architecture and Marine Engineering. Each and every one of them have been the key reason I stayed at the University of New Orleans to continue my education. I will always admire and appreciate their dedication and enthusiasm for teaching. I’d especially like to thank my thesis advisor, Dr. Brandon Taravella, for always making time for me when I needed help and advising me on my project. My classmate and teacher Chris McKesson has supported me not only as an advisor but as a friend in times when I needed reassurance. Also, Dr. Thomas Dobie advised me with his practical knowledge on flight from his experience flying in WWII. Last but not least, I’d like to thank my thesis board, including Dr. Lothar Birk and Dr. Pingsha Dong, who always displayed a willingness to help me over hurdles with my research.

Lastly, I would like to thank my family. My Dad, Mom, and Grandma have always believed in me and supported my dreams. The foundation of self-motivation and independence in thought which I was raised on gave me the confidence to take on any life goal. I am eternally grateful for them.

TABLE OF CONTENTS

List of Figures

LIST OF TABLES

TABLE OF SYMBOLS

Von Karman (1929)

P_{max}	*Maximum pressure*
v_O	*Impact velocity at the moment of first contact or sinking speed*
ρ	*Density of fluid*

Wagner (1932) and Faltinsen (2005)

c	*Wetted half beam*
dc/dt	*Speed of propogation of the wetted-semi width*
dV/dt	*Vertical acceleration*
n_b	*Vertical distance of the surface height relative to the body*
p	*Hydrodynamic pressure*
p_a	*Atmospheric pressure*
t	*Time*
V	*Constant vertical velocity*
x	*Coordinate along the beam of pressure*
ρ	*Mass density of the water*
β	*Deadrise angle*

Blundell and Jones (1938)

b	*Span or beam*
K	*Constant whose value depends on the position of the pressure station*
P_{max}	*Maximum pressure, psi*
V	*Tangential or horizontal velocity of the keel of the V-shape at impact*
V_n	*Velocity normal to the keel*
v_O	*Vertical velocity at impact*
W	*Seaplane weight*
$\emptyset$	*Angle between the normal to the plate and the vertical, i.e. deadrise angle*
α	*Angle of incidence at impact, i.e. trim angle*
θ	*Angle between a side of the V-shape and the horizontal*

Mayo (1945)

ds	*Thickness of plane*
F_n	*Hydrodynamic force in the Vn direction*
F_p	*Force normal to the keel registered by an individual flow plane*

K	*Theoretical coefficient, varies according to angle of deadrise*
m_p	*Virtual mass of the flow in the plane*
m_s	*Virtual mass of flow plane at step, per unit distance in keel direction*
m_w	*Virtual mass associated with hydrodynamic flow beneath float*
s	*Initial intersection of keel line and water surface to an individual flow plane*
V_n	*Velocity normal to the keel*
V_p	*Velocity of the float parallel to keel, rate at which flow planes Slide along and off step*
y	*Depth of immersion, normal to plane of water surface*
z	*Penetration in the plane*
τ	*Angle between flight path and plane of water surface*
β	*Angle of deadrise*

Crewe (1946)

dV_n/dt	*Acceleration of the craft normal to the craft bottom*
g	*Acceleration due to gravity*
h	*Draft of the bottom of the hull, usually that of the keel at the step*
K'	*Associated mass coefficient*
K_S	*Pressure area coefficient*
p	*Pressure, psi*
q	*Constant that depends on the relationships between the various forces acting on a particular impact condition*
r	*Constant that depends on the relationships between the various forces acting on a particular impact condition*
s	*Constant that depends on the relationships between the various forces acting on a particular impact condition*
S	*Pressure area by projecting the surface of the bottom supporting the water pressure*
t	*Time measured from the instant the bottom first touches the water in the impact period considered*
u	$(W/g)u$ *is the pure impact associated water mass, which u' is related and equal to* $u(cos\,\tau)^2$
u'	$u(cos\,\tau)^2$
u'_m	u'*at maximum acceleration of the craft normal to the craft bottom*
V_H	*Craft velocity parallel to water*

V_n	*Craft normal velocity relative to the bottom*
V_v	*Craft velocity perpendicular to water*
ω	*Flight path angle parameter*
ω_O	*Initial value of the flight path angle*
W	*Craft weight*
x	*Constant which is dependent on the dimensional classic impact theory and is equal to 3 for 3D cases and 2 for 2D cases*
τ	*Angle between craft bottom plane and water plane, i.e. keel altitude*

Benscoter (1947)

m	*Additional mass of water or virtual mass*
$\bar{M}$	*2-dimensional mass of the seaplane*
r_m	*Ratio of flight path angle to the tangent of the trim angle at instant of maximum acceleration*
r_o	*Ratio of flight path angle to the tangent of the trim angle at instant of entry*
s_m	*Step draft normal to keel at instant of maximum acceleration*
t_m	*Time at instant of maximum acceleration*
u_m	*Ratio of additional mass of water to mass of seaplane at instant of maximum acceleration*
V_o	*Velocity at instant of entry*
$\ddot{z}_m$	*Maximum acceleration normal to the keel*
z_m	*Displacement or draft normal to the keel at instant of maximum acceleration*
$\dot{z}_0$	*Velocity normal to the keel at instant of maximum acceleration*
α_1	*Factor occurring in the definition of the coefficient that defines the additional mass of the water*
α_2	*Factor occurring in the definition of the coefficient that defines the additional mass of the water*
$\bar{\epsilon}$	*2-dimensional coefficient that defines the additional mass of the water*
β	*Deadrise angle*
λ	*Length parameter*
τ	*Trim angle*

Hamilton (1955)

c	*Wetted half beam*
K	*Constant in Wagner's maximum pressure formula, equals 132 for design purposes when Pmax is in psi*
P	*Hydrodynamic pressure*
P_{max}	*Maximum value of hydrodynamic pressure*
P_{mean}	*Mean distributed pressure*
V_n	*Velocity component normal to keel*
x	*Distance from keel to point at which pressure is being measured*
θ_L	*Local deadrise angle at any point on the hull planing bottom, degrees*
θ	*Deadrise of line joining keel to chine*
η	*Where,* $\eta = x/c$
ρ	*Density of water*

Crewe and Gerry (1977)

b	*Planing beam*
C_Δ	*Beam loading coefficient*
m	*Mass of the seaplane*
ρ	Density of the water

Code of Federal Regulations

C_2	*Constant*
C_3	*Constant*
K_2	*Hull station weighting factor*
P_{ch}	*Pressure at the chine, psi*
P_k	*Pressure at the keel, psi*
V_{s1}^2	*Seaplane stalling speed at the design water takeoff weight with flaps extended in the appropriate takeoff position, knots*
β	*Deadrise angle at the chine for each station*
β_k	*Deadrise angle at the flare tangency*

Current Work

C_p	*Coefficient of pressure*
E	*Young's modulus*
V_h	*Horizontal velocity or forward velocity*
V_n	*Normal velocity to the keel*

V_p	*Velocity parallel to the keel*
V_r	*Resultant velocity*
V_v	*Vertical velocity or rate of descent or sink rate*
τ	*Trim angle of plane*
β	*Angle of resultant velocity relative to the normal velocity*
α	*Flight path angle*
σ_{cr}	*Critical stress*

I. ABSTRACT

Flight and drop tests of the Martin 270 (M270) seaplane were conducted in 1955. Theoretical and empirical pressures were determined by use of Wagner's theory and also by the Code of Federal Regulations (CFR). The pressure results from the experimental tests on the hull were compared with pressures calculated from Wagner's theory to determine how well the theory correlated with the measured pressures. The experimental pressure data was also compared with the CFR results to determine how the current industry standard of estimating impact loads compares with actual pressures a seaplane is subjected to.

Using the structural design and geometry of the M270 the seaplane hull was modeled in Maestro with a coarse mesh finite element model. The pressures from Wagner's theory and the CFR were applied to the model of the M270 hull. The structural reactions of the drop test section were compared with the reactions determined from Maestro.

Key Words: Seaplane, flying boat, float plane, planing, impact, slam, drop test, chine wetted

II. INTRODUCTION

The purpose of this paper is to review seaplane impact theories studied by various authors and to determine theories which are applicable for the determination of impact loads on an actual fuselage. The project is governed by two different departmental criteria sets and requires two deliverables. The first of which was outlined by the Center for Innovation in Ship Design (CISD) at NAVSEA Naval Surface Warfare Center (NSWC) Carderock Division for the Naval Research Enterprise Intern Program (NREIP) and the second was outlined by the University of New Orleans' School of Naval Architecture and Marine Engineering for a master's thesis. CISD serves as mentor for the literature search and supplied the majority of the data and information needed to support the project. This project is the deliverable for the NREIP as well as for the master's thesis requirements. The objectives of this project are to:

- Review past seaplane impact theory
- Complete a master's thesis study

The literature review was conducted the summer of 2011 to review past methods of determining seaplane impact loads. The study considered a wide range of papers including theoretical and experimental studies; however, due to the limited time frame of the 10 week duration of the research phase of the project, the literature search does not include all impact load theories available.

The master's thesis for the University of New Orleans in the School of Naval Architecture and Marine Engineering expands on the studies done during the summer of 2011 for CISD at NAVSEA NSWC Carderock. The objective of the master's thesis study is to apply the theoretical impact load theory previously studied to an existing seaplane hullform and compare the water loads on the hull to experimental results. After the determination of loads, a structural analysis is completed using Maestro, which is a global coarse mesh structural analysis tool, to compare the structural reactions from the experimental test to the structural reactions determined by Maestro.

Due to the lack of reference materials for seaplane structural drawings, very few seaplane possibilities to use for the study exist. The only structural arrangement that could be found is for an experimental flying boat, the Martin 270.

The study was completed November, 2011 at which time a second and final paper was submitted to CISD at NAVSEA NSWC Carderock and the University of New Orleans' graduate school.

III. INTRODUCTION TO SEAPLANES

Seaplanes are divided into two categories: the flying boat and the float plane. The two types differ in their hullforms. Flying boats are fixed winged seaplanes where the fuselage is the hull and sponsons are normally installed under the wings for stability purposes. An example of a WWII flying boat where the fuselage serves as the hull of the plane is seen in Figure 1. For the floatplane (Figure 2), floats or pontoons are attached to the underside of the fuselage through struts and serve as the hull of the seaplane. Further, a floatplane pontoon design can be done in two different arrangements. The most common is the twin float design where two floats are attached on the underside of the fuselage. The second arrangement is the single float, where one larger float is attached underneath the fuselage and sponsons are attached under the wings for stabilization.

Whether the seaplane is a flying boat or a floatplane, the hull of the plane enters the water causing an impact load on the hull structure due to the force exerted by the water on the hull. These forces are related to the rate of growth of the waterplane area. The development of impact theory has been a main focus in seaplane engineering since the late 1920s and later gave rise to slamming theory on planing hulls. Key contributors such as Von Karman (1929), who studied conservation of momentum imparted from the seaplane to an associated water mass of the hull, and Wagner (1932), who studied transverse pressure distributions and wave rise during impact, helped set the baseline for other impact theories.

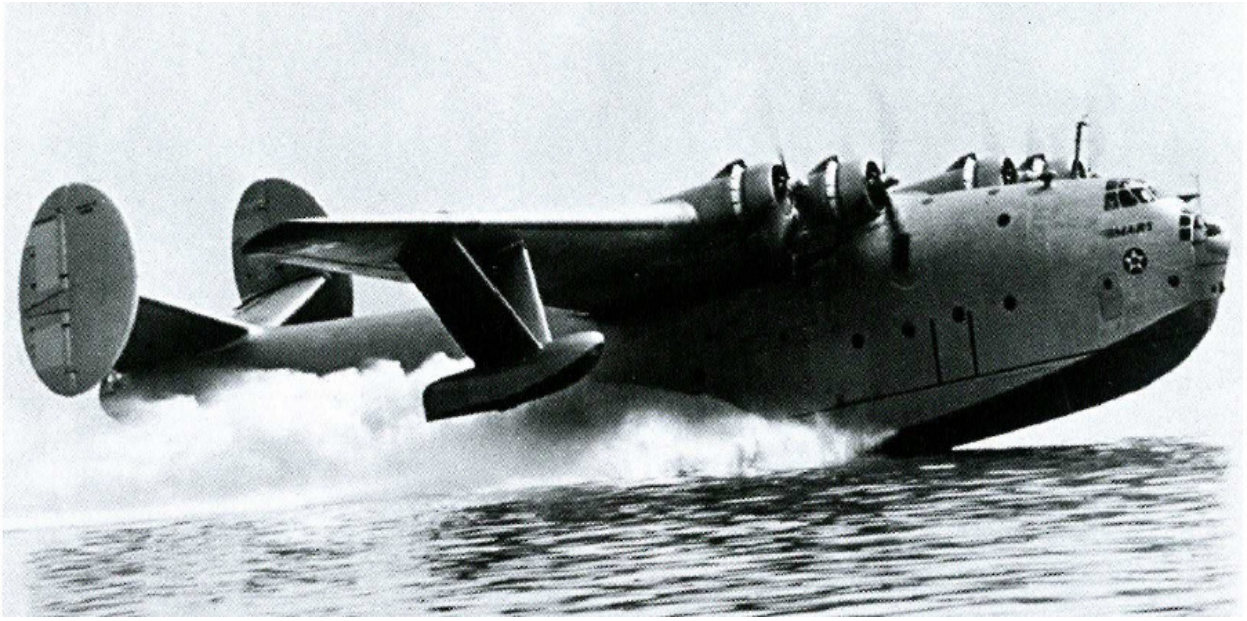

Figure 1. XPB2M-1 Martin Mars prototype classed as a flying boat type seaplane (Yenne 1977).

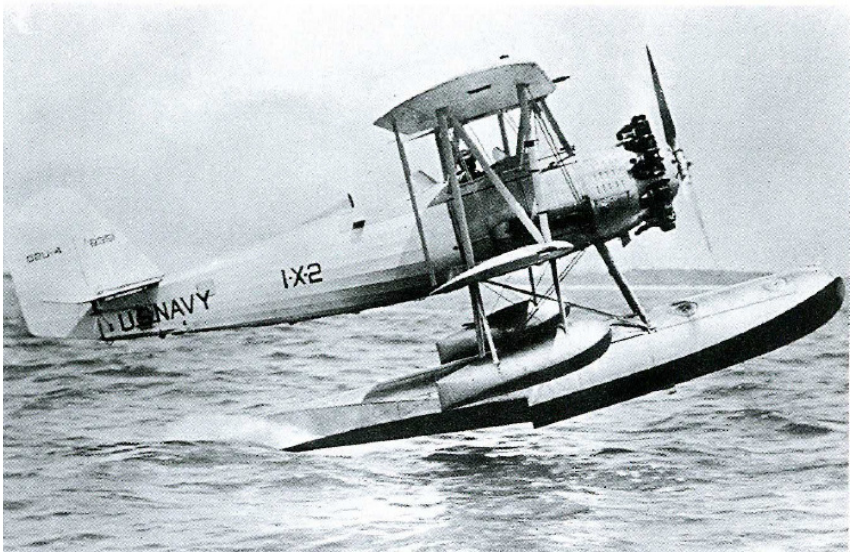

Figure 2. Vought 02U-4 Corsair classed as a floatplane type seaplane (Yenne 1977).

Early impact theories assumed that the momentum of the seaplane imparted to the virtual mass remained constant. However, this is only true in the case of vertical drop where the velocity parallel to the keel is zero. For typical oblique seaplane landings depicted in Figure 3, momentum of the seaplane is not only imparted to the virtual mass of the water connected or associated with the impact area of the hull but also to the downwash as the water slides off the step or the rear of the plane. The cross section at the step determines the momentum imparted to the downwash, whereas the forward cross sections have more effect on the virtual mass. Thus, applying equations that solely consider the vertical velocity during impact and not the resultant velocity of both vertical and horizontal velocities like in oblique landing, neglect the momentum imparted to the downwash (Mayo 1945).

Seaplanes with constant trim during landing will skip like a rock does when thrown nearly horizontally off the water. Each of these "skips" are impact periods and during each of these periods the force exerted on the hull from the water goes from zero before initial impact to a maximum force and then back to zero when the hull leaves the water. The first impact period produces the maximum impact force, and this decreases with each consecutive impact period.

During the impact period the lift force on the wing is about equal to the weight of the entire seaplane, so most theories assume they are equal. Benscoter (1947) shows this type of landing approach in Figure 4, and the reaction during the impact period of a "skip." In most theories the horizontal velocity component of the seaplane during impact is kept constant. According to Crewe (1946), this is also true for full scale conditions.

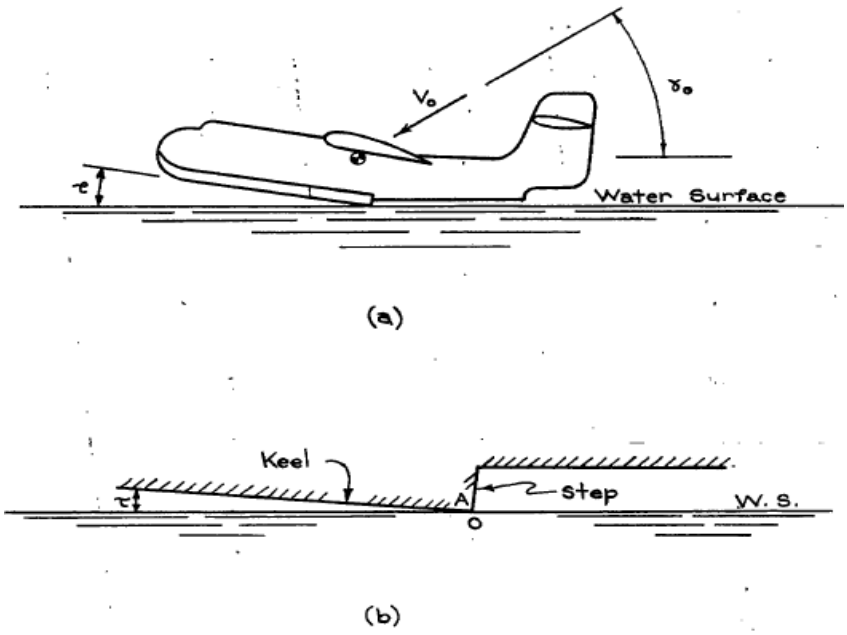

Figure 3. Typical oblique seaplane step landing (Crew 1946).

It is important to determine the impact loads in order to perform a structural analysis on the hullform. Severe structural damage can be done to the plating and framing of the fuselage if the loads are not estimated appropriately. Since hydroelasticity is ignored in most seaplane impact theories assuming a rigid body, the average pressure is of importance to the structural response (Faltinsen 2005).

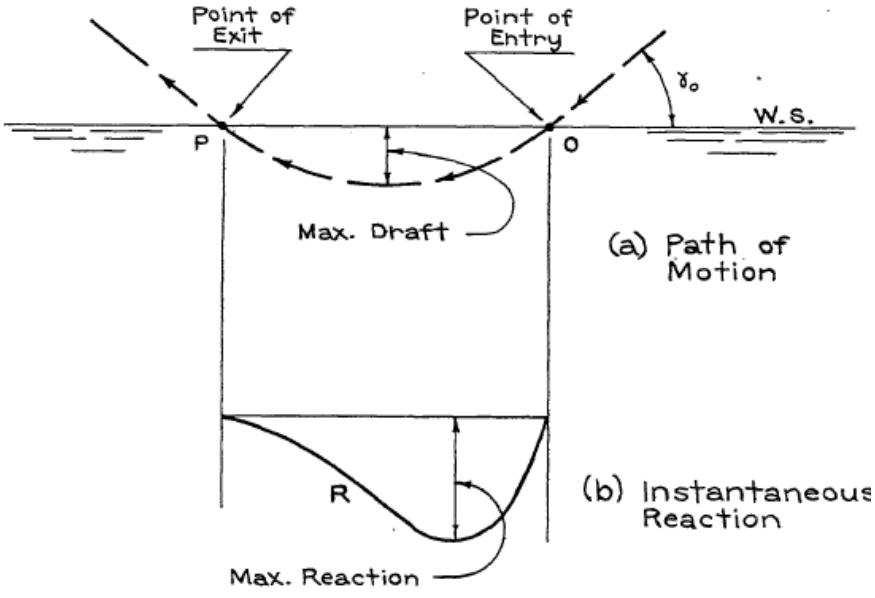

Figure 4. Draft and reaction variations during impact period (Benscoter 1947).

IV. IMPORTANT CONSIDERATIONS USING IMPACT THEORY

In much of the theory reviewed, there are several assumptions and physical conditions inherent in seaplane impact which is usually ignored. Thus, a review of some key underlying assumptions should be addressed in order to understand the limitations of the methods proposed. Important considerations discussed include planing data, model test results, hullform rigidity, 2-dimensional versus 3-dimensional analysis, and chine immersion.

A. PLANING DATA

Some theories suggest using planing data in order to predict the impact loads; however a cautionary note should be advised when doing so. Overall, impact pressures are related to the rate of growth of the waterplane area. However, when using pure-planing data versus impact data, differences arise in local pressure. Crewe and Gerry (1977) conclude that local pressures in steady planing cannot exceed the water stagnation pressure, however in impact the local pressures maybe up to several times this amount. Therefore, planing conditions do not see these peak pressures near the water surface intersection during impact. The authors suggests determining the pressure distribution by a strip method calculation by means of both “planing theory” of a 2-dimensional longitudinal plate on a stream of finite depth proposed by Green (Green 1935) and vertical impact theory for lateral hull sections proposed by Wagner (Wagner 1932).

B. MODEL TEST RESULTS

To validate impact theory, the theoretical equations to predict such loads are usually compared with either model or full scale tests. Comparing experimental results with theoretical has its complications for many reasons since many effects that a normal seaplane experiences are not included in theory. These effects include, but are not limited to the following: airframe elasticity which affects the inertial loads, the aerodynamic lift which varies during impact, ground effect on the wing lift which may greatly affect the trim and initial flight path, and after-body effects. Thus, additional safety factors should be applied when using theoretical loads (Crewe and Gerry 1977).

C. RIGIDITY

When developing the theory for seaplane impact loads the hullform can either be considered elastic or rigid. For elastic structures, hydroelasticity is important for both local and global effects of impact. Hydroelasticity refers to the fact that both the fluid flow and the structural elastic reaction have reciprocated interaction. Local hydroelastic effects are important for high impact pressures for very short durations and should be

considered for small deadrise angles. Rigid structural analysis however, does not consider hydroelasticity or dynamic effects (Faltinsen 2005). The theories discussed for the most part assume a rigid hullform.

D. 2-DIMENSIONAL VERSUS 3-DIMENSIONAL

Many theories consider only 2D impact as opposed to 3D. The importance of 3D flow affects the maximum pressure by a ratio of 0.66 when comparing a cone and a wedge with small deadrise and constant velocity. Beukelman (1991) showed with experimental data that the forward speed has a strong influence on the pressure level when the deadrise angle is lower than around 2 degrees for 3D bodies (Faltinsen 2005).

E. CHINE IMMERSION

Another consideration sometimes not dealt with in theory is chine immersion. Most theories assume no chine immersion. Due to the effect of free water surface wave rise during penetration of impact, the chines may immerse before maximum acceleration occurs. In this case the acceleration would be less than if the chines had not been immersed. An estimate for the rule of chine immersion given in the equation below, is that for length-to-beam ratio hulls of around six, the maximum acceleration and sometimes maximum penetration or draft occurs without chine immersion with normal loading or in other words typical beam loading coefficient in the order one (Crewe and Gerry 1977).

$$C_{\Delta} = \frac{m}{\rho b^3}$$

V. LITERATURE REVIEW

A. VON KARMAN AND WATTENDORF (1929)

Empirical equations are derived by Von Karman (1929) to find the maximum pressure experienced by the float at initial impact. The theory is based on a prismatic wedge hull dropped vertically and striking a horizontal water surface. The force is derived using the momentum theorem, and can only be used by assuming a closed system and conservation of momentum. Thus the effect of buoyancy decreasing momentum is neglected.

Von Karman determined that the added mass for the seaplane float is equal to the mass of the water contained in a semicircular cylinder of the diameter equal to the waterplane breadth in the still water condition. The paper outlines that this can be

assumed if the undersurfaces are not too sharply inclined. The following equation predicts the maximum pressure acting on the float and includes a dynamic pressure part which corresponds to the impact velocity and a term which correlates to the theoretical factor of increase for differing angles of deadrise.

$$Pmax = \frac{\rho v_o^2}{2} \pi \cot \alpha$$

The empirical formula corresponds well with experimental results performed for the paper; however, a limitation is that this method is not compared with oblique impact velocity component parallel to the keel.

B. WAGNER (1932)

Wagner's (1932) method assumes blunt body impact and considers the local uprise of water. Wagner's slamming model of a local small deadrise angle completed in 1932 is useful in the fact that it provides simple analytical results and has practical uses. Faltinsen's (2005) forms of Wagner's equations were also used in this section of review of theory.

Wedge drop tests show that spray is close to atmospheric pressure and thus is not as important as the large pressures occurring at the spray root where there is green water loading, or where the air isn't mixed with the flow. At the spray root large pressure gradients accelerate the water at high velocities into a "jet flow" causing a high free-surface curvature or wave uprise which then turns into spray under the influence of surface tension. Wagner devised the impact problem in separate domain theories. The proposed method concentrates on Wagner's outer flow domain theory, which excludes the flow in the jet domain, which turns into spray, and also excludes the inner domain which includes the flow in the spray root (Faltinsen 2005).

This outer domain theory uses the intersections between the water surface and the hull surface, which is very close to the location of the spray roots (Faltinsen 2005). Figure 5, shows an impacting hull with the water surface in the outer flow domain where the hull hits with constant entry velocity. The derived pressure equation is given below where *c* is the wetted half beam, *P* is the hydrodynamic pressure, P_a is the atmospheric pressure, ρ is the density of water, $^{dV}/_{dt}$ is he vertical acceleration, $^{dc}/_{dt}$ is the speed of propagation of the wetted semi-width, and *x* is the coordinate along the beam of pressure (Faltinsen 2005).

$$p - p_a = \rho V \frac{c}{(c^2 - x^2)^{1/2}} \frac{dc}{dt} + \rho \frac{dV}{dt} (c^2 - x^2)^{1/2}$$

The first term in this equation is the slamming pressure and is related with the rate of change of the wetted surface and the second term which is considered the added mass pressure (Faltinsen 2005). After chine immersion, the wetted half beam is constant, so the slamming pressure term goes to zero. Thus, after chine immersion the only pressure acting on the hull is due to the associated added mass of the hull.

Several variables in the pressure equation need further insight on how to determine them. Wagner's theory is capable of handling non-prismatic hullforms, where the vertical distance of the surface height relative to the body, $n_b(x)$, can be defined a series which captures the bottom surface geometry and is given by the equation below.

$$n_b(x) = \beta x + \beta_1 x^2 + \beta_2 x^3 + \beta_3 x^4 + \beta_4 x^5 + \cdots$$

To determine a function which relates the normal velocity to the speed of propagation of the wetted semi-width as the body submerges, the function *u* is defined by formula below (Wagner 1932).

$$u = u(c) = \frac{V_n}{\frac{dc}{dt}} = \frac{2}{\pi}\beta + \beta_1 c + \frac{4}{\pi}\beta_2 c^2 + \frac{3}{2}\beta_3 c^3 + \frac{16}{3\pi}\beta_4 c^4 + \cdots$$

With the function u calculated at a particular wetted half beam of interest, the speed of propagation of the wetted semi-width can be determined given an impact velocity. This quantity can then be substituted into the pressure equation to determine the hydrodynamic pressure on the hullform.

As previously stated Wagner's theory is useful since it provides simple analytical results and is practical. The theory is of value since it is capable of computing pressures for non-prismatic hullforms. However, the equations only use vertical impact velocity and chine

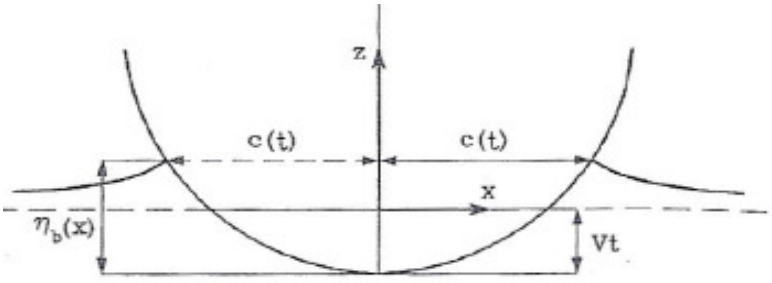

Figure 5. Definition of parameters to determine the impact forces on a hull using Wagner's outer domain theory (Faltinsen 2005).

un-wetted conditions, which is not the impact scenario for typical oblique seaplane landing. Since Wagner's theory is derived with only the vertical impact velocity, the momentum imparted to the downwash is not considered.

C. BLUNDELL AND JONES (1938)

Pressure and total impact force measurements were conducted on a variety of seaplane hulls including the Southampton and Perth seaplanes, the Singapore IIc, and on a V-shape hull by Blundell and Jones (1938). The Southampton and Perth seaplanes were tested to seaplane alighting impact conditions, whereas the Singapore IIc was tested in purely vertical impact. The results were then compared with impact theory using the equation below.

$$P_{max} = \frac{V_n^2}{K} \cot \emptyset \,, \qquad where \ \cos \emptyset = \cos \theta \cos \alpha$$

The equation given above is derived from V-shape model tests and gives the relation of the pressure, where the constant K varies depending on the location of impact interest and the loading. In previous tests, K equaled 68 for a location close to the chine and 47 for a location near the keel. This shows that the impact pressure is higher at the keel than at the chine for a V-shape hull. The pressure near the chine depends on the loading as well as the striking velocity, whereas the pressure near the keel is independent of the weight, or the loading, of the hull. It is however dependent on the deceleration through the water. It is important to note that this equation with the values of K provided is only for hull forms with the same order of loading on the hull bottom as the experimental hull form.

Figure 6 shows the varying hull shapes used in the paper and the peak pressures across transverse sections of each hull form. The Perth hull is of particular interest with the drastic change of the local deadrise from keel to chine varying from 5.5 degrees to 41 degrees. Table 1 summarizes a good agreement between the theoretical and experimental results of one transverse section and the pressure distribution on the Perth hull, where station 11 is close to the chine and station 14 is close to the keel.

Table 1. Perth Hull pressure distribution along one transverse section ($V = 60\frac{ft}{s}$, $v_o = 7\frac{ft}{s}$, $\alpha = 7.5°$, and K=55)

	Station	Deadrise Angle $\theta°$	Empirical Pressure (psi)	Recorded Pressure (psi)
Near Chine	11	5.5	24.5	22.0
	12	14.0	14.2	14.0
	13	22.5	9.1	-
	14	41.0	4.5	6.2
	16	41.0	9.0	8.0
Near Keel	17	41.0	18.0	17.0

The experimental and theoretical results also show that at constant immersion, regardless of the impact velocity, the maximum force of impact occurs. Also under this condition, the experimental results showed that for all three seaplane hulls the chine was nowhere near chine wetting when the maximum force was measured. The theory also shows and is verified by experimental results that the pressure midway between the keel and the chine is proportional to the cotangent of the deadrise angle at a given impact velocity which is normal to the keel except when this angle is very small.

Comparing the recorded pressure of the three seaplane hulls and the V-shape used for experimental study with the maximum peak pressure equation, the results showed good agreement. Since there was good agreement with the seaplanes with curved transverse sections, Blundell and Jones imply that the theoretical equation can be applied not only to flat V-sided hulls but to curved hullforms and to hull forms with deadrise varying longitudinally. However, because the value of constant K seen in the pressure equation is deduced from experimental results from the seaplane hull forms listed, it is important to note that this method is limited to hullforms similar to those tested.

An important aspect of Blundell and Jones' work is a series of tables of experimental results performed on the V-shape hull specimen that shows the peak pressures registered at two points on the transverse section. The experiments used constant vertical velocity at impact with varying deadrise angles, trim angle during impact, and tangential or horizontal velocities. This shows that the simple empirical pressure equation, gives good estimates for oblique impact landing conditions.

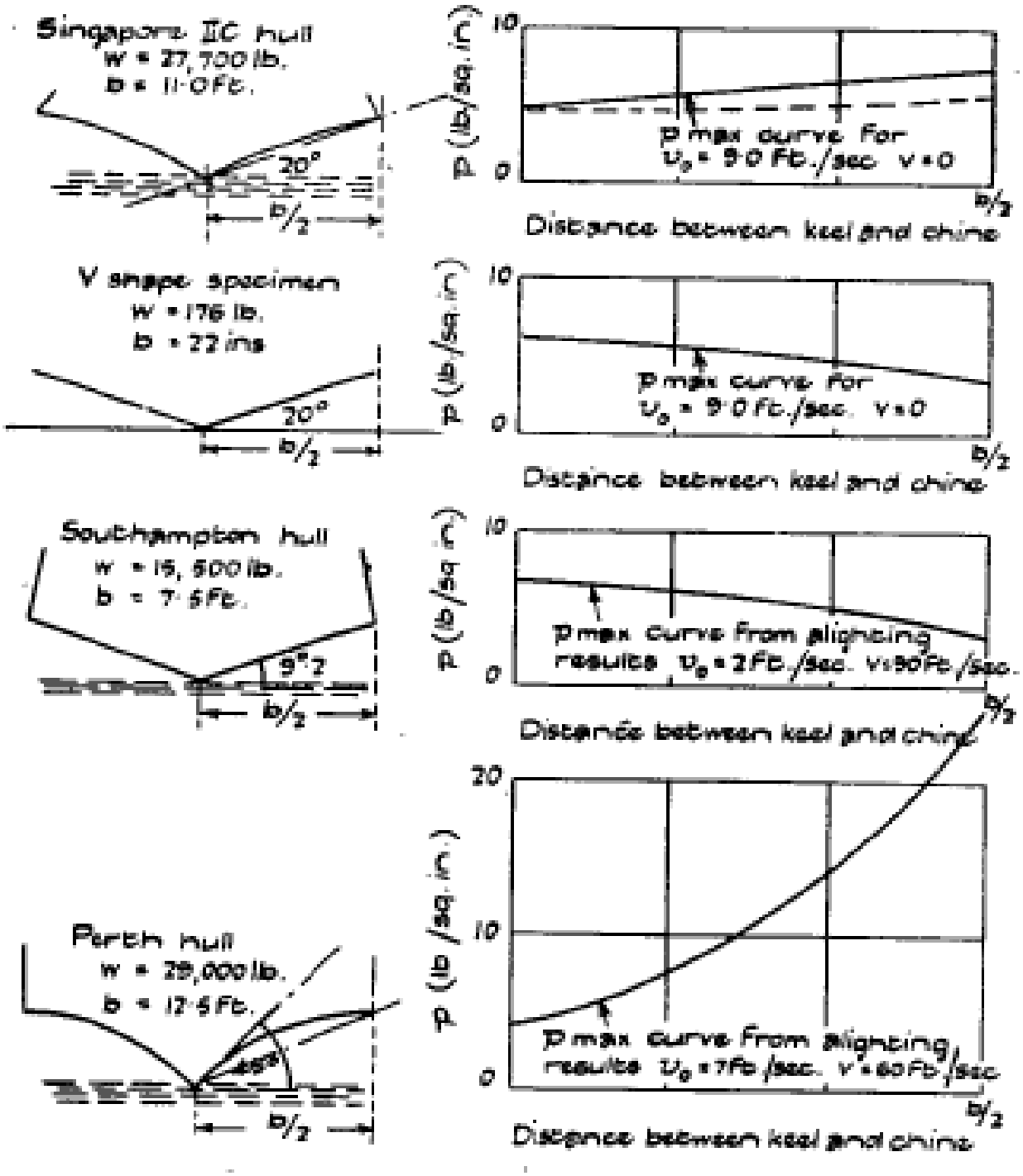

Figure 6. Transverse pressure distribution of the four hullforms used in experimental testing (Blundell and Jones 1938).

D. MAYO (1945)

By correcting previous impact theory, Mayo (1945) develops an improved theory to determine the force acting on the hull during impact of a prismatic hull with positive trim. The key contributions to the impact problem that Mayo considers include: flow in transverse planes, momentum equations, aspect-ratio corrections, effect of generated wave on the virtual mass, distribution of surface pressure, and conditions for maximum impact force.

The forward velocity of the seaplane float causes momentum to be passed into the hydrodynamic downwash. For impact with trim the rate of penetration is determined not only by the velocity component normal to the keel but also by the velocity component parallel to the keel, which tends to reduce the penetration.

The motion of the hull for oblique impact considers not only perpendicular but parallel flow motions in respect to the keel. The paper considers transverse "flow planes" which are fixed in space and can be seen in Figure 7. The hull passes through these flow planes and when the step clears a flow plane the flow plane then becomes a part of the wake. Thus for oblique impact the flow plane comes into contact with all cross-sections as the hull form passes through it with time, whereas for solely vertical impact the flow plane is in contact with only one cross section.

For an ideal fluid, the growth of the of the intersected hull cross section as it passes a particular plane will only be used to determine the flow in that particular plane. The entire flow process for an individual plane begins when the keel line penetrates the individual plane and ends when the planes slide off the step or the rear of the hull.

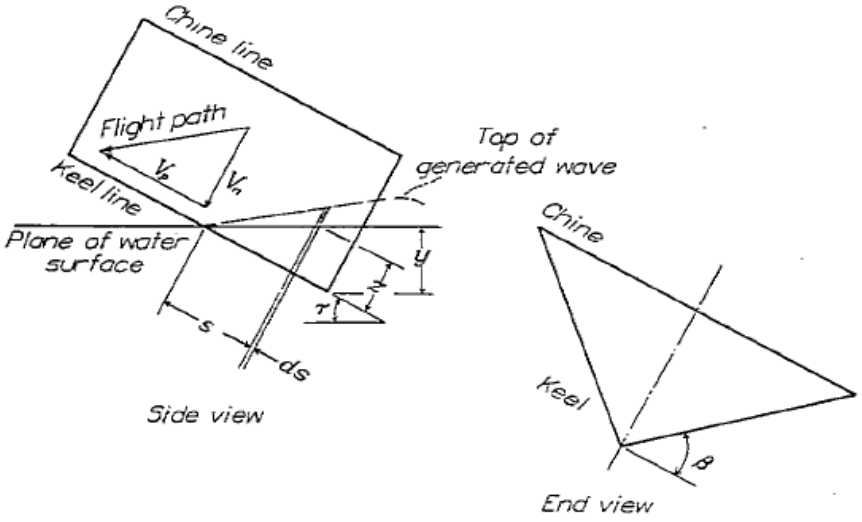

Figure 7. Prismatic float showing the velocity components and normal transverse flow plane (Mayo 1945).

For vertical impact with a hull with some trim angle, the accelerated water during impact is in the direction normal to the plating, thus the stationary plane in which the fluid moves is in the direction normal to the keel. As the keel immerses there is a difference in depth along the keel and this difference causes longitudinal pressure gradients. These longitudinal pressure gradients change the end effects of the flow and the cross-plane-flow. To account for the various differences in flow caused by the longitudinal pressure differences, an aspect-ratio factor is applied to the pressure equation.

The total impact force is found by total rate of change of momentum, which is equal to summing all the reactions of the individual flow planes that the hull encounters and also the momentum that is passed on to the downwash along with the flow planes that slide off the step. The total hydrodynamic force in the direction of the velocity normal to the keel is defined by the equation below.

$$F_n = \frac{d}{dt}(m_w V_n) + m_s V_n V_p$$

However, in order to get the longitudinal load distribution, each reaction of each individual flow plane affected by the impact at a particular instant of loading must be determined.

In order to apply the equation above, this force equation is derived again with empirical equations for virtual mass and aspect-ratio corrections for the distributed load. A brief summary is provided, with key equations that determine the end result of the force acting normal to the hull.

The force acting on the hull due to an individual transverse flow plane given in the equation below, considers the momentum of the flow in that transverse plane.

$$F_p = \frac{d}{dt}\left(Kz^2 ds \frac{dz}{dt}\right)$$

To obtain the total force, the forces acting on the hull from each individual flow plane can be integrated over the effected length of the hull. For fixed trim impact a total force equation is defined by the following equation, where the first term is related to the virtual mass of the flow beneath the hull and the rate at which the momentum of the seaplane is imparted to the downwash.

$$F_n = \frac{Ky^2 \frac{dV_n}{dt}}{3 \sin\tau \, (\cos\tau)^2} + \frac{Ky^2 V_n^2}{\sin\tau \cos\tau}$$

To account for the virtual mass of the flow in the transverse plane, Sydow's theoretical equation for flow in normal planes of a triangular prism along with Pabst's empirical aspect ratio factor to correct for end loss were used. The effective aspect ratio used in this case, is the length to mean-beam ratio. However, to correct for the inaccuracy of Pabt's aspect-ratio factor determined by submerged vibration test a correction factor of 0.82 derived from experimental results was introduced into the equation for the virtual mass of the flow in the transverse plane. The resulting equation is given below.

$$m_p = 0.82\left(\frac{\pi}{2\beta} - 1\right)^2 \pi \frac{\rho}{2} z^2 ds \left(1 - \frac{\tan\tau}{2\tan\beta}\right)$$

The equation above can only be used for small deadrise angles due to the aspect-ratio factor. With further substitutions and knowing that the total force equation already stated was derived on the relationship that $K = m_p/z^2 ds$ the m_p equation can be substituted into the normal force equation and gives the following final total force formula.

$$F_p = 0.82\frac{\rho}{2}\left(\frac{\pi}{2\beta} - 1\right)^2 \left(1 - \frac{\tan\tau}{2\tan\beta}\right)\frac{\pi y^2}{\sin\tau\cos\tau}\left(\frac{y\frac{dV_n}{dt}}{3\cos\tau} + V_n^2\right)$$

When comparing this method to experimental data for planing, vertical drop, and oblique impact, the theory shows good agreement for the loss of momentum imparted to the downwash. Also, the oblique impact data shows that old theory used greatly overestimates the impact force, thus the proposed theory gives good results especially for seaplanes landing with higher trim angles.

E. CREWE (1946)

Crewe's (1946) theory assumes that the hull has a tangential-to-keel velocity relative to the water. The impact motions in this case have other forces in addition to the classical impact theory. These additional forces are the same types that occur in steady planing motions. Crewe refers to these forces as impact-planing forces. The impact-planing forces could be less than the similar forces developed during planing due to the impact not lasting long enough for the forces to build up entirely. The equations used to predict these impact-planing forces include a 'time-lag' coefficient to account for this lack of full force build-up as compared to the steady planing condition.

The total water force in impact depends on the draft, attitude, geometry of the hull bottom, pressure area, and the velocity components during impact. The forces that Crewe considers which affect the impact include the following: the classical or pure impact force, impact gliding force, and possibly normal drag or a form drag. The pure

impact is dependent on the virtual mass. Like other impact methods, Crewe assumes that a hull form in motion has a corresponding mass of water that attaches itself with the hull, however the virtual mass moves with the normal-to-bottom velocity component during impact. All water effects except the inertia forces of the added mass are neglected.

The impact gliding force is considered when the velocity component in the vertical direction is zero and the Froude number is large. These forces are due to the tangential velocity of the water relative to the bottom and are similar to that in a steady planing case. The normal drag comes from the component of flow of the water in the direction past the bottom.

Additional derivations of important quantities such as the pure impact added mass at the moment of peak acceleration are given in the text, however one of the most unique and important aspects of the paper are the series of cures of numerical cases. These are very good for making seaplane performance estimates and they also include the time history of impact which many theories do not. The hull form shown in Figure 8 was used for the calculations for the curves is a "single keeled rectangular prismatic bottom."

Important physical quantities can be determined in the Table 2. The product of columns 2, 3 and 4 give the quantities in column 1. In order to get values at the moment of peak acceleration, the prime term of the pure impact associated water mass value, u', and the flight-path-angle parameter, ω, should be replaced by their values at maximum acceleration in column 4 formulas. The series of curves of numerical cases discussed later provide the values for the columns in the table.

The quantities for determination in column 1 include: the draft of the bottom of the hull, usually that of the keel at the step, *h*, the pressure area by projecting the surface of the bottom supporting the water pressure, *S*, the time measured from the instant the bottom first touches the water in the impact period considered, *t*, the craft velocity perpendicular to the water, V_v, the acceleration of the craft normal to the craft bottom, (dV_n/dt), and average water pressure over the pressure area, *p.* Other quantities listed in columns 2, 3, and 4 are described in Appendix A, however for this report details and equations to determining these values are not provided and the main text should be referenced.

Table 2. Physical quantities during impact

Quantity Required		Functions Plotted	
Column 1	Column 2	Column 3	Column 4
h	$(W/g)^{(1/x)}$	$1/K'^{(1/x)}$	$u'^{(1/x)}$
S	$(W/g)^{(1-1/x)}$	$K_s/K'^{(1-1/x)}$	$u'^{(1-1/x)}$
t	$(W/g)^{(1/x)}/V_H$	$1/K'^{(1/x)} \tan\tau$	$\frac{u_m'^{(1/x)}}{\omega_O}\int_0^{(u'/u_m')^{(1/x)}} \frac{d(u'/u_m')^{(1/x)}}{(\omega/\omega_O)}$
V_v	V_H	$\tan\tau$	ω
(dV_n/dt)	$V_H^2/(W/g)^{(1/x)}$	$K'^{(1/x)}(\tan\tau)^2$	$xsu'^{(1-1/x)}, (\omega^2+q\omega+r)/(1+u')$
p	V_H^2	$K'(\tan\tau)^2/144K_S$	$xs\,(\omega^2+q\omega+r)/(1+u')$

Some of the quantities that can be determined from the design curves to apply to important design parameters include peak acceleration, time to reach peak acceleration to determine wing stresses, wetted area and draft when the velocity component perpendicular to the water has become zero to determine frame stresses, average pressure at moment of first contact with water to determine plating stresses, and the variation of average pressure with pressure area to determine frames and plating strengths. Example graphs to determine the peak acceleration are included in Figures 9 and 10, where both graphs are used simultaneously to determine the value.

This method gives an in-depth analysis of the forces affecting the impact condition, and allows for various impact conditions. The graphs hold value in their ability to give easy design estimates. Also, there is a lot of additional information in the paper which allows a designer to change design parameters quickly and determine how the changes affect other parameters. There is limited experimental evidence to support the theoretical formulas, but the numerical work can be used for a range in deadrise angles from 10 to 30 degrees.

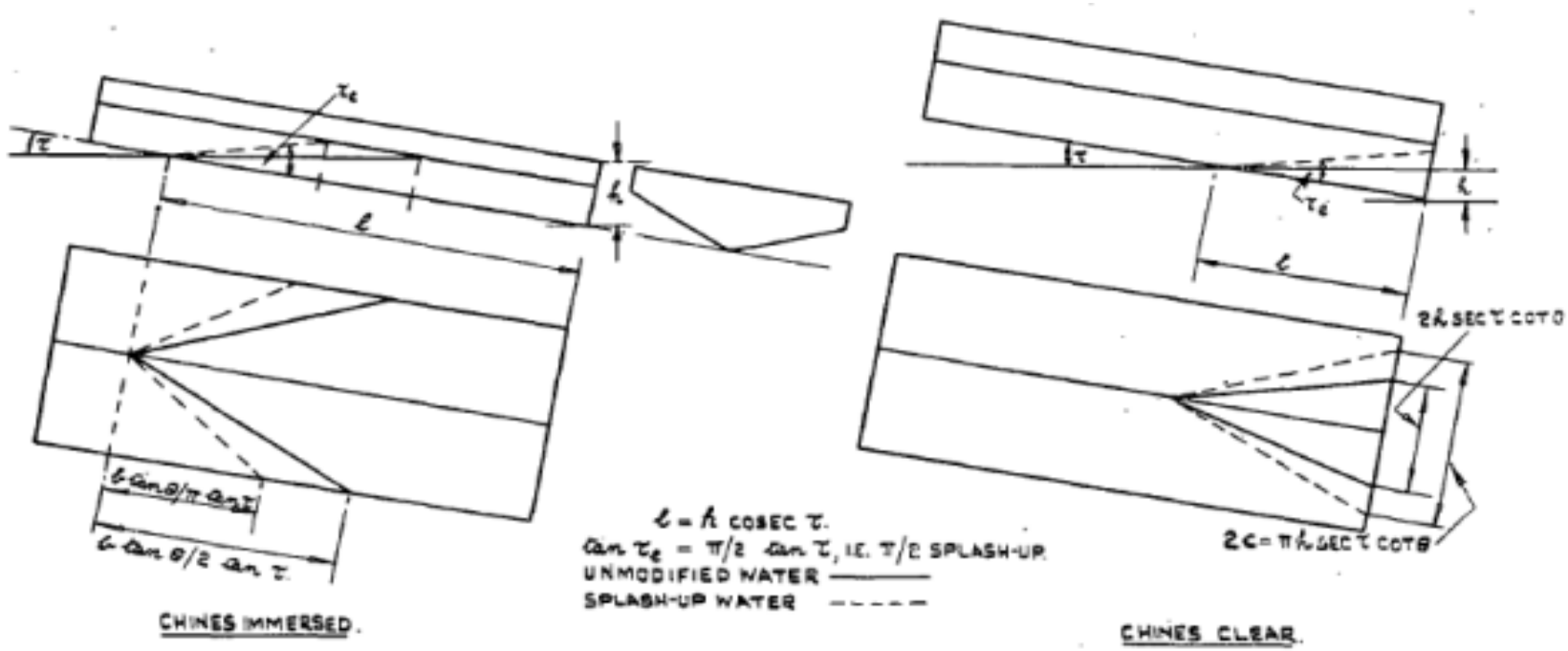

Figure 8. Idealized single keel rectangular prismatic bottom hull form for both chine immersed and clear cases. Shows the splash-up of impact and the dimensions of pressure area (Crewe 1946).

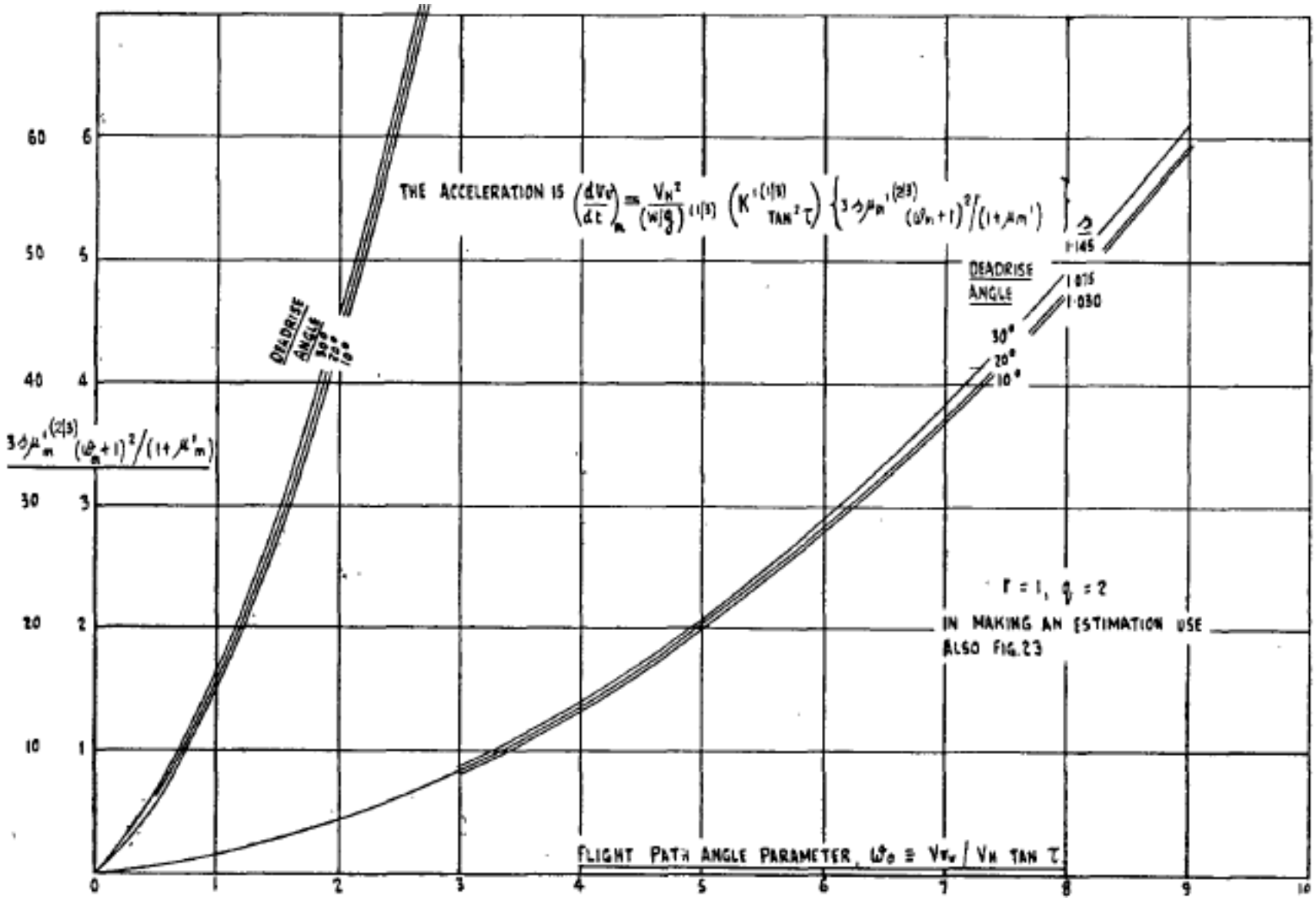

Figure 9. Curves for estimating peak acceleration (Crewe 1946).

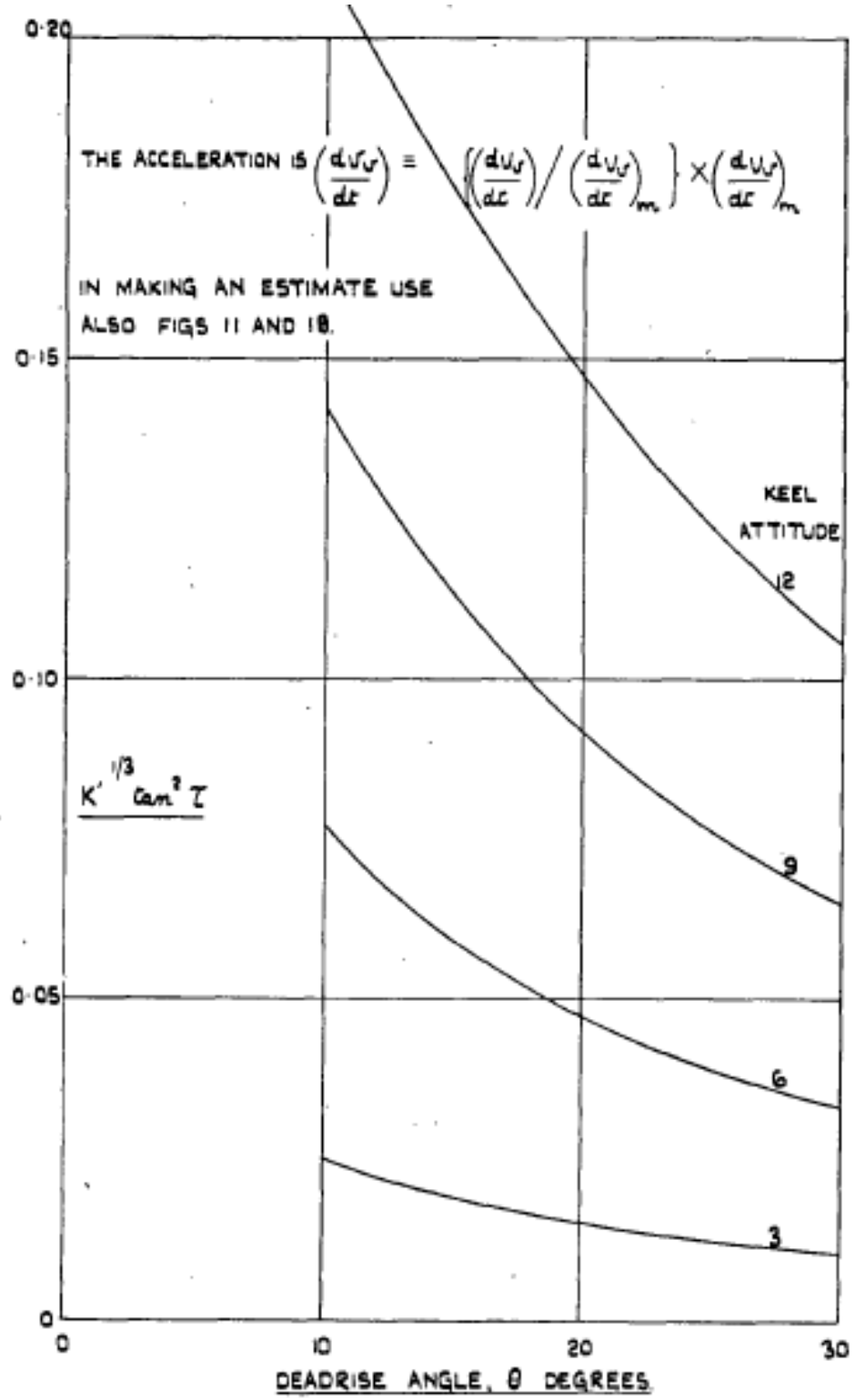

Figure 10. Curves for estimating peak acceleration (Crewe 1946).

F. BENSCOTER (1947)

A step landing is proposed by Benscoter (1947) for an infinite beam and length wedge starting at the step with a flat-bottom without flare and no afterbody. The trim angle is assumed to remain constant and the initial velocity is in the direction of the flight path angle. In most analysis, the velocity component parallel to the keel is kept constant during the impact period. However, since for stepped landings the trim angle is kept small, then the horizontal velocity component will be kept constant which produces just slightly different results if the velocity component parallel to the keel were kept constant.

As shown in the introduction section of the paper and Figure 4, the seaplane enters the water at the intersection of the keel and the step, which is marked at point O. Point O is considered the initial part of the "skip" where the plane enters the water and point P is where the plane exits the water.

We can see in Figure 4 that the seaplane's reaction reaches a maximum upward acceleration before the point of maximum draft. This is proven in both experimental and theoretical results. Also it is important to note that this bottom reaction, throughout the course of the impact period of the seaplane, is only proportional to the vertical acceleration when the wing lift equals the weight. It can also be concluded that the maximum acceleration is proportional to the initial velocity squared and inversely proportional to the draft at the time of maximum acceleration.

Benscoter considers the important parameters that affect the loading or motion of the seaplane to include the deadrise along the hull and the mass of the plane. If the plane is large then elasticity of the structure may also be important, however in this analysis it is ignored. As seen in Figure 11, the loaded area of the hull is similar to that of a triangle. However, the "calm water" intersection of the hullform is not enough to analyze. Due to water pile-up of the spray root, the transverse pressure distribution must be analyzed along with the longitudinal pressure distribution.

Now the problem has been turned into a 3D analysis with a longitudinal distribution. The problem could only be handled in the proposed state of Benscoter's work via an aspect-ratio factor applied to the pressure at all the points along the loaded area. To analyze the total reaction distribution along the length of the hull, unit transverse strips of the loaded area are analyzed at stations along the longitudinal loaded area and then integrated along this longitudinal length of loading. Each individual strip's reaction force is dependent on the draft of the keel at this particular station and the velocity components normal to the keel. The 2D case is used to determine the reaction force on

each individual unit strip. This method lacks the ability to determine the transverse pressure distribution as in Figure 11. Possible incorporation of other methods, such as Wagner's, maybe integrated into this method.

First analyzing the 2D case, the theory considers a wedge dropped vertically in the water and the added mass associated with the impact. To account for the water pile-up, the added mass is multiplied by a correction factor. The theory shows that the water mass is proportional to the square of the displacement. The reaction force is caused by the rate of change of momentum of the fluid, where this momentum change is due to the change of velocity of the hull and also the change of added mass due to the change of the loaded width.

When creating the equation for the maximum acceleration that the hull experiences with its corresponding draft and time of occurrence, the buoyancy term is omitted because for maximum accelerations the buoyancy force is very small at the

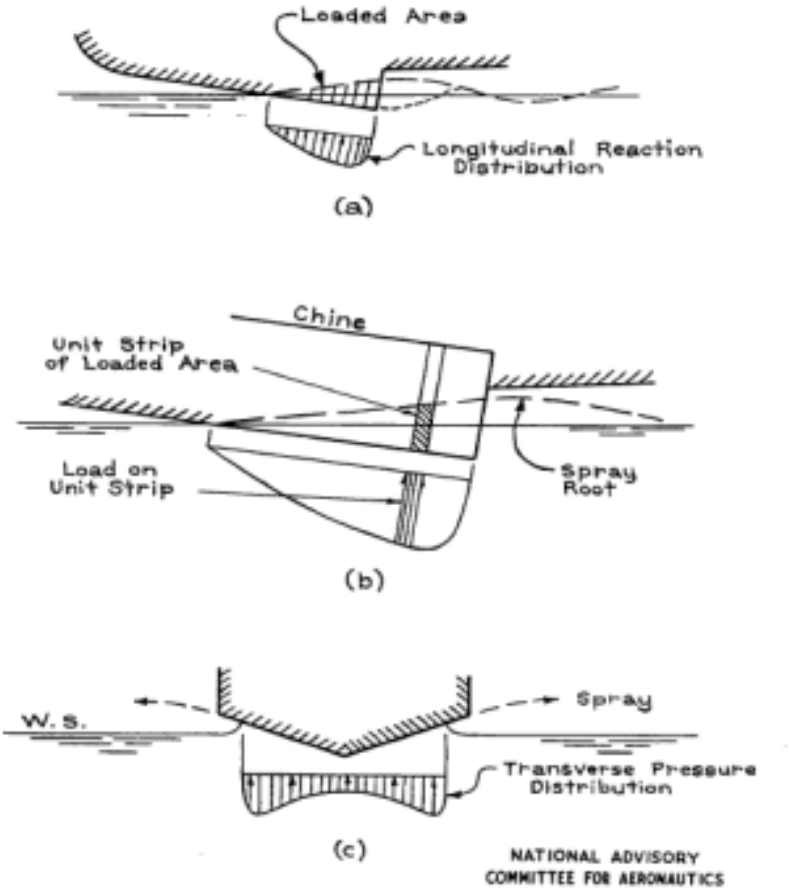

Figure 11. Longitudinal and transverse reaction distribution on the loaded hull area (Benscoter 1947).

corresponding displacement. The equation below is for the maximum acceleration in the 2D case and is the final result of a series of substitutions and assumptions. It is in terms of the physical properties of the float as well as the initial sinking speed.

$$\ddot{z}_m = -\left(\frac{25}{108}\right)\frac{z_o^2}{z_m}$$

Also the displacement, or draft, at the maximum acceleration is dependent on the mass of the seaplane and the coefficient of added mass and is defined by the equation below.

$$z_m = \sqrt{\frac{\bar{M}}{5\ \bar{\epsilon}}}$$

Lastly, for the 2D case, the time for the maximum acceleration is defined in the following equation.

$$t_m = \frac{16}{15}\left(\frac{z_m}{\dot{z}_o}\right)$$

For 3D flow, the motion of each unit slice described in 2D flow is assumed to act independently of the adjacent unit slices, where the fluid of the loaded area is divided into unit slices that are perpendicular to the keel. The velocities, displacements and accelerations of each slice are assumed to act normal to the keel. The reaction on the hull is assumed to be the combined widths of the slices which then equal the entire wetted length of the hull.

A 3D virtual mass is derived in the paper and it contains the reduction factor for the aspect-ratio effect to compensate for the varying loaded area in the longitudinal direction. Through a series of assumptions and substitutions, the force per unit slice is integrated over the entire wetted length of the hull and produces the equation for maximum acceleration given below.

$$\ddot{z}_m = -\frac{1}{s_m}\left(\frac{3u_m}{1+u_m}\right)\frac{(1+r_m)^2 V_o^2(\sin\tau)^2}{1+r_o^2(\tan\tau)^2}$$

The paper also gives formulas that are approximate for design. The formula for maximum acceleration given above is re-written in the following form below, where the factor α_1 is brought into the approximate design formula to account for the primary effects of trim angle and deadrise angle on the virtual mass of water and the factor α_2 is introduced to account for the secondary effects. The secondary effects include aspect-

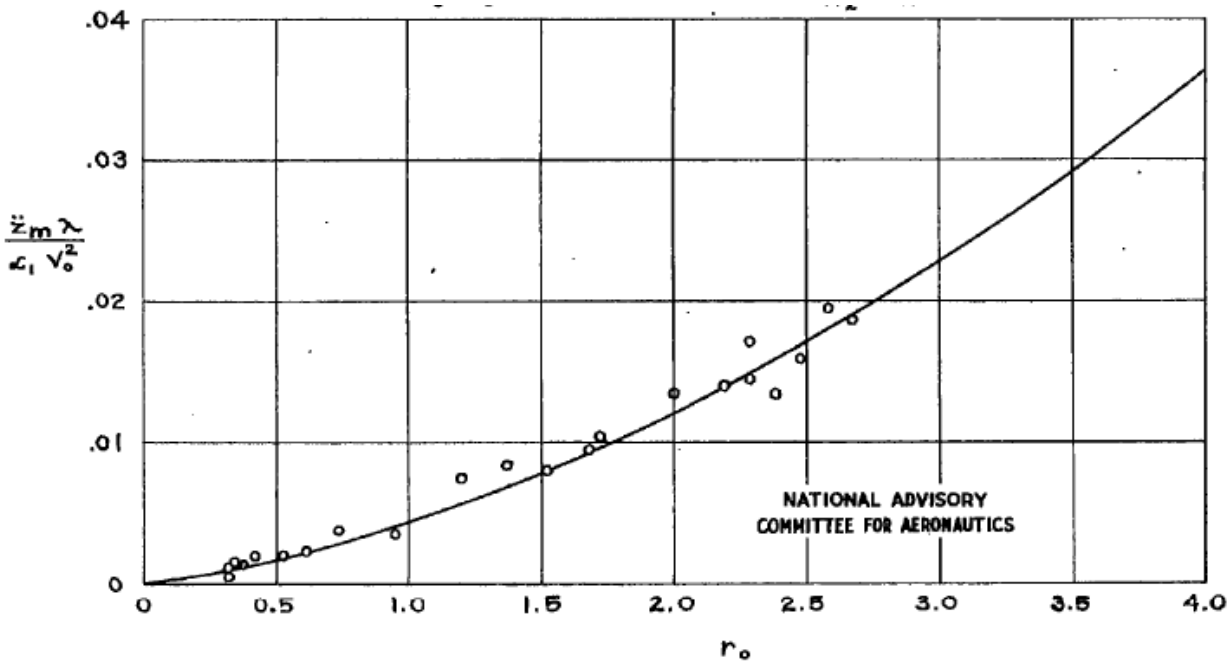

Figure 12. Ratio of maximum acceleration to squared initial speed for $\tau = 3°$ (Benscoter 1947).

ratio effect, the effect of piled-up water, and the dead-rise angle correction to flat-plate theory.

$$\frac{\ddot{z}_m \lambda}{\alpha_1 V_0^2} = -\frac{\alpha_2}{\sqrt[3]{u_m}}\left(\frac{3u_m}{1+u_m}\right)\frac{(1+r_m)^2(\sin\tau)^2}{1+r_o^2(\tan\tau)^2}$$

From Figures 12 and 13 which use an average value of $\alpha_2^3 = 1.1$ and two different values of trim angle, the approximate maximum acceleration of any hullform can be determined. To get the reaction force, the acceleration determined from the graphs is simply multiplied by the mass of the seaplane. The longitudinal reaction distribution can then be determined as shown in Figure 14. There are two parts to the individual force acting on each individual strip which include a quadratic variation and a linear variation.

The theory for maximum acceleration gives good agreement with experimental results. However, the comparison between draft in theory and experimental results is harder to determine and more work should be done on this matter. Overall, the proposed theory gives a good method for determining the longitudinal variation the loading. However, more detailed work should be done on incorporating a more complete theory that includes the transverse pressure distributions.

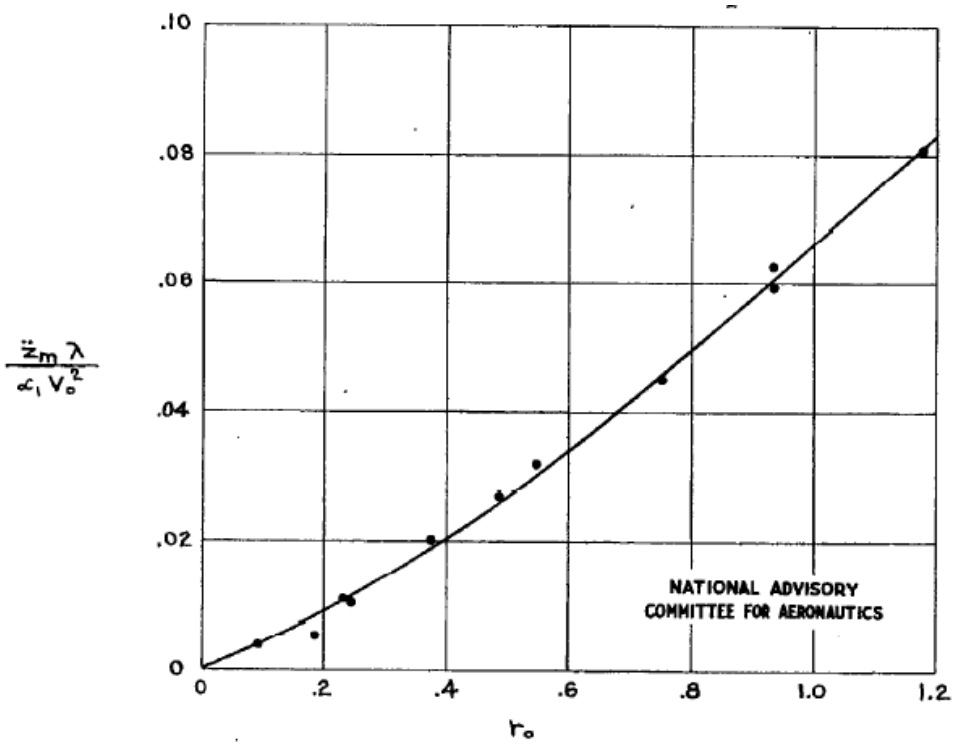

Figure 13. Ratio of maximum acceleration to squared initial speed for $\tau = 12°$ (Benscoter 1947).

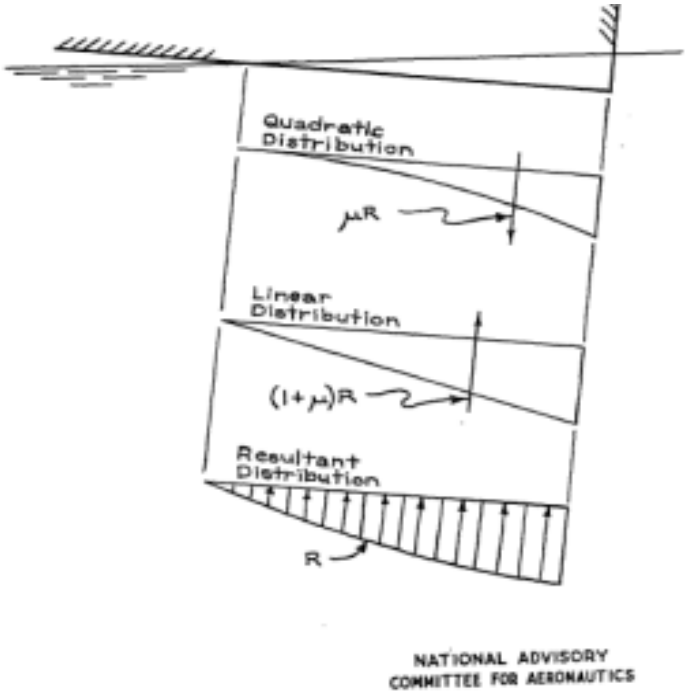

Figure 14. Longitudinal distribution of reaction (Benscoter 1947).

G. HAMILTON (1955)

To demonstrate the full scale impact forces and pressures and the magnitude different parameters affect the total outcomes, Hamilton (1955) used the Sunderland Mk.5 in full scale tests and compared the results with Wagner's theory on pressure. Figure 15 shows where the experimental pressure pick-up positions were located longitudinally on the hull with three different rows along with transverse pick-ups on each of those rows for the experimental impact test.

To determine the maximum hydrodynamic pressure on a planing bottom for local impact, Wagner's equation below was used for the theoretical calculations. Although this equation is for a wedge with flat-sides, Hamilton says it can be used for curved cross-sections because of the use of the local deadrise angle in the equation.

The value for the constant in Wagner's maximum pressure formula, K, differs from full scale derivation to Wagner's theory by an additional value of 8, and is respectively as follows, 132 and 144 when the maximum pressure is given in psi. The paper suggests K should be used as 132 for design purposes, and are the transient peak pressures near the leading edge of the pressure wave.

$$P_{max} = \frac{1}{2}\rho\frac{V_n^2}{K}\left[\left(\frac{\pi}{2}\cot\theta_L\right)^2 + 1\right]$$

Figure 16 plots every pick-up point's maximum pressures against the impact velocity squared along with Wagner's theory. Individual plots at each pick-up row can found in the paper.

To show the transverse pressure distribution of individual cross section rows at the transverse pick-up points, Figures 17, 18, 19, and 20 show several experimental runs versus Wagner's theoretical transverse pressure distribution for rows A and B. There are two methods to determine the experimental pressure distributions. Figures 17 and 19 are generated by experimental method 1 and Figures 18 and 20 are generated by experimental method 2. Method 1 finds the transverse distributions from pressures indicated simultaneously on several pressure pick-ups in the rows, whereas method 2 finds the transverse distributions taken from the pressure time histories of one pick-up in each row by assuming that the pressure wave has a constant velocity for the considered time interval. Wagner's equation to equate the transverse pressure distributions shown in the Figures 17, 18, 19, and 20 is given by the following formula.

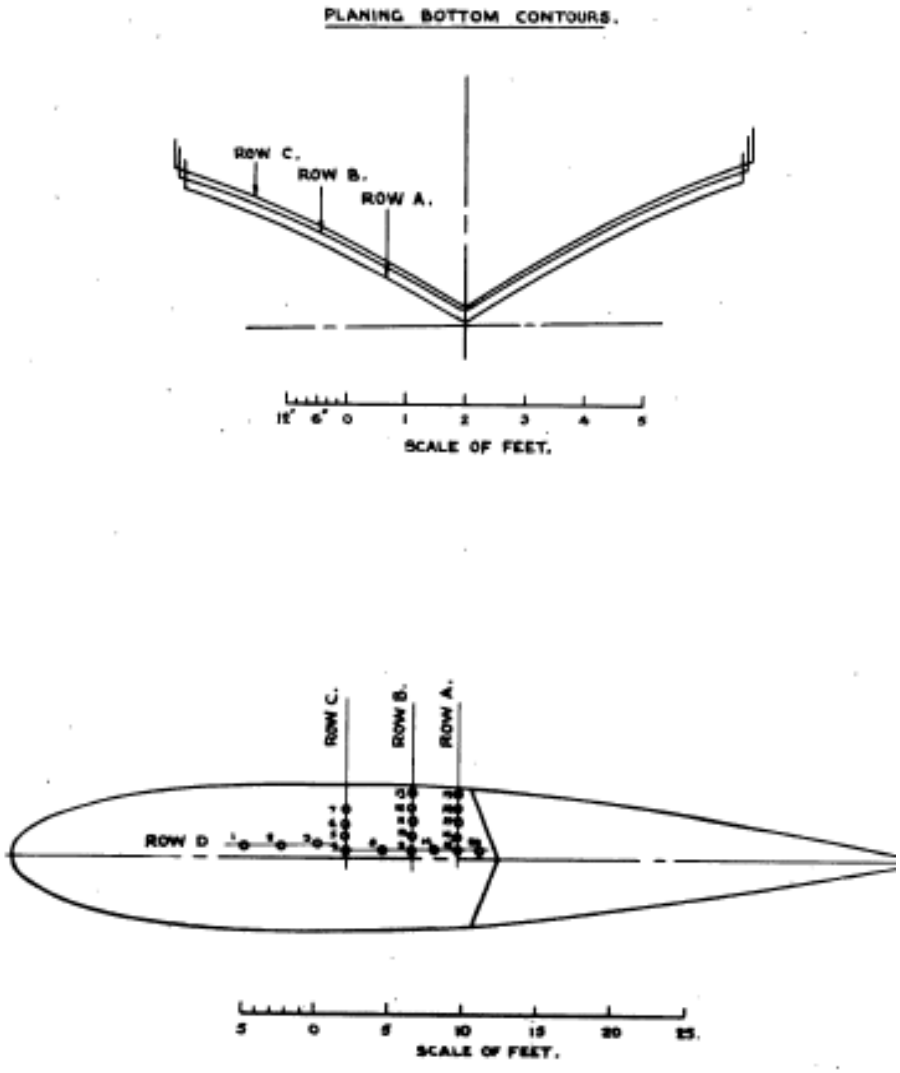

Figure 15. Pressure pick-up positions on the Sunderland Mk 5 (Hamilton 1955).

$$P = \frac{1}{2}\rho V_n^2 \left(\frac{\pi \cot \theta_L}{\sqrt{1-\eta}} - \frac{\eta^2}{1-\eta^2} \right)$$

To account for other factors that may affect impact loads such as chine immersion, hull and wing flexibility, and afterbody effects the following conclusions were made during experimental tests. Chine immersion is small and takes place after the theoretical time of maximum acceleration. As far as structure flexibility, wing vibrations were not amply excited to cause great differences in maximum acceleration and also hull flexibility is negligible.

Lastly, in order to convert the peak pressures, or the pressures confined to a small area, to the design pressures, or the pressures over larger areas, for 2D hulls a simple

expression is derived for the relative magnitude of peak and the mean distributed pressures.

$$\frac{P_{max}}{P_{mean}} = \frac{\left(\frac{\pi^2}{4}\, cot^2\theta + 1\right)\eta}{\pi \cot\theta \sin^{-1}\eta + \eta - \frac{1}{2}\log_e \frac{1+\eta}{1-\eta}}$$

Overall this paper shows good agreement between the experimental and theoretical maximum pressures. However, the Sunderland Mk.5 hull almost matches the description of a wedge shaped prismatic hull of constant deadrise that Wagner uses in his theory. Although the paper says that the theory can be used for curved cross-sections because of the local deadrise angle, additional experiments should be conducted on other hull forms to verify the theory's validity with hull form types of non-constant longitudinal deadrise and flare. Also it should be noted that the paper showed that the theoretical time to reach the maximum impact force is nearly half of that measured by the experimental results. This could be due to afterbody effects not accounted for.

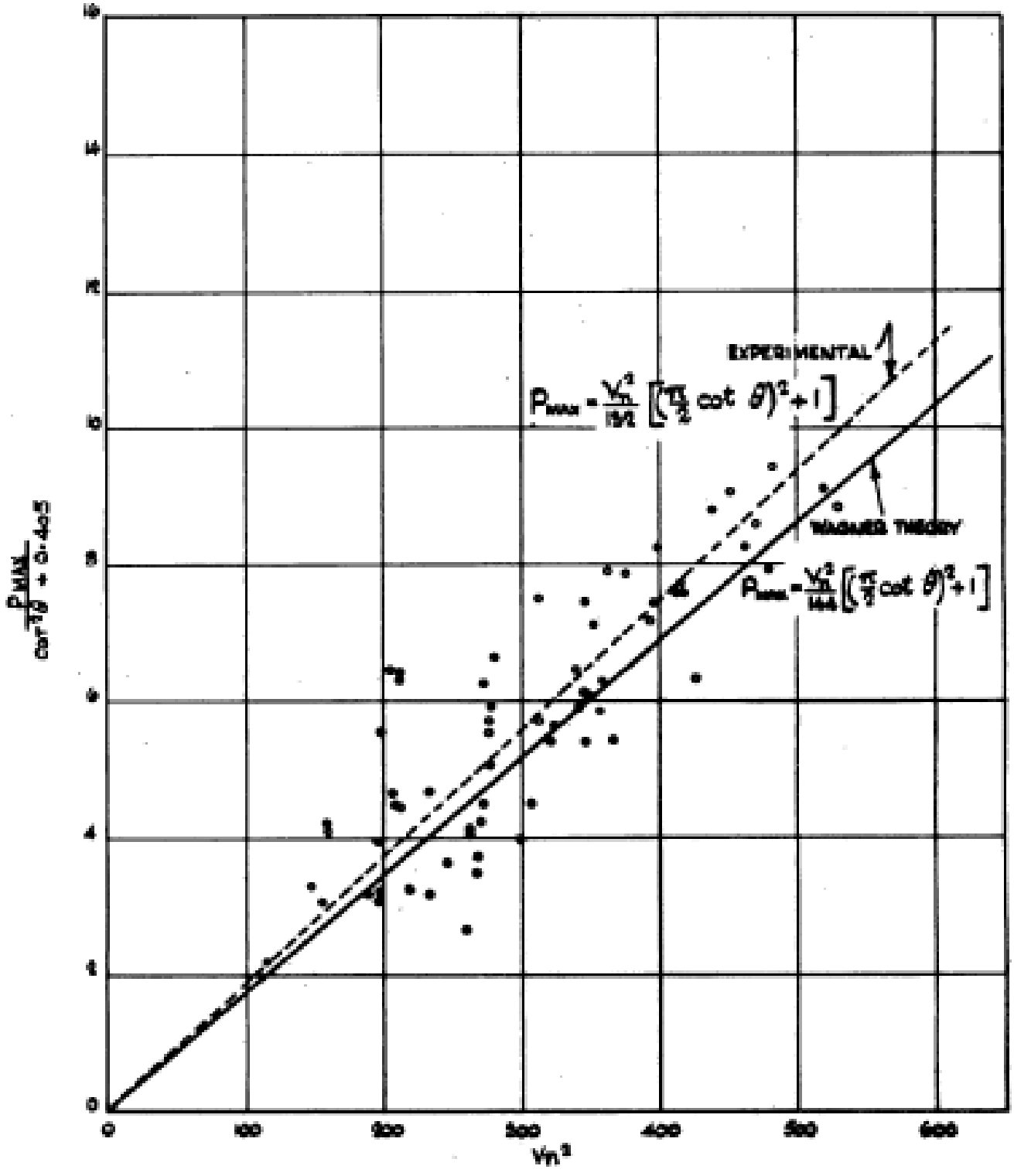

Figure 16. Measured maximum local pressures on rows A,B,C, and D compared to Wagner's theoretical results (Hamilton 1955).

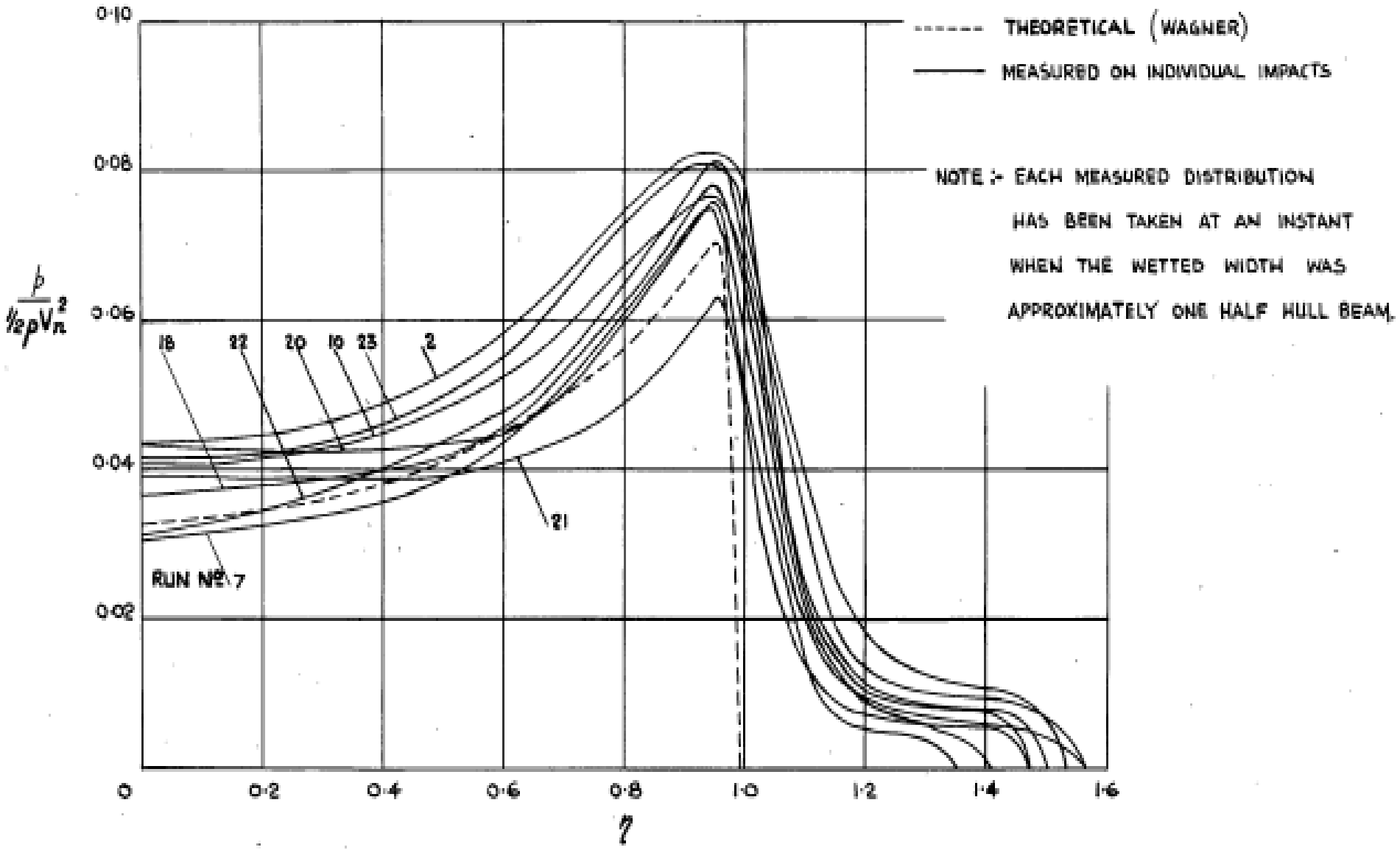

Figure 17. Measured vs. Wagner's theoretical transverse pressure distribution in row A via method 1 (Hamilton 1955).

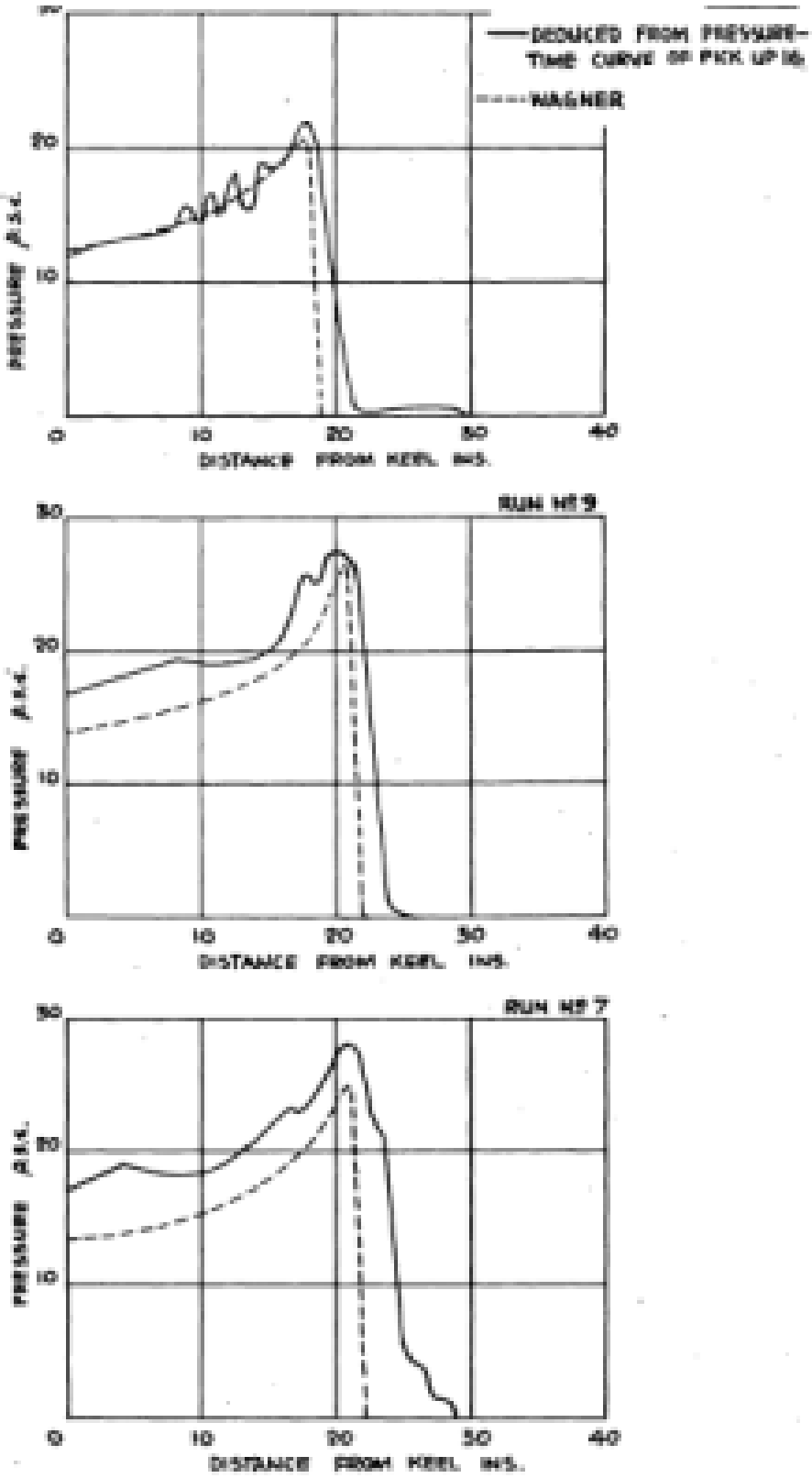

Figure 18. Measured vs. Wagner's theoretical transverse pressure distribution in row A via method 2 (Hamilton 1955).

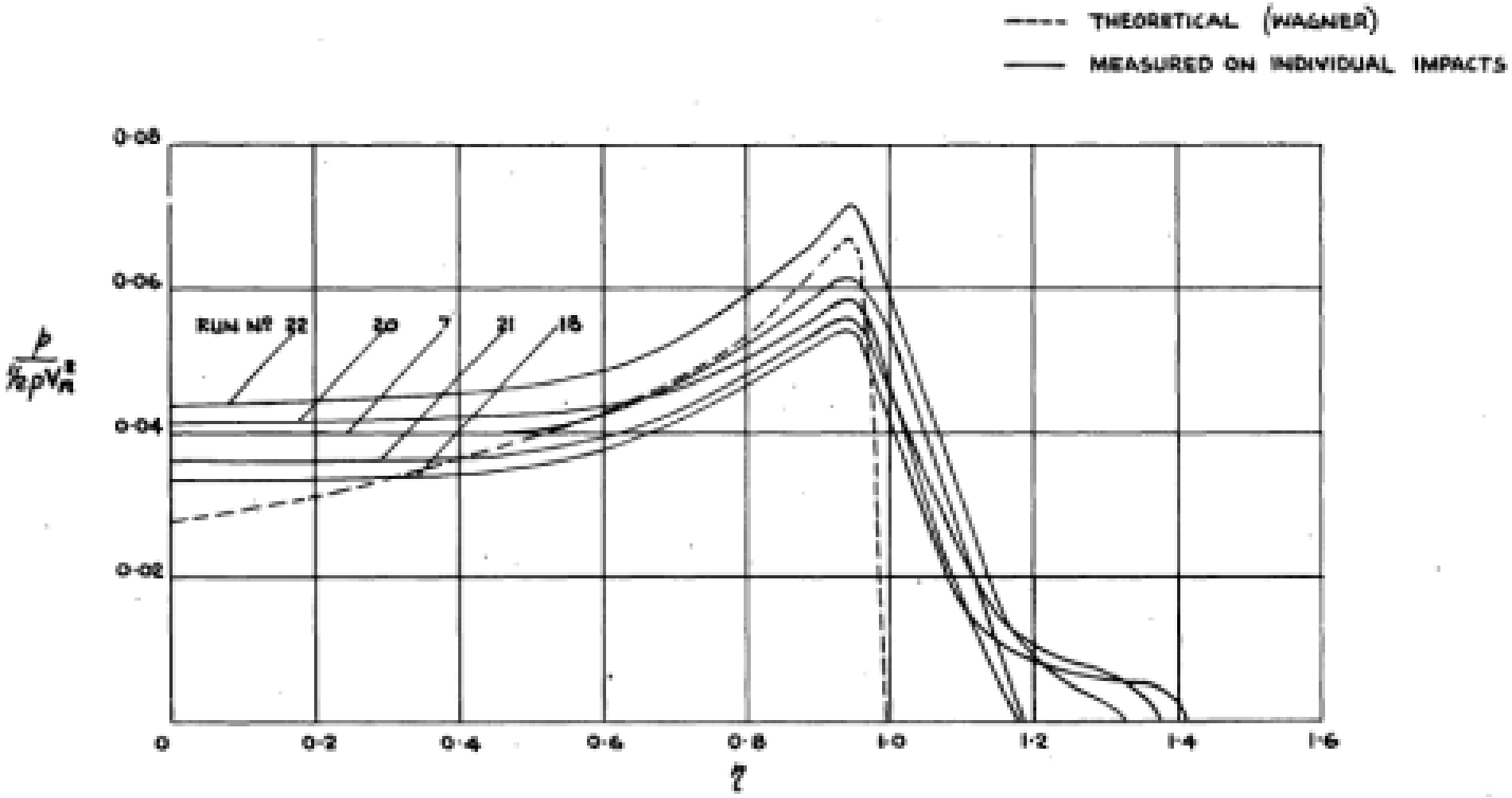

Figure 19. Measured vs. Wagner's theoretical transverse pressure distribution in row B via method 1 (Hamilton 1955).

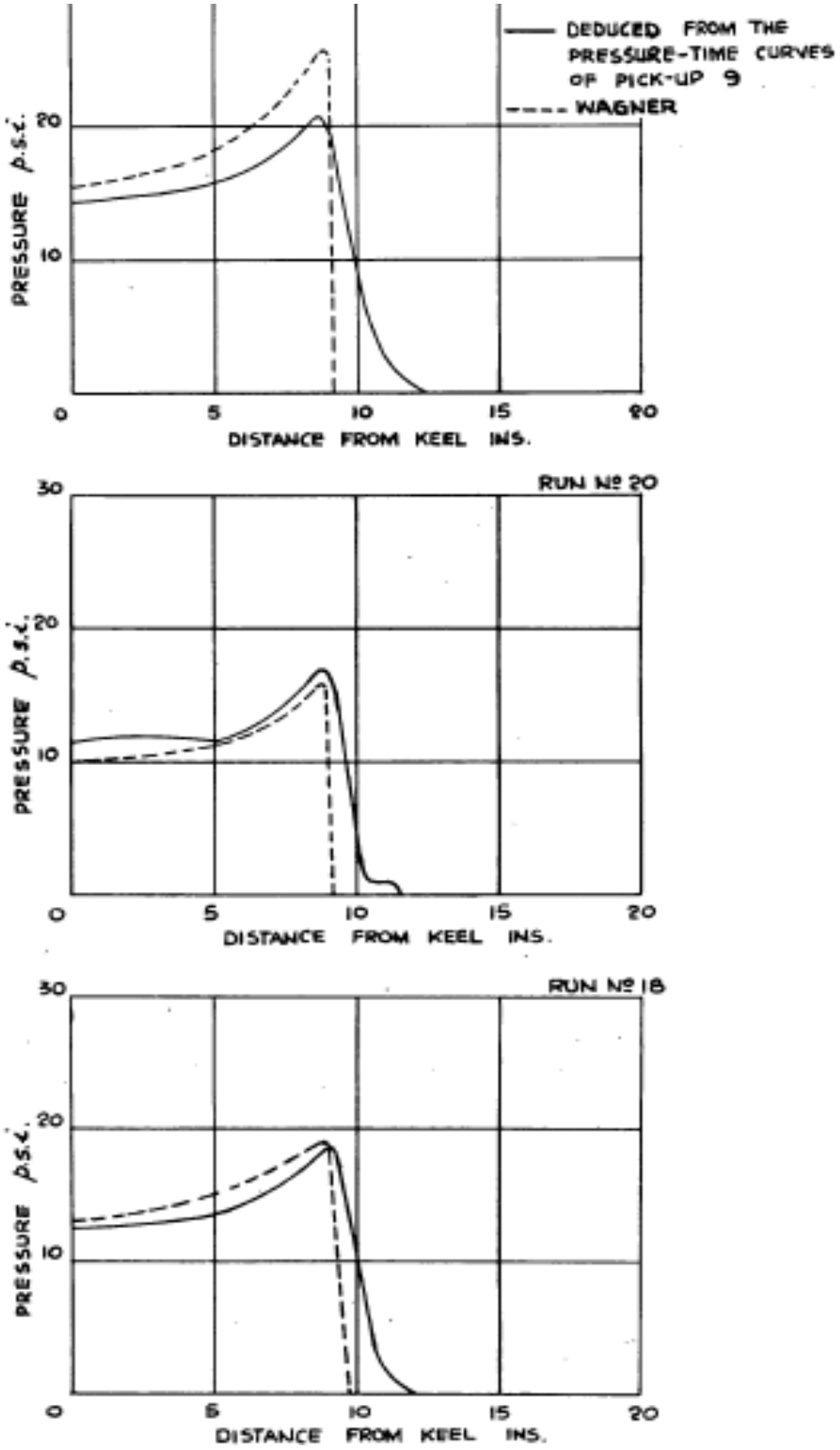

Figure 20. Measured vs. Wagner's theoretical transverse pressure distribution in row B via method 2 (Hamilton 1955).

H. AREAS OF FURTHER STUDY

After reviewing the theories outlined, it is concluded that additional research should be conducted in many aspects of the impact problem. Again it should be noted that there are many other theories that propose solutions to seaplane impact loading and further that the review of the theories described in this paper does not address every factor considered in the original papers. However several conclusions can be made on further areas of possible study, include the following:

1. Many theories do not provide a variation of pressure distribution with time along with the variation of penetration or draft with the corresponding pressure distributions. This is necessary in order to further analyze the pressure distribution in both longitudinal and transverse direction.

2. More research in determining the virtual mass corresponding to the actual shape of the seaplane hull should be conducted. As previously discussed, the momentum of the seaplane is imparted to the virtual mass of the water connected or associated with the impact area of the hull and also with the downwash as the water slides off the step or the rear of the plane. Therefore, the virtual mass is critical in determining the impact loading.

3. As far as the effect of the afterbody, in main step landings, a suction force may occur on the afterbody. From experimental results such as the Sunderland Mk.5 this force was not calculated. The suction force is also not included in the theoretical calculations seen in the papers reviewed. Further investigation in measuring experimental suction forces and incorporating them into theory is needed.

4. The theories studied only considered single step hull forms. A theoretical and experimental study could be done on multiple step seaplane hulls.

5. To account for non-calm water conditions, relative vertical motions and velocities between the hullform and the water where the hullform will hit is needed. It would be beneficial to account for the interactions between the impact loads and hullform motions.

6. For impacting bodies like seaplanes it is not only important to consider the local curvature but also the time history of the angle and curvature, so a more in depth analysis on this subject should be done.

I. IMPACT THEORY TRADE-OFF STUDY

The pressure data for the entire plane was limited to only a few stations and buttock locations. A theoretical method to determine the pressure distribution that could accurately depict the pressure distribution for the M270 stations was needed in order to capture the complete picture of the loads acting on the hull during impact.

A simple trade-off study was conducted between the impact theories, where rating extends from three being the highest importance in each parameter to one being the lowest. Several impact theories were combined since they were related to one another. It is important to note, that the restricted timeline for the project to actually utilize the theory was a consideration.

The parameters used to rate the theories include the following: (1.) the theories practicality to apply to a preliminary study,(2.) the availability of required information from the Martin Model M270 Water Loads Investigation (1955) report needed for the theory, (3.) the theories validation with experimental tests, (4.) the theories ability to be applied to non-prismatic hullforms, (5.) and the theories ability to capture the entire impact process. The ranking from the trade-off study is shown in Table 3. After the trade-off study was completed, it was concluded to use Wagner's impact theory should be used for the theoretical study.

Table 3. Trade-off study between theories in literature search

	Trade-off Study Parameters					
	(1.)	(2.)	(3.)	(4.)	(5.)	Sum
Wagner (1932), Faltinsen (2005) and Hamilton (1955)	3	3	3	3	2	14
Von Karman and Wattendorf (1929)	3	1	2	3	1	10
Blundell and Jones (1938)	2	3	3	3	1	12
Benscoter (1947)	1	1	3	1	3	9
Mayo (1945)	2	1	3	2	2	10
Crewe (1946)	1	2	1	2	3	9

VI. HULLFORM DESCRIPTION

A. GENERAL HULLFORM PARAMETERS

The M270 general dimensions shown in Figure 21 from Martin (1955) include: full loading of 71,000 pounds, length of the waterline of 1186.8 inches, maximum beam of 90 inches, and the beam at the step of 80 inches. Station spacing is one inch and is defined by the following stations: station -65 is at the forward perpendicular, station 435.8 is the first section of the step, station 489 is the later end of the step, and station 1121.8 is at the aft perpendicular. The forebody extends between station -65 and 420, while the afterbody extends between station 420 and 1121.8 (Martin 1955).

B. UNIQUE ATTRIBUTES

The M270 experimental plane's hullform was unique and combined several design parameters not considered in other seaplane design. Each design feature was chosen in order to decrease the impact loads. These design features include: high length-beam ratio hull, rounded forebody keel, long afterbody, and faired V-step.

Unlike traditional flying boat designs with a straight transverse step, the M-270 was designed to have a V-shaped step with deadrise of 60 degrees. For a step landing at reasonable angles of trim, the V-step should result in a smaller impact load when compared to a more traditional step design. This is due to a more gradual entry of the step as it enters the water.

Along with the V-step, the long afterbody with high angles of deadrise produces milder impacts for landing with stern impact conditions and in general the high length-beam ratio of 15:1 leads to lower impact loads in rough water landings than would a smaller length-beam ratio hull. (Martin 1955).

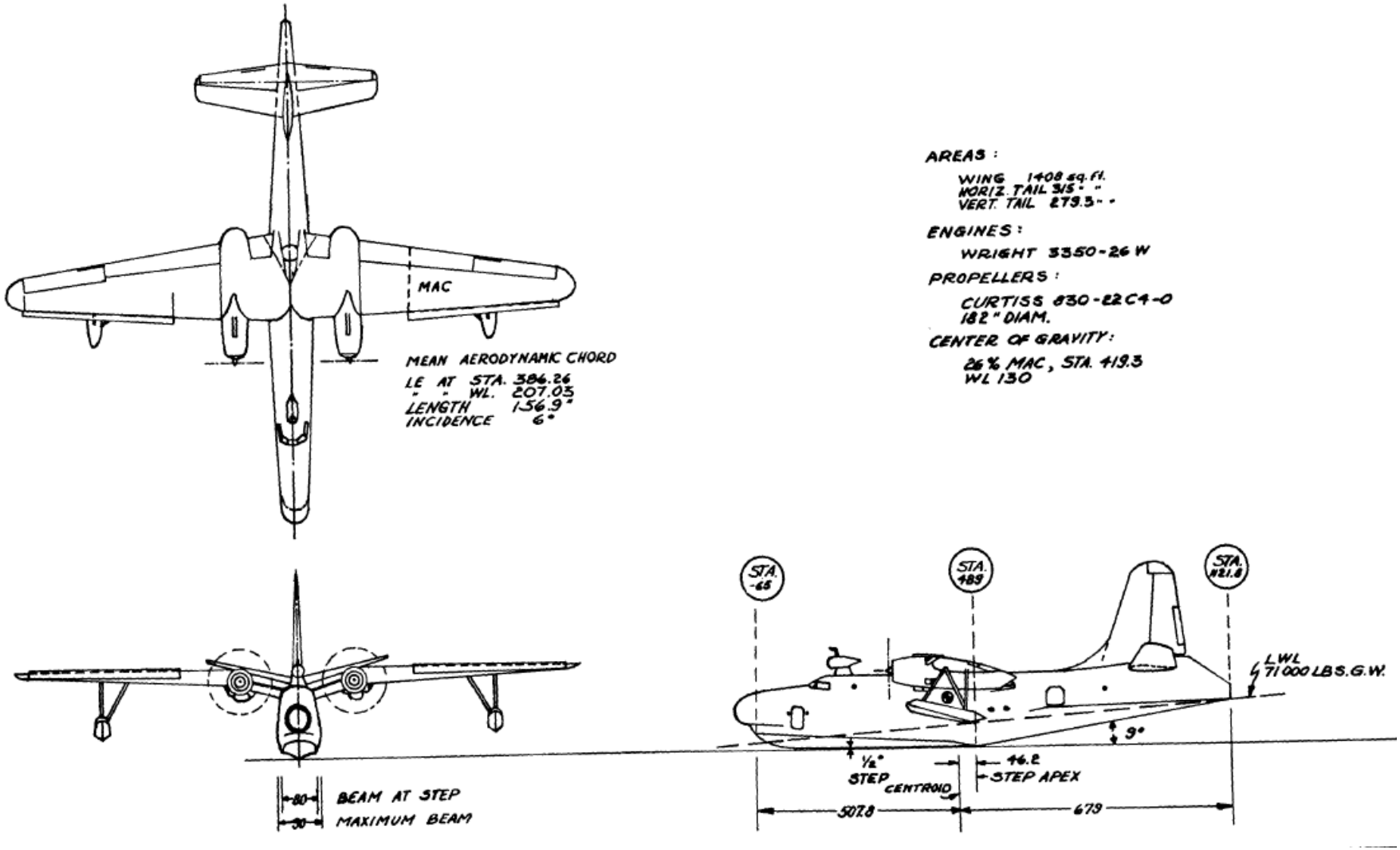

Figure 21. M270 general dimensions and characteristics (Martin 1955).

C. GEOMETRY

The Martin (1955) report included drawings of the forebody plan, however a scale was not provided. Therefore, in order to produce an accurate scaled drawing of the station geometry of the forebody a comparison study was preformed between the body plan of the forebody and a geometric parameters graph of the forebody, shown in Figure 22.

As stated, there was no scale for the buttock lines on the x-axis or the waterlines on the y-axis on the forebody plan. Therefore the maximum beam of the fuselage provided on the basic airplane parameters drawing, Figure 21, was used to scale the drawing to the maximum beam of 90 inches. Stations 431 to 469 taken from the forebody plan, is where the maximum beam is located. Therefore the forebody plan half-breadth was scaled to the 90 inch beam or 45 inch half-breadth.

The discrepancy arose when comparing the scaled offsets of the body plan drawing with the geometric parameters of the forebody. Both sources of geometry data show dimensions from centerline to the following locations: round bottom tangency, inner chine flare tangency, outer chine flare tangency and chine semi-width. Table 4 summarizes the percent difference in the offsets taken from the scaled body plan in comparison to the offsets taken from the geometric parameters graph for various stations ranging from station -45 to station 420.

Table 4. Percent difference between the two sources to determine geometric parameters of forebody relative to centerline

Station	Bottom Tangency	Inner Flare Tangency	Outer Flare Tangency	Chine Semi-Width
-45	N/A	13%	2%	17%
-25	N/A	19%	14%	17%
22	24%	17%	18%	17%
75	12%	17%	17%	17%
149	16%	17%	17%	17%
257	19%	18%	17%	17%
300	16%	18%	18%	17%
350	14%	18%	18%	18%
396	12%	18%	18%	18%
420	8%	19%	17%	17%
Greatest	24%	19%	18%	18%
Lowest	8%	13%	14%	17%
Average	15%	17%	15%	17%

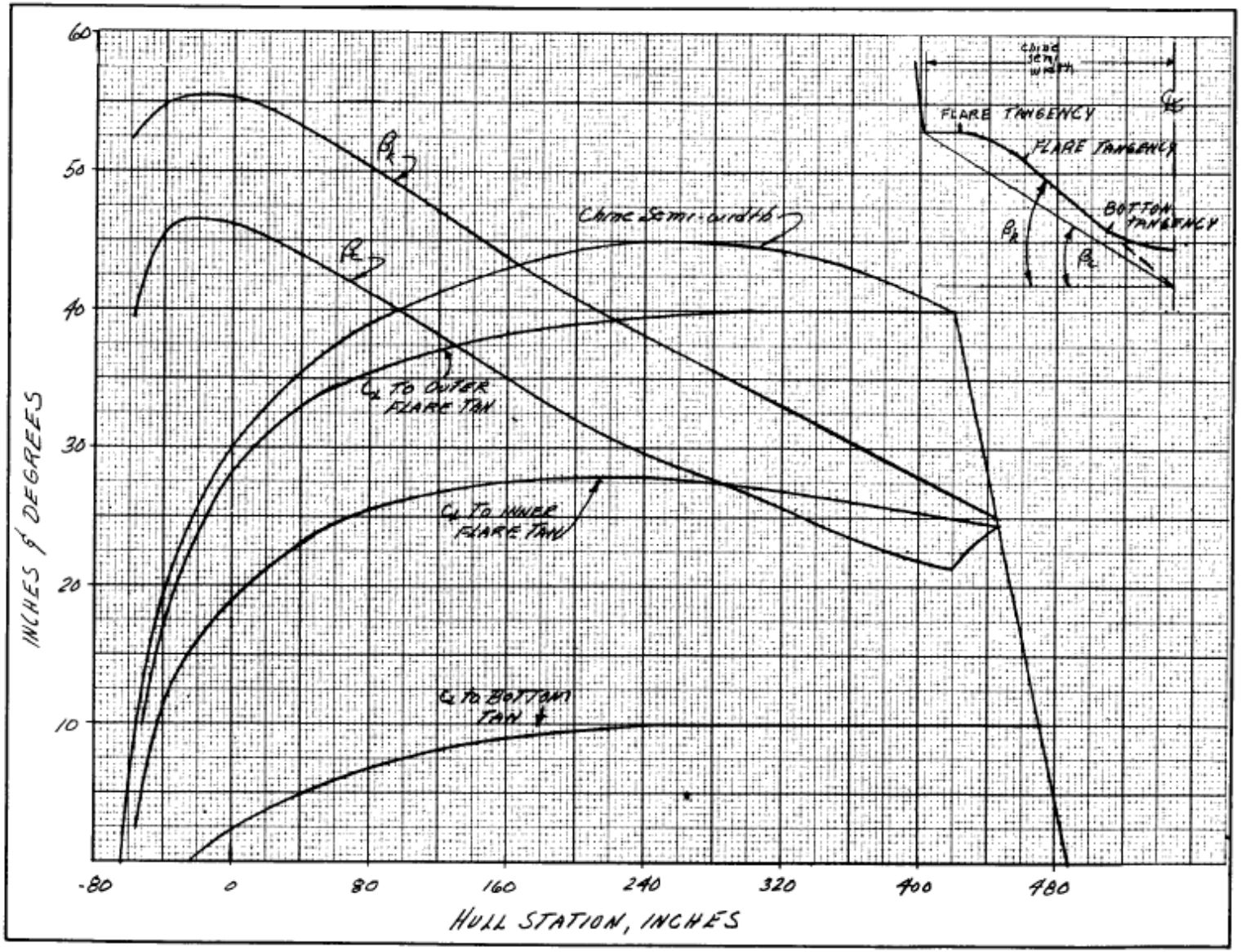

Figure 22. Geometric parameters of forebody (Martin 1955).

There is an average percent difference of 15% for the bottom tangency distance, 17% for the inner flare tangency, 15% for the outer flare tangency, and 17% for the chine semi-width, all of which are referenced from centerline. Since the chine semi-width had the least range of offset percent difference at each station, the body plan drawing was scaled to the chine semi-width offsets taken from the geometric parameters of the forebody table.

To validate the results of the geometry, the structural drawing for frame 328, provided by the Martin (1955) report was scaled to fit the station offsets. A direct correlation between the structural drawings centerline height of 72 inches and the scaled body plan was found. Thus, the comparison confirmed the newly scaled forebody geometry.

With the new scale imposed on the body plan drawing, the waterline and buttock spacing were determined to be one inch. The geometry was modeled in Rhinoceros 4.0 and the revised body plan of the forebody showing the floor frame stations 391 to 139 is shown in Figure 23.

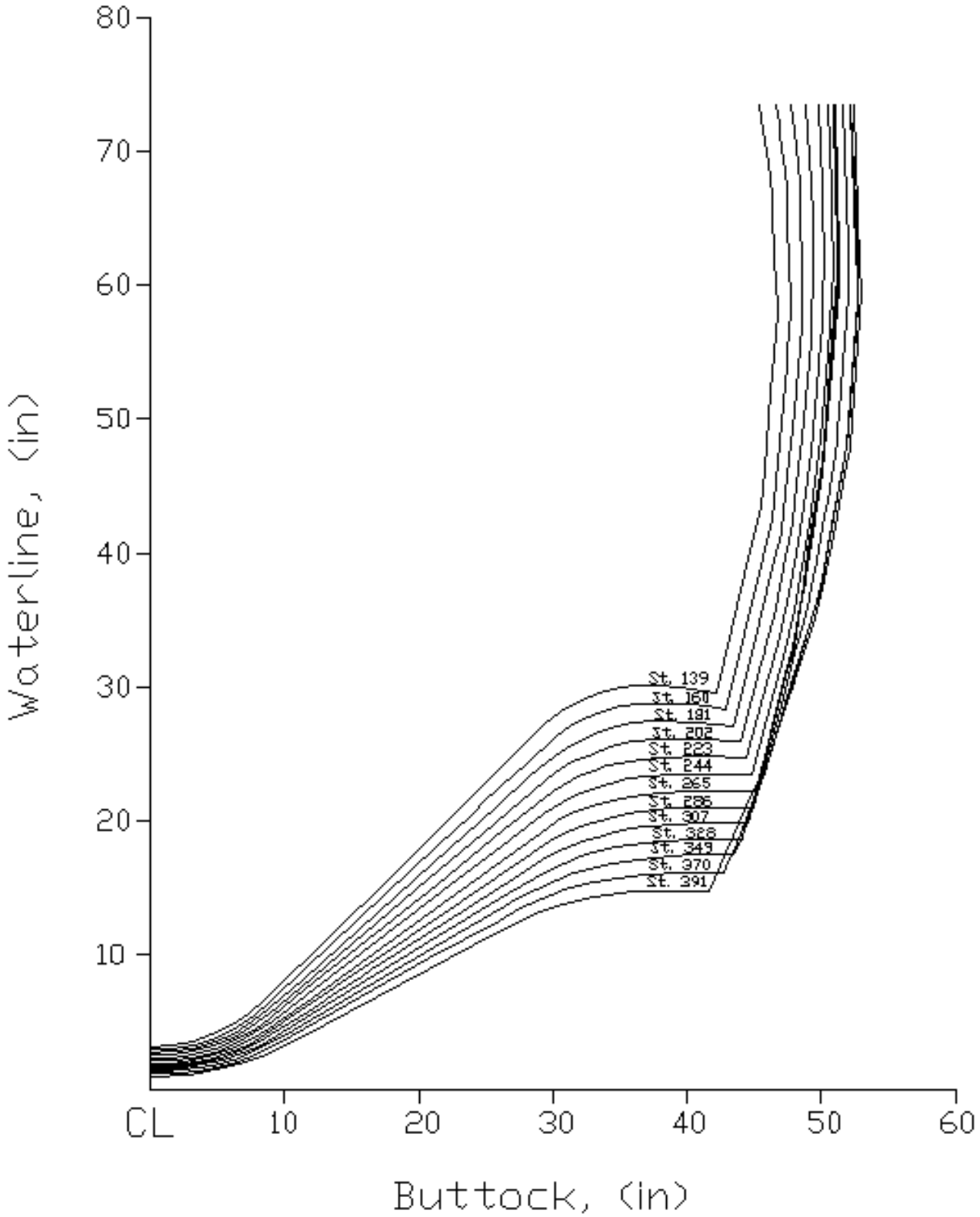

Figure 23. Forebody plan of station 391 to 139.

VII. MODEL TESTS

A. DROP TEST

1. MODEL DESCRIPTION

The drop test specimen section tested in the Martin (1955) report was chosen since it was near the maximum pressure load on the hull. The cross section which the specimen dimensions were based on was for station 328-5/8. Overall the specimen is a constant deadrise section with a depth of 72 inches and longitudinal length of 71 inches as seen in Figure 24, illustrating the test specimen under construction.

Overall the specimen represents roughly one-sixth of the length of the M270's forebody and the gross weight of the specimen was designed to be one-third of that of the M270 equaling 20,000 pounds. However, the actual maximum weight of the structure was only 19,800 pounds. This structure was ballasted to reach this weight, thus other loading conditions include: 19,800, 15,500, 11,590, and 10,584 pounds.

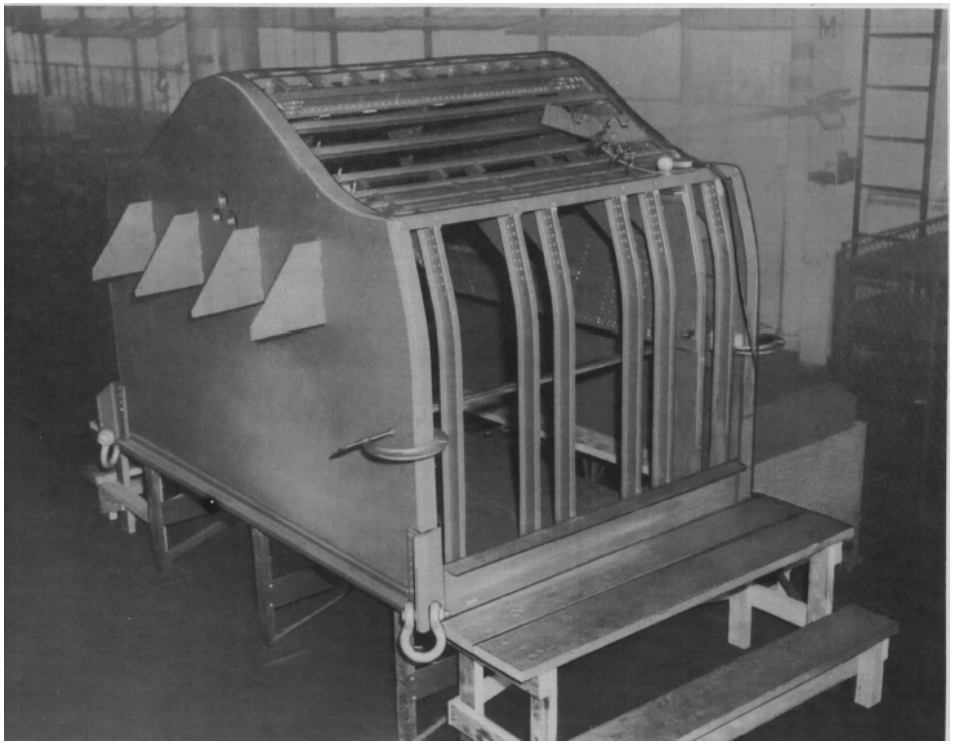

Figure 24. Drop test specimen under construction (Martin 1955).

2. STRUCTURAL DESIGN

The M270 drop test specimen section represents a floor frame design that was typical to Glenn L. Martin Company structural designs (Martin 1955). The frames for the test specimen include 3 floor frames spaced 21 inches apart and a total of six intermediate floor frames, two frames in between each floor frame, and spaced seven inches from the floor frames.

The specimen is a riveted structure and was constructed of 75ST Alclad aluminum alloy with material properties given in Table 5 (Niu 1988). Keel plating in the structure was designed to be removed in order to test different plate thicknesses during impact tests. Standard keel plate thickness for the M270 is however, 0.156 inches thick.

Table 5. Material properties used in the M270 design.

Material Properties					
	Young's Modulus, E	Density, ρ	Poisson Ratio	Yield Stress	Ultimate Tensile Strength
	(psi)	(lb/in^3)	(-)	(ksi)	(ksi)
75 ST-AL	1.03E+07	0.101	0.33	70	78
75 ST-AL Extrusion	1.04E+07	0.101	0.33	70	78

Structural details for the floor frame at station 328 are shown in Figure 25. The web plate is stiffened by channels running perpendicular to the bottom plating. At the chine and keel locations where high water pressure occurs during impact, doubler plates were added. At low areas of water pressure between the doubler plates, the bottom plating is only supported by longitudinal stringers.

The intermediate frames are attached to the side shell and the chine knees by the angle clips to longitudinal stringers S6A, S6, and S5A. Additional support at each intermediate frame is provided with shallow former plates attached to the five stringers on and closest to centerline.

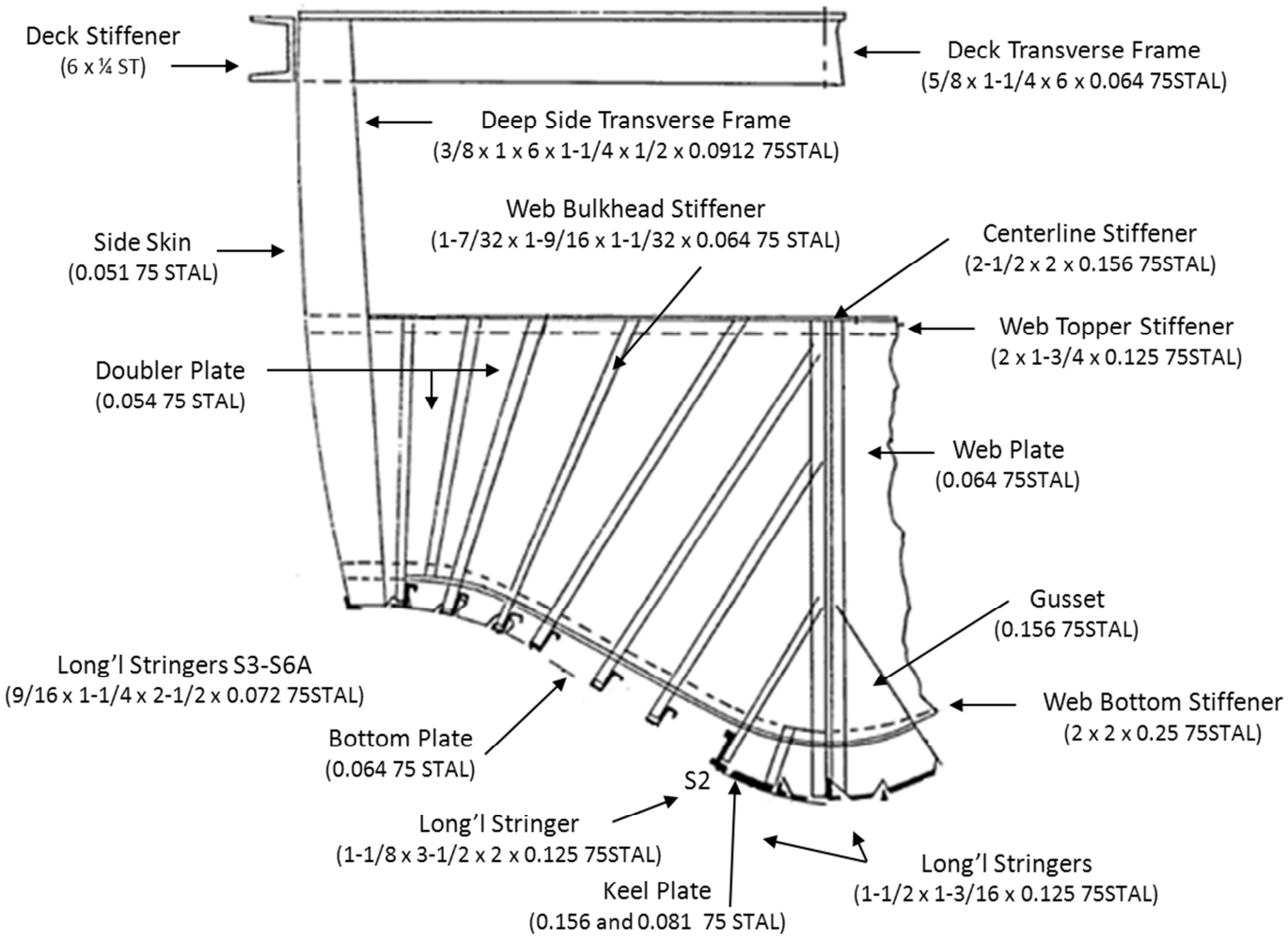

Figure 25. Structural drawing of floor frame 328 (Martin 1955).

The specimen only represents the hull of the seaplane and not the entire fuselage, therefore longitudinal steel channels were fastened to the upper corners of specimen. These channels simulate the skin and frames that would exist on the fuselage above the test specimen's 72 in waterline. In addition, for model testing purposes end plates were attached the specimen ends, which projected roughly one foot below the bottom of the specimen. Table 6 summarizes the frames, stiffeners, and plate properties used in the construction of the test specimen that is typical of Glenn L. Martin Structural design and construction.

Table 6. Structural members used in the M270 design

Scantlings Table					
	Structural Member	Shape	Size (in)	Grade	Extruded
Plate	Side Plate	Plate	0.051	75 ST-AL	Normal
	Keel Plate	Plate	0.156, 0.081 versions	75 ST-AL	Normal
	Bottom Plate	Plate	0.064	75 ST-AL	Normal
	Web Plate	Plate	0.064	75 ST-AL	Normal
	Doubler Plate	Plate	0.054	75 ST-AL	Normal
	Gusset	Plate	0.156	75 ST-AL	Normal
Stiffener Profiles	Deck Stiffener	Channel	6 x 0.25	24 ST	Normal
	Centerline Stiffener	T	2-1/2 x 2 x 0.156	75 ST-AL	Extruded
	Web Topper Stiffener	T	2 x 1-3/4 x 0.125	75 ST-AL	Extrusion
	Web Bulkhead Stiffener	Channel	1-7/32 x 1-9/16 x 1-1/32 x 0.064	75 ST-AL	Normal
	Longitudinal Stringer S0 and S1	L	1-1/2 x 1-3/16 x 0.125	75 ST-AL	Normal
	Longitudinal Stringer S2	Z	1-1/8 x 3-1/2 x 2 x 0.125	75 ST-AL	Extruded
	Longitudinal Stringer S6A - S3	Capped Z	9/16 x 1-1/4 x 2-1/2 x 0.072	75 ST-AL	Normal
	Web Bottom stiffener	L	2 x 2 x 0.25	75 ST-AL	Extruded
Frames	Deck Transverse Frame	Capped Z	5/8 x 1-1/4 x 6 x 0.064	24 ST-AL	Normal
	Deep Side Transverse Frame	Capped Z	3/8 x 1 x 6 x 1-1/4 x 1/2 x 0.0912	75 ST-AL	Normal
	Intermediate Transverse Side Frame	Z	1 x 2 -1/2 x 1 x 0.072	75 ST-AL	Normal

3. TEST OUTLINE

The drop test preformed on the model was tested in the Martin (1955) report at 4 different weighted ballast conditions including 19,800, 15,500, 11,590, and 10,584 pounds. The weights lower than 19,800 pounds correspond to the lighter gross loads of the M270. However, only the 11,590 pound condition is studied in this report, since this was the only ballast condition that the structural reactions of the members were measured in the Martin (1995) report.

Various keel plating thicknesses were changed out of the model in order to determine when and under what loading conditions the plating would fail. Keel thicknesses of 0.156 inches corresponds to the full scale keel thickness of the M270 and thickness of 0.081 inches are studied in this report which corresponds to the drop test outlined in the structural analysis section.

The drop test was performed at a constant trim angle of zero degrees and at the following contact speeds: 20, 25, 30, and 40 ft/s. The drop test was performed twice for each given speed.

4. INSTRUMENTATION

To measure the local pressure, load locations, and the stresses in specimen test during impact in in the Martin (1955) report, various instrumentation was attached to the hull for two different test phases as follows: pressure tests and stress tests.

For the pressure tests, pressure transducers were attached longitudinally at stations and transversely at different buttock locations during a series of impact loading conditions and speeds. However, for the stress tests, only 10 pressure transducers were attached to the hull, six down the centerline keel and four on the corners of the specimen. Additionally, a total of 12 stress strain gages were attached to the test specimen, including one shear stress strain gage and 11 axial stress strain gages. The locations of the stress strain gages are shown in Table 7.

Table 7. Stress strain gage locations on the drop test specimen.

Stress Strain Gages			
	Section	Location on Section	Longitudinal Location
Shear	floor frame web	Top Flange	St. 328
Axial	Stringer S0	Top Flange	St. 328
	Stringer S0	Top Flange	10. 5 inch offset from St. 328
	Stringer S1	Top Flange	St. 328
	Stringer S1	Top Flange	10. 5 inch offset from St. 328
	Stringer S2	Top Flange	St. 328
	Stringer S2	Top Flange	10. 5 inch offset from St. 328
	Stringer S5	Top Flange	St. 328
	Stringer S5	Bottom Flange	10. 5 inch offset from St. 328
	Top of Floor Frame Web	-	7 inch offset from St. 328
	Top of Keel Former	-	10. 5 inch offset from St. 328
	Keel Plating	Between S0-S1	10. 5 inch offset from St. 329

5. LOADING RESULTS

The drop tests indicated the highest hull bottom pressures for the longitudinal distribution were normally midway between the ends of the specimen and decreased at the ends of the specimen section. For the transverse pressure distribution, test results show that the peak pressures recorded by the pressure transducers are near the keel and chines.

The 11,590 pound drop test specimen used in this study does not represent the fully loaded portion of the M270 at 71,000 pounds. However, the effect of gross weight of the specimen loading conditions for other drop tests studied in the Martin (1955) report was negligible in its effect on peak pressures. An impact

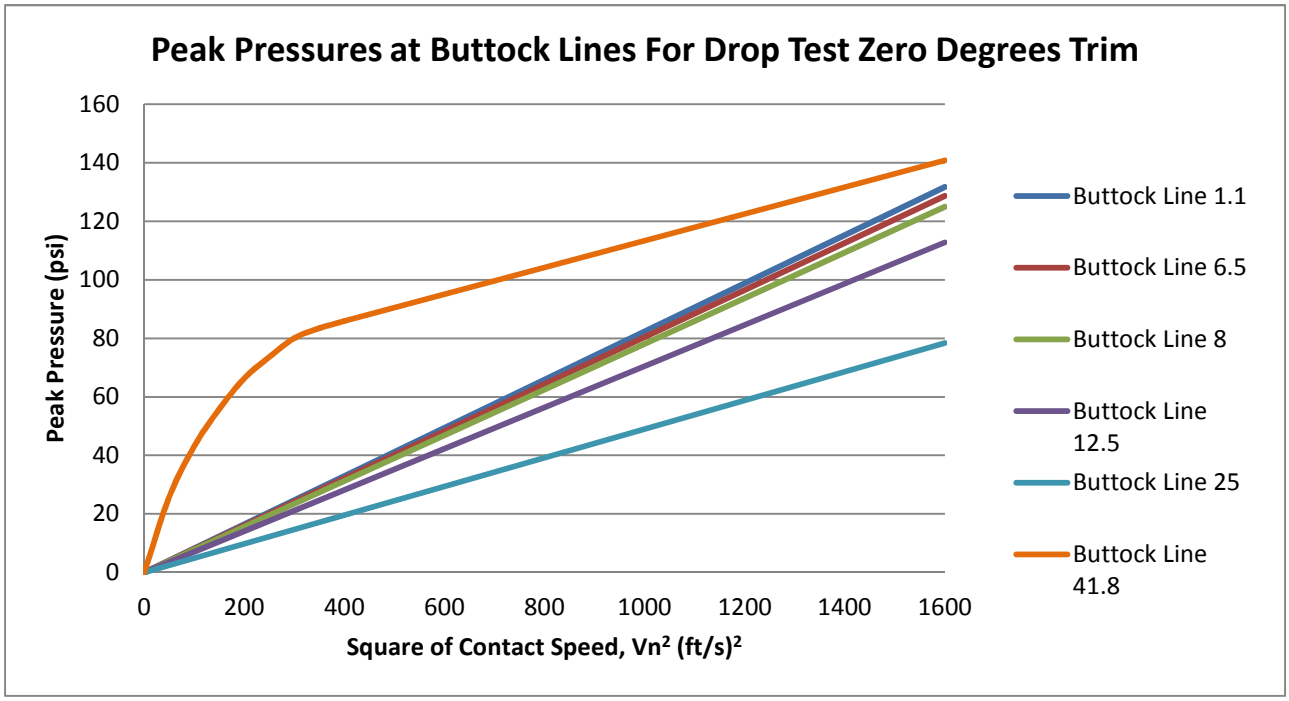

Figure 26. Drop test peak pressure trend as a function of the squared contact speed for zero degrees trim.

pressure line was fitted through drop test data of several pressure pick up points along buttock lines at various speeds and specimen loading conditions. Thus, the negligible differences in peak pressures for different weights are averaged out into a 'best-fit' line through the data. The 'best-fit' lines for each buttock line are shown in Figure 26.

It is concluded that the there is a linear relationship between peak pressure and the squared contact speed except near the region of chine flare. In the region of chine flare, the ratio of pressure to the squared contact speed is lower at high speeds and greater at lower speeds.

The effect of the end plates attached to the model was also studied. Although the end plates were tightened to the model to reduce pressure leakage, there was still an effect on the longitudinal pressure distribution due to the end plates. As shown in Figure 27, the effect of the end plates on the longitudinal pressure distribution smoothed out the pressure distribution whereas without the endplates the peak pressure measured longitudinally along the hull would have been greater than that recorded with the end plates and the distribution was more uneven. Only results with end plates installed were used in this study to compare with theoretical results (Martin 1955).

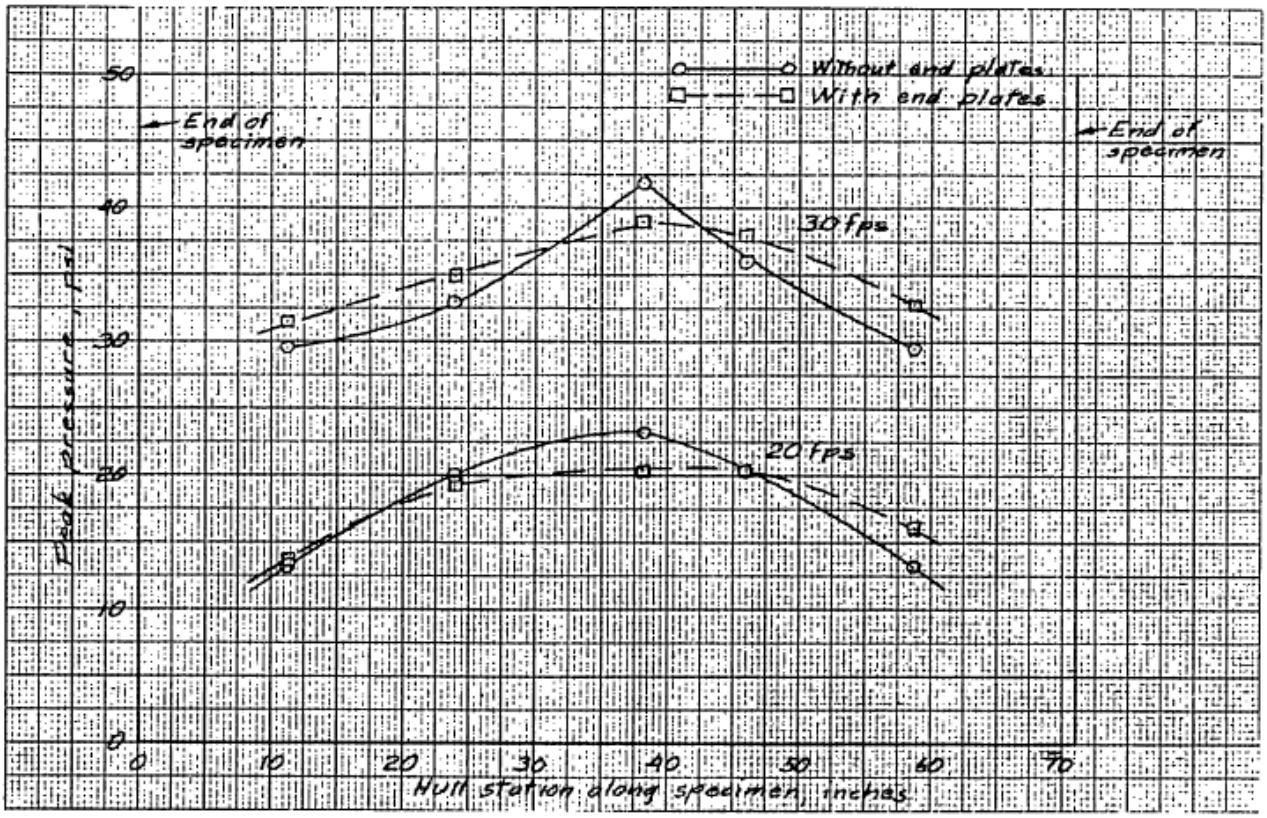

Figure 27. End Plate effects on longitudinal distribution of peak pressures for zero degree drops ballasted at 10,000 pounds (Martin 1955).

Peak pressures experienced on the hull bottom with end plates installed for the zero degree trim case with a keel plate thickness of 0.156 and 0.081 inches, and for impact velocities of 20, 25, 30, 35, and 40 ft/s are shown in Figure 28. The peak pressures are shown by their coefficient of pressure, C_p, where the pressures are normalized by their normal to keel impact velocity, which in this case is the same as the vertical impact velocity. The equation of the coefficient of pressure is given below which is composed of the pressure, *P*, normalized by the density, ρ, and the normal velocity, V_n.

$$C_p = \frac{P}{\frac{1}{2}\rho V_n^2}$$

The location and water density that the experimental tests were conducted in were not provided. However, from in the Martin (1955) report, which further describes the testing conditions in depth, it is presumed that the tests were

conducted in salt water. The equation for the coefficient of pressure given above is assumed to have a density of salt water of 1.99 slugs/ft^3.

For impact velocities of 20, 25, and 30 ft/s there is an increase in trend of coefficient of pressure from the keel to the chine. Impact of velocities of 35 and 40 ft/s show a roughly constant transverse distribution of coefficient of pressure. It is important to note, that these pressures represent the maximum pressure that the specimen encountered at each pick up point during a series of tests, and not a time series of pressures at one time recording. Time histories for pressures that the hull was subjected to for each drop case, during the course of submergence were not provided in the Martin (1955) report.

It is deduced from the drop test description in in the Martin (1955) report that chine immersion did occur during the drop test. However, as stated previously, the transverse pressure distribution that reflects the onset of chine immersion is unknown.

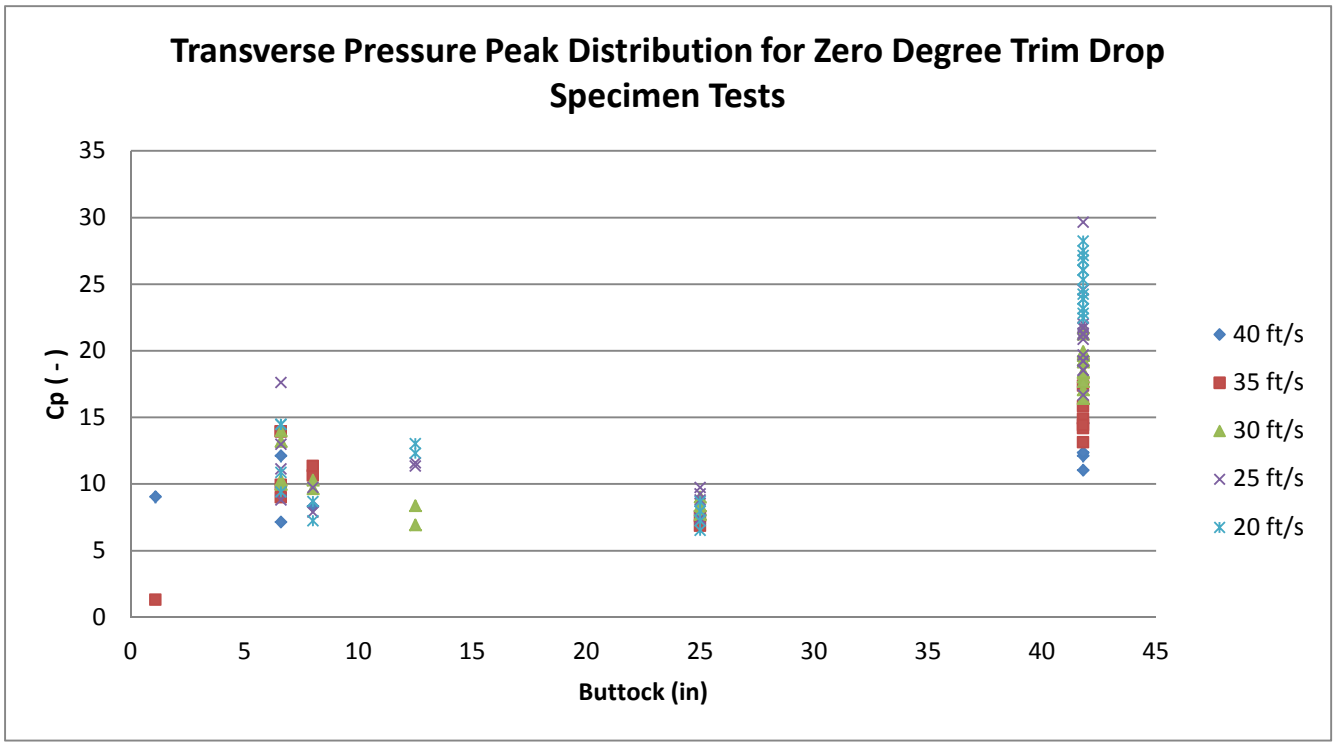

Figure 28. Transverse peak pressure distribution for drop test specimen at zero degrees trim at impact velocity of Vn = 20, 25, 30, 35 and 40 ft/s.

6. Structural Reaction

After a series of drop tests performed in the Martin (1955) report, using the M270 design keel plate thickness of 0.156 inches, there was no failure of the structural components. It was not till after the keel plating was replaced with 0.081 inch thick plate that structural failure occurred in the internal members and severe sets in the plating was formed.

After a series of 20, 25, 30, and 35 ft/s drops were conducted twice, the following structural failures occurred after the last 35 ft/s drop: slight buckling of the centerline stiffener where it attaches to longitudinal stringer 2, slight buckling of two chine knees, and a set of 0.10 inches in the keel plate.

After repairing the failed structure, the specimen was dropped at 40 ft/s and the following structural failure occurred: shear failure at the longitudinal stringer and web bulkhead stringer at longitudinal stringer numbers 4 and 5, buckling of longitudinal stringer 6A, buckling of chine knee gussets, and a considerable wrinkling of the test specimen's bottom.

B. Flight Test

1. Model Description

The Geometry used in the flight test is the full-scale seaplane geometry described in Chapter VI.C and should be referenced in that section.

2. Test Outline

Flight tests performed on the M270 (Figure 29) included a series of oblique impact tests with flight test parameters including glide flight path angle, trim, impact velocity, and ballast conditions. The varying wave heights and wind speeds were measured during the flight test, and these affected the pilot's landing capabilities and extremities of operation with the flight test parameters.

In total 4 flight tests were used in this study, each with a series of varying landing approaches shown in Table 8. There were a total of 5 flight tests conducted in in the Martin (1955) report; however in flight test 31, data for the flight path angle was not recorded.

Table 8. Flight test landing approach parameters

	Landing Number	Rate of Descent of Airplane (ft/s)	Resultant Velocity of Airplane (ft/s)	Normal Velocity (ft/s)	Trim (degrees)	Flight Path Angle (degrees)	Resultant Angle (radians)
Flight 27 (64,000 lb)	2	1.70	143.24	11.69	4.00	0.68	1.49
	3	3.00	138.63	13.86	4.50	1.24	1.47
	5	5.10	138.52	15.94	4.50	2.11	1.46
Flight 28 (64,000 lb)	1	4.50	161.17	14.33	3.50	1.60	1.48
Flight 29 (64,000 lb)	1	4.50	161.17	10.12	2.00	1.60	1.51
	2	4.50	185.51	10.97	2.00	1.39	1.51
	3	7.70	165.29	24.92	6.00	2.67	1.42
	4	13.30	156.99	25.53	4.50	4.86	1.41
	7	11.10	168.82	21.36	3.50	3.77	1.44
Flight 30 (71,000 lb)	2	1.90	170.10	21.14	6.50	0.64	1.45
	3	5.10	171.91	23.03	6.00	1.70	1.44
	4	3.60	185.84	19.78	5.00	1.11	1.46
	5	3.40	162.35	23.16	7.00	1.20	1.43
	6	2.90	161.33	25.32	8.00	1.03	1.41
	7	8.00	232.72	46.28	9.50	1.97	1.37

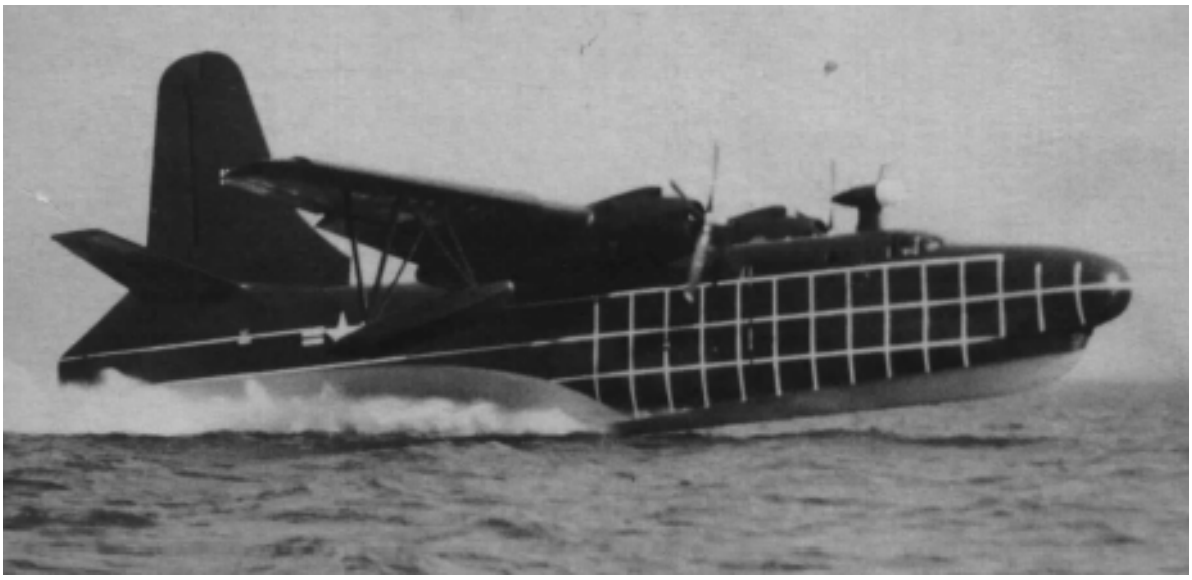

Figure 29. M270 flight test (Martin 1955).

Velocities and their angles in an oblique impact are shown in Figure 30, where V_v is the rate of descent or the sink rate, V_h is the horizontal velocity or forward velocity, V_r is the resultant velocity which is has a flight path angle, α, relative to the horizontal of an earth fixed axis, V_p is the velocity parallel to the keel, V_n is the velocity normal to the keel, τ is the trim angle of the plane, and β is the angle of resultant velocity relative to the normal velocity.

Only the rate of descent or the vertical velocity, trim angle, and flight path angle were given in in the Martin (1955) report, thus the equations to determine the other velocity components and their angles are defined below.

$$V_r = \frac{V_v}{\sin(\alpha)}$$

$$V_n = \sin(\alpha + \tau) \cdot \frac{V_v}{\sin(\alpha)}$$

$$\beta = 90° - \alpha - \tau$$

In typical landing approaches the pilot preforms a flare just before landing by increasing the angle of attack or flight path angle, which results in a reduced impact velocity. Prior to flare the aircraft has a constant attitude and sink rate. Consideration of flare and the results on the impact velocities are neglected in this study and it is assumed that constant attitude and sink rate were maintained during landing.

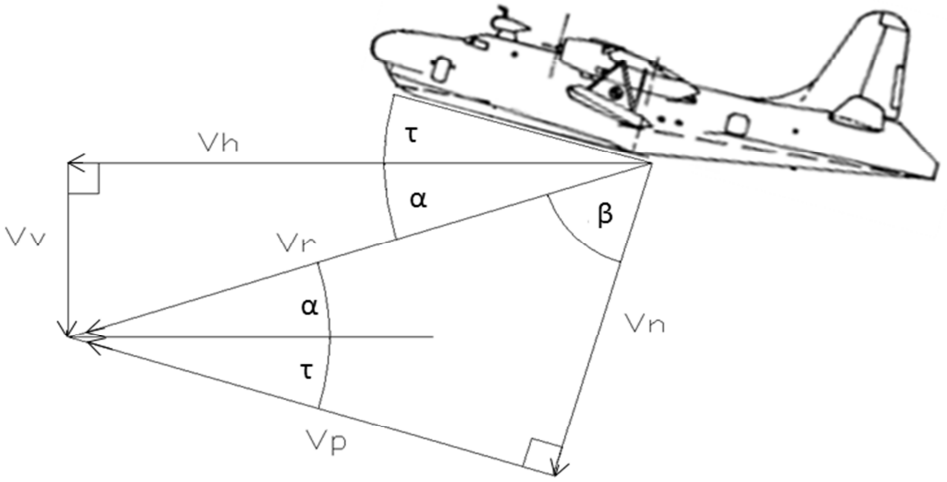

Figure 30. Impact velocity components and angles.

3. INSTRUMENTATION

To measure the external water loads applied to the hull during impact, various instrumentation were attached to the hull longitudinally at stations and transversely at different buttock locations on the M270 (Martin 1955). The local pressure, total load, load locations, and the stresses at several locations along the hullform were determined during the model testing. The instrumentation attached to the hull to determine these measurements include pressure transducers and strain gages. Table 9 summarizes the station and buttock locations of the instrumentation.

Table 9. Instrumentation locations of pressure transducers

Pressure Transducer		
Station	Buttock	Stb/Port
152 1/8	1.4	Stb
152 1/8	6	Stb
152 1/8	41.5	Stb
249	1.4	Stb
249	6.3	Stb
249	16	Stb
249	43.8	Stb
249	43.8	Port
309 3/4	1.4	Stb

Table 9 continued

391	6.6	Stb
309 3/4	16.6	Stb
331 1/2	1.4	Stb
331 1/2	6.6	Stb
331 1/2	17	Stb
331 1/2	37.5	Stb
331 1/2	37.5	Port
391	1.4	Stb
448	1.4	Stb
448	6.6	Stb
448	18.2	Stb

Strain gages were used in the flight tests; however their locations were outside of the region of fuselage location considered with this project. Many of the strain gage locations were located in the hull crown however this portion of the fuselage was not modeled in Maestro. The flight tests for oblique landings did use strain gages in floor frame 328 and in the bottom plating, however only vertical impact cases are applied to the Maestro loading conditions. Therefore test data from the strain gages used the specimen impact test are used for comparison.

4. STRUCTURAL DESIGN

The only structural drawing provided by in the Martin (1955) report, for the M270 was for floor frame 328 5/8. Due to limited resources on the structural design on the M270, it was assumed that the structural design is similar at the other mid-forebody sections of the hull. Thus, the floor frame and intermediate frame spacing was kept constant throughout the hull.

The assumptions of using the same design as that used in the test specimen, was supported by the P5M-2, the Martin Marlin, basic frame layout which the M270 design was based off of (Glenn L. Martin Company 1951). The floor frame, intermediate frame, and longitudinal stringer spacing layout description reflected that of the M270. The structural design of the P5M-2 included four watertight bulkheads in the forebody, however structural details were not provided for the P5M-2. Since only the structure below the hull crown was modeled, estimations on the watertight bulkhead structure were also neglected in the modeling. However, the steel channel was used to account for the actual stiffness of the entire fuselage structure.

Forebody stations 139 through 391 were only considered for analysis. From a preliminary design standpoint, in regards to only having one structural station drawing, the structure could only assume to remain constant through these sections of the forebody. Thus, the region of the step and the after body are not considered.

The stiffener sizes from frame 328 were used for the other transverse floor frames, web structure, and intermediate transverse frames. The stiffener spacing was scaled for each floor frame based on the spacing measured from station 328. The spacing was scaled based on the circumference of the bottom geometry.

Scaling was also used to determine the end connectivity of the bulkhead stiffeners from where they butted with the longitudinal stringers to where they connected with the top of the web. For this case, the spacing was scaled by the half beam of the hull at the top of the web bulkhead. The spacing for web bulkhead stiffeners which connected to the centerline stiffener was kept the same as the spacing used in frame 328, since the difference in bulkhead height differences was negligible. Likewise, the web bottom angle stiffener toe connectivity location was scaled based on the total length of each web stiffener, by using the connectivity locations determined from frame 328.

5. LOADING RESULTS

It was beneficial to study how the flight path pressures for oblique impact conditions vary since tests do not have a constant normal velocity. The most appropriate method to show flight path data relationships are by comparing the coefficient of pressure to the resultant angle as seen in Figure 31. The data shows a trend among all buttock lines except for buttock 37.5, that there is an increase in pressure as the resultant angle increases. More test data is required for buttock 37.5 and also buttock 1.4 to make a more accurate trend in the data. Individual plots of the transverse distribution of the coefficient pressure for available flight test data at various stations, is shown in Chapter VII section 3.

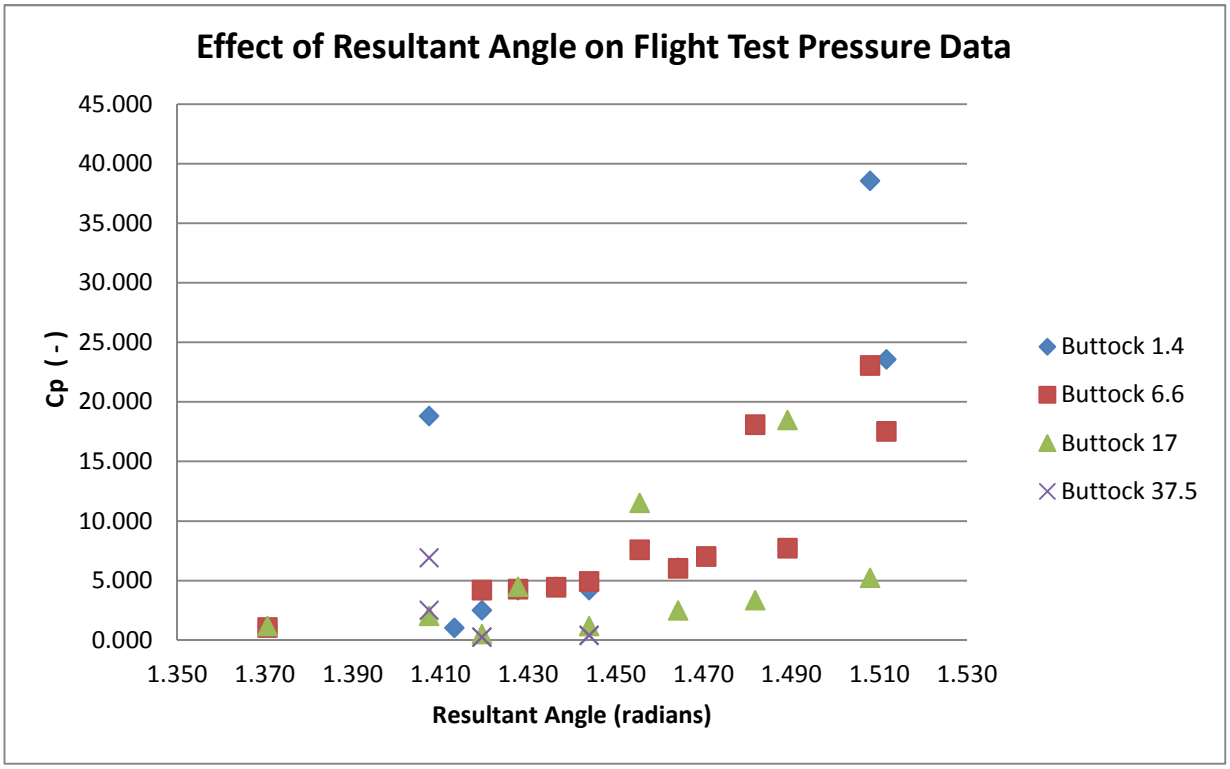

Figure 31. Effect of the resultant angle on the flight test peak pressure data at each pressure transducer buttock location.

6. STRUCTURAL REACTIONS

Stresses from flight test data was not provided in the Martin (1955) report. However the report did conclude that locally, the pressures and their effects on the structure over the wetted area should be the same for both the airplane and drop test specimen since the structure is the same. The longitudinal bending moments caused by the impact during landing can assumed to be simulated by the drop test specimen. The mass was primarily located at the ends of the specimen due to the ballast location, and this most likely caused a similar bending moment as that experienced by the seaplane. Thus a fore-and-aft tensile or compressive stress in the bottom plating and stringers exist in both cases.

VIII. MAESTRO MODELING

A. APPLIED LOADING

1. DESIGN LOADING OF M270

The uniqueness of the M270 hull required upon designing the seaplane, the determination of the applicability of then current specifications for water loads. In general, impact loads were found by determining the momentum of the hull imparted to the water. The reaction of the water on the hull is equal to the rate of change of momentum of the water in contact with the hull, along with the rate at which momentum is imparted to downwash. To account for the uniqueness of the hull design several assumptions were made in the impact theory including:

- Water loads were calculated without using reductions for a high length-to-beam ratio hull, even though specifications suggest significant reductions impact loads for increases in length-to-beam ratio.

- Specification use straight V-bottom hulls, however since the M270 has chine flare it was assumed that the rounding of the keel was small. Thus the loads were calculated with a sharp keel extending off the straight portion of the hull bottom to centerline.

- Design water pressures were seemingly calculated using empirical equations from conventional straight-V bottom hulls of deadrise of 20 to 25 degrees. The hull bottom regions outboard of the rounded keel were calculated using these equations, however for the rounded keel pressures were estimated from theoretical peak pressures of low deadrise planing surfaces at M270 take off speed.

The water load pressures used to design the M270 greatly underestimates the peak pressure experienced at the chine by the test specimen at floor frame 328 as seen in Figure 32. However, the rounded keel design pressures are slightly higher than that recorded during the impact test.

The pressure loads that the structure was designed too proved adequate for the chine structure and the plating for the normal M270 keel plate thickness of 0.156 inches, however permanent sets in the stringers and skin between stringers resulted from the impact loading (Martin 1955).

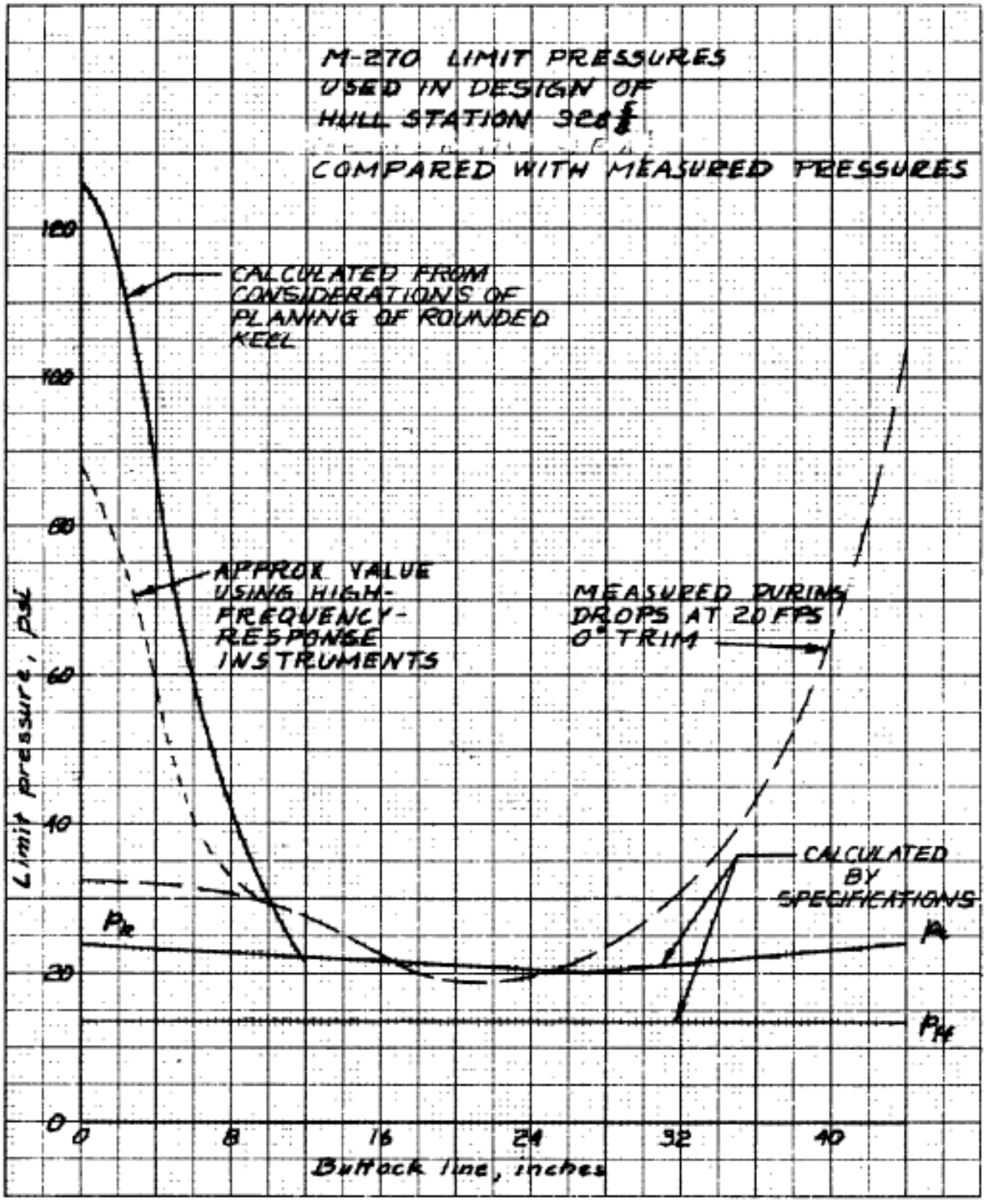

Figure 32. Pressures used in the design of the drop test specimen compared with the measured peak pressures (Martin 1955).

2. CODE OF FEDERAL REGULATIONS LOADING

Seaplane water loads restricted by the Code of Federal Regulations (14 CFR Ch. I 2010) were determined in order to apply them to the FEA model and to compare with the loading results experienced by the seaplane during impact testing. The CFR regulations outline the pressures to design the structural components of the seaplane including: frames, bulkheads, stringers, and bottom plating. Using the CFR seaplane water loads regulations provides a good method to determine if the loading the structure outlined in the Martin (1955) report was designed to, meets current design standards.

In summary, the CFR states that seaplane subjected to loads corresponding to their calculated load factors can be applied and distributed over the hull by using pressures not less than those calculated by the local pressure equations. The design of stringers and their attachments to their supporting structure along with the bottom plating must be designed with the applied pressure distribution at the keel and chine. Between the keel and chine the pressure distribution varies linearly. The applied pressure distributions to the chine, P_{ch}, and keel, P_K, are given respectively in the following equation in psi.

$$P_{ch} = \frac{C_3 K_2 V_{S1}^2}{tan\beta}$$

$$P_k = \frac{C_2 K_2 V_{S1}^2}{tan\beta_k}$$

The variables used in the equations include the following: K_2 is the hull station weighting factor, V_{S1} is the seaplane stalling speed in knots at the design water takeoff weight with flaps extended in the appropriate takeoff position, β is the angle of deadrise at the chine for each station, β_k is the deadrise angle at the flare tangency, and C_2 and C_3 are constants.

The seaplane stalling speed assumed to correspond to the CFR requirements is at 135 ft/s or roughly 80 knots. The deadrise angles were measured in the same manner as that done by in the Martin (1955) report, in the design pressures for the M270 assuming a sharp keel extending off the straight portion of the hull bottom to centerline.

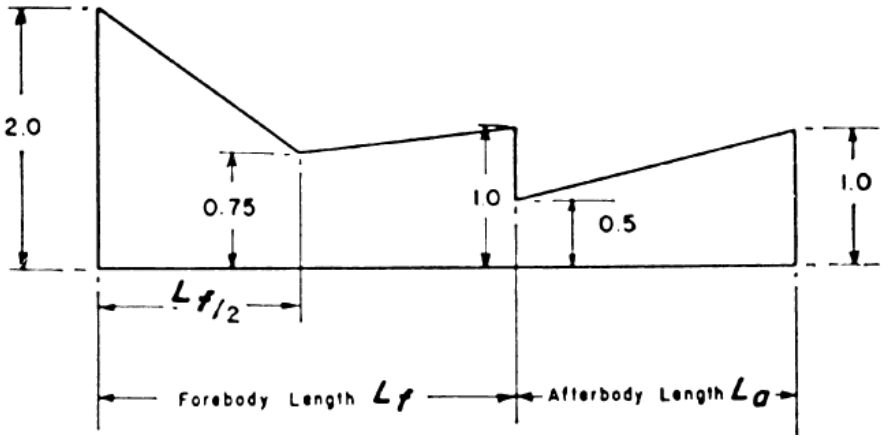

Figure 33. Hull station weighting factor, K_1 for calculating bottom pressures (14 CFR Ch. I 2010)

The hull station weighting factors were determined using CFR guidelines using the M270 forebody length of 485 inches extending from station -65 and 420. The hull station weighting factors for the forebody was calculated at each station using Figure 33 and are summarized in Table 10 for each station. Table 10 also shows the results of the CFR loading requirements and equations for hull stations 139 to 391. The maximum pressure experienced by the hull was at station 391 which is defined by the smallest deadrise angle.

Table 10. Hull station weighting factors and pressure distribution for each floor frame.

		Pressure at Longitudinal Stringers (psi)									
Floor Frame	K_2	S0	S1	S2	S3	S4	S5	S5A	S6	S6A	Chine
391	0.97	24.779	24.784	24.791	24.797	24.803	24.810	24.814	24.819	24.824	24.830
370	0.95	22.871	22.902	22.942	22.980	23.015	23.055	23.078	23.109	23.138	23.175
349	0.93	21.123	21.168	21.226	21.280	21.331	21.389	21.422	21.467	21.510	21.563
328	0.91	19.602	19.644	19.697	19.747	19.794	19.847	19.877	19.919	19.959	20.006
307	0.88	18.166	18.202	18.248	18.292	18.333	18.379	18.405	18.442	18.477	18.519
286	0.86	16.856	16.890	16.933	16.973	17.010	17.053	17.077	17.112	17.145	17.183
265	0.84	15.628	15.674	15.731	15.784	15.833	15.889	15.921	15.967	16.011	16.065
244	0.82	14.465	14.528	14.605	14.677	14.744	14.820	14.864	14.926	14.987	15.062
223	0.80	13.413	13.471	13.541	13.606	13.667	13.736	13.776	13.832	13.888	13.955
202	0.78	12.430	12.476	12.532	12.582	12.630	12.684	12.715	12.759	12.803	12.858
181	0.75	11.432	11.475	11.526	11.572	11.616	11.665	11.692	11.732	11.773	11.824
160	0.84	12.015	12.050	12.091	12.127	12.162	12.201	12.223	12.253	12.287	12.328
139	0.95	12.744	12.785	12.832	12.874	12.914	12.960	12.984	13.020	13.060	13.107

3. WAGNER'S IMPACT THEORY

Wagner's (1932) theory was calculated to compare with the CFR (14 CFR Ch.I 2010), the drop test, and the flight test results from the Martin (1955) report. Several assumptions were made before calculating the theoretical pressures. It was assumed that chine immersion occurred during the drop tests and also that the hullform is a rigid structure, thus hydroelasticity was not considered in the analysis.

Wagner's theory is not defined for cases of chine immersion. Since the chine immersion case is considered, it is assumed that the intersection between the outer domain water surface elevation and the hull surface, c, is at the chine half-beam for each station. Since Wagner's formula is invalid for chine immersion and the denominator in the equation explodes at x = c, and the pressure goes to infinity, the x coordinate was set 0.001 ft off the actual chine width.

It is also assumed that the velocity remains constant through the entire impact period. With limited data on the acceleration distribution of each hull station and buttock line, it is assumed that each location on the hull bottom impacts the water with the same acceleration.

In order to use Wagner's pressure equation given by Faltinsen (2005), the acceleration at which the hullform contacted the water had to be calculated. Peak acceleration data for hull ballast conditions of 15505, 11590, and 10584 pounds was averaged for each loading case and compared with the contact speed at which the averaged accelerations occurred. Figure 34 shows this relationship and was used to determine the impact pressure.

To determine the function u, each station's geometry was plotted and fitted with a polynomial trend line of order 5. As previously stated, using the wetted half beam as the chine half beam, the function *u* was determined at each station and the values are shown in Table 11. Accordingly the speed of propagation of the wetted semi-width for each of the floor frame stations for various vertical impact speeds are shown in Table 11, however only impact speed of 40 ft/s is used in the study. From the table it can be seen that the speed of propagation decreases as the impact velocity does.

Table 11. Function u, speed of propagation, wetted semi-width, normal velocity, and acceleration used to calculate pressures at each station.

			Speed of Propagation dc/dt (ft/s)									
			Vn (ft/s)	dV/dt (ft/s^2)	Vn (ft/s)	dV/dt (ft/s^2)	Vn (ft/s)	dV/dt (ft/s^2)	Vn (ft/s)	dV/dt (ft/s^2)	Vn (ft/s)	dV/dt (ft/s^2)
Station	c (in)	u (-)	40	18.278	35	16.591	30	15.128	25	13.891	20	12.878
391	41.597	0.106	376.191		329.167		282.143		235.119		188.096	
370	42.675	0.120	334.571		292.749		250.928		209.107		167.285	
349	43.494	0.129	311.170		272.274		233.378		194.481		155.585	
328	44.055	0.139	288.302		252.264		216.226		180.188		144.151	
307	44.567	0.140	285.168		249.522		213.876		178.230		142.584	
286	44.941	0.138	289.251		253.095		216.938		180.782		144.626	
265	45.059	0.130	308.801		270.201		231.601		193.001		154.400	
244	44.821	0.146	273.454		239.272		205.090		170.909		136.727	
223	44.361	0.145	275.214		240.812		206.411		172.009		137.607	
202	43.977	0.139	288.117		252.102		216.088		180.073		144.059	
181	43.467	0.135	295.527		258.586		221.645		184.704		147.764	
160	42.905	0.143	279.941		244.949		209.956		174.963		139.971	
139	42.188	0.144	276.883		242.272		207.662		173.052		138.441	

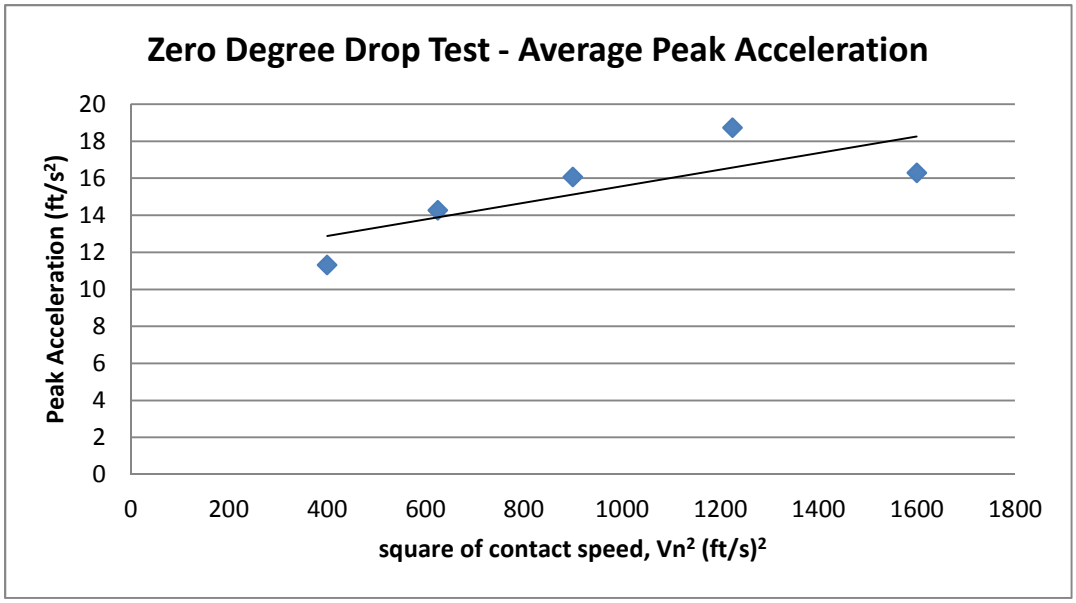

Figure 34. Drop test specimen averaged peak accelerations as a function of square contact speed for zero degree drop tests.

The pressure at each station was calculated using Wagner's theory and plotted against the non-dimensional buttock normalized by the chine beam at the corresponding station as seen in Figure 35. The pressure steadily increases from the keel to right before the chine, where there is a concentrated and peak pressure. The pressure distribution peaks and is concentrated very close to the spray root (Faltinsen 2005).

In order to record pressures of this magnitude, pressure transducers must be of high sampling frequency (Faltinsen 2005). Thus, these measurements are not reflected in model test data most likely due to the pressure transducers capability to record these high pressures. It is important to note that the trend in a peak and concentrated pressure near the spray root is not reflected at station 307, and reasons for this is unknown.

A comparison between pressures calculated using Wagner's theory and those found from drop tests at station 328 is shown in Figures 36, 37, 38, 39, 40. Only the buttock locations for pressure transducers used in drop tests were plotted, therefore coordinates near the chine were not used and a clearer image of the pressure distribution before the pressure peak is given. All vertical drop test impact velocities are given to show the accuracy of Wagner's theory for the pressure prediction at station 328. The trend of the test data is similar to the trend that Wagner's theory shows. Like stated before, the recording abilities of

the pressure transducers might not be as accurate to record high pressures of short duration.

Also, in the occurrence of chine immersion the pressure distribution would be more evenly distributed across the plate, or in other words the peak and concentrated pressure at the chine region would no longer be present. Thus, if the transducers were unable to measure the magnitudes of the peak pressures of short duration, only the pressures of smaller magnitude after before or after chine immersion would have been recorded. It is also important to note, the drop test pressures are peak pressures and not a time history of pressure and draft. Therefore it cannot be determined during what condition of immersion the individual peak pressures were recorded at. Wagner's theory subsequently gives the pressure distribution at a particular draft and time.

Overall, Wagner's theory gives fairly accurate transverse pressure distribution estimations. Test data for pressures at the chine are not given. Thus conclusions on the correlation between Wagner's theory and the test results for the concentrated peak pressure in the vicinity of the spray root, which as previously stated was set in the vicinity of the chine, cannot be determined.

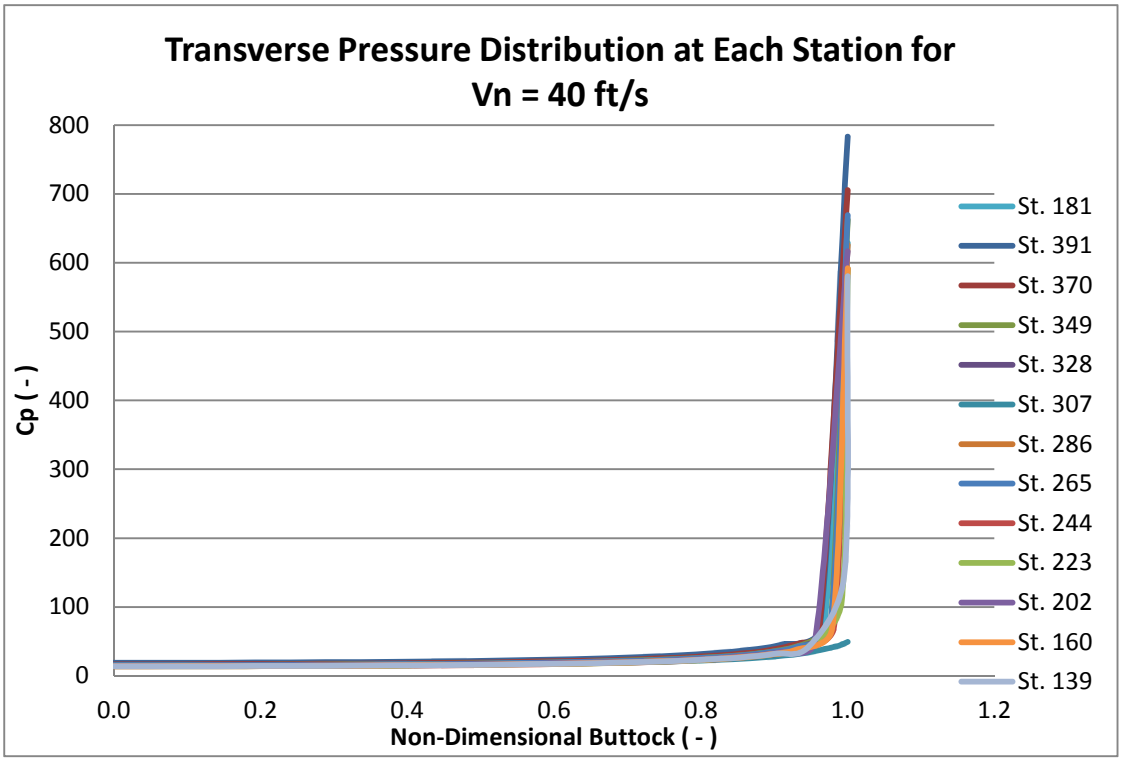

Figure 35. Transverse pressure distribution at each floor frame calculated using Wagner's theory.

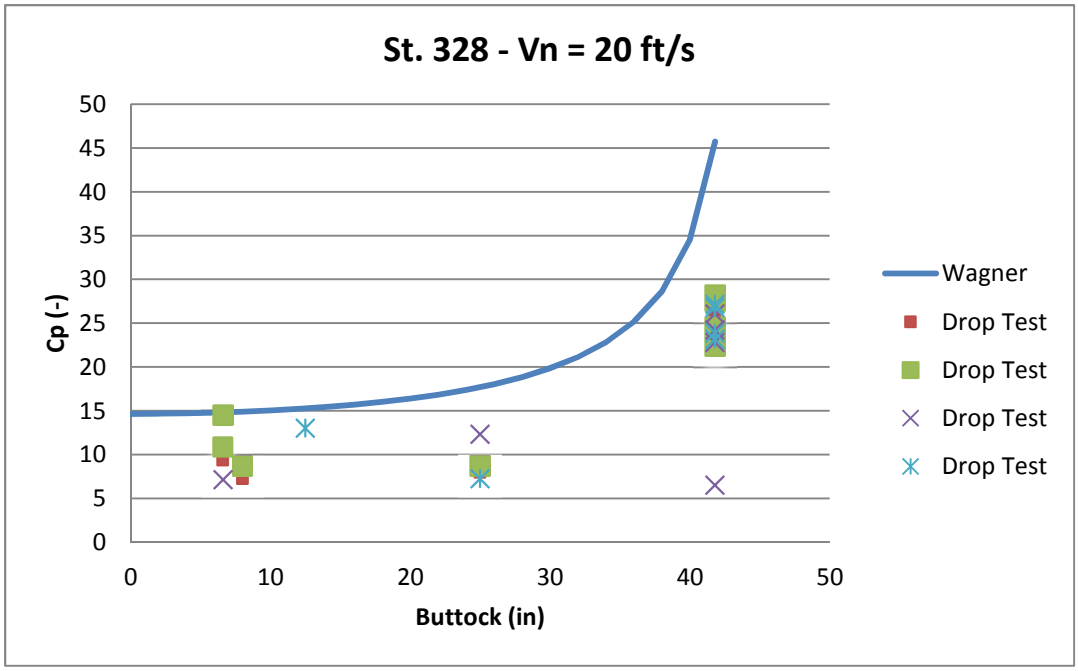

Figure 36. Wagner's pressure distribution compared with zero degree trim drop tests at 20 ft/s impact speed.

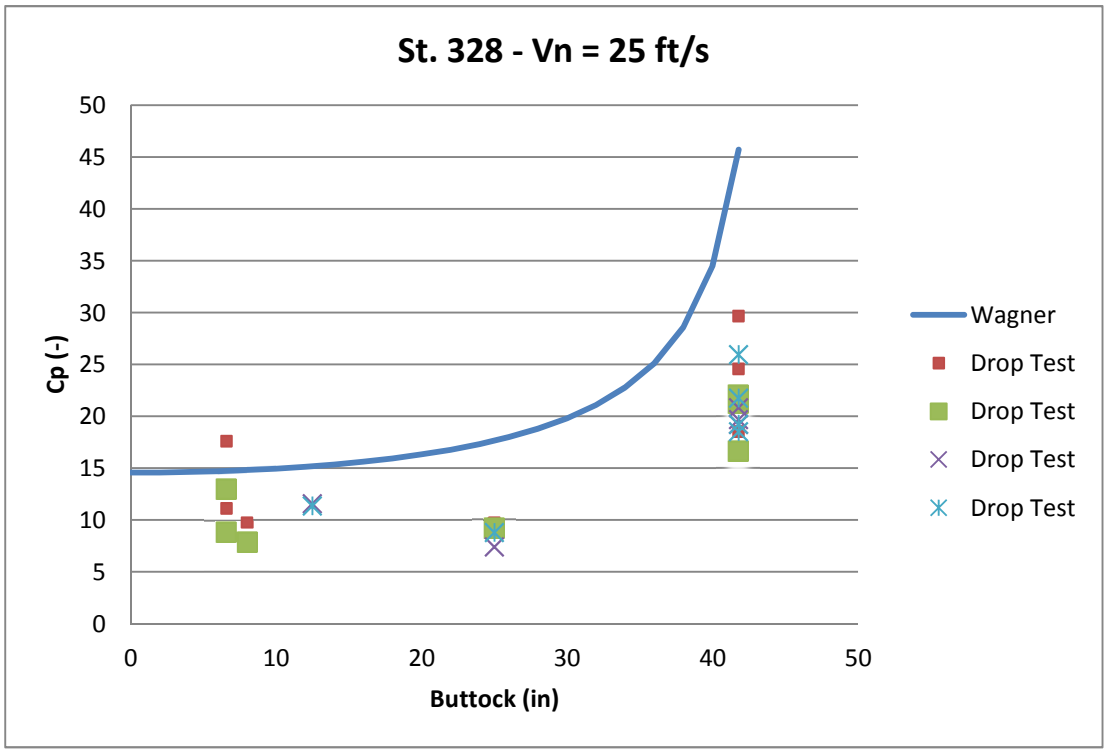

Figure 37. Wagner's pressure distribution compared with zero degree trim drop tests at 25 ft/s impact speed.

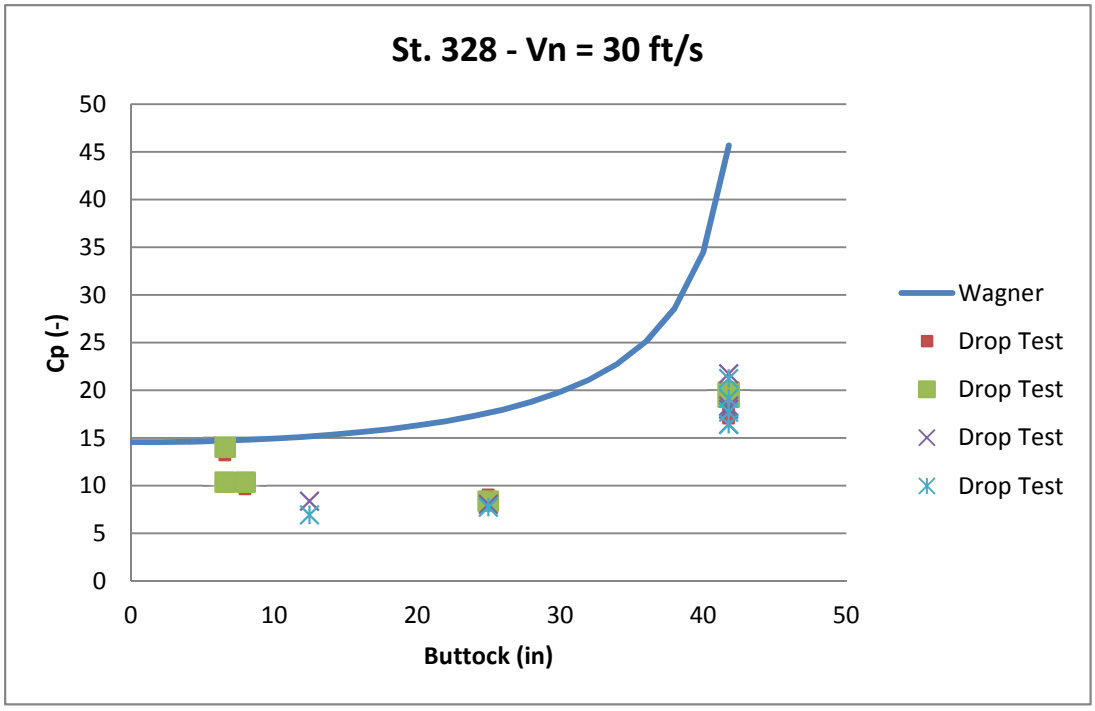

Figure 38. Wagner's pressure distribution compared with zero degree trim drop tests at 30 ft/s impact speed.

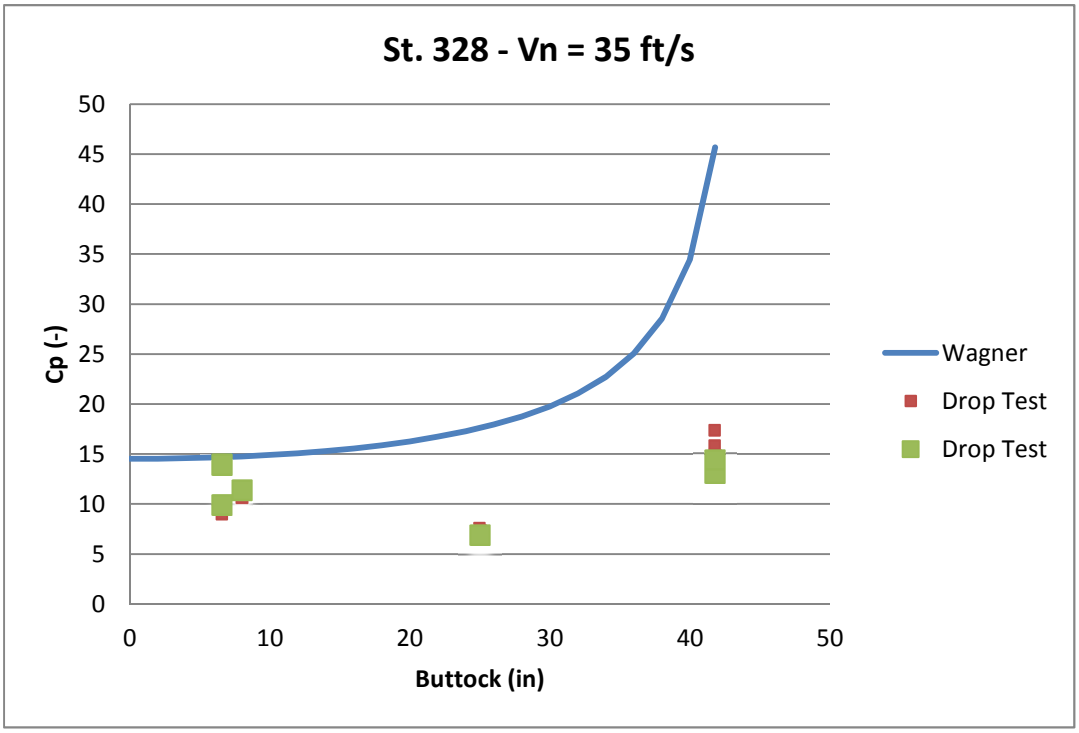

Figure 39. Wagner's pressure distribution compared with zero degree trim drop tests at 35 ft/s impact speed.

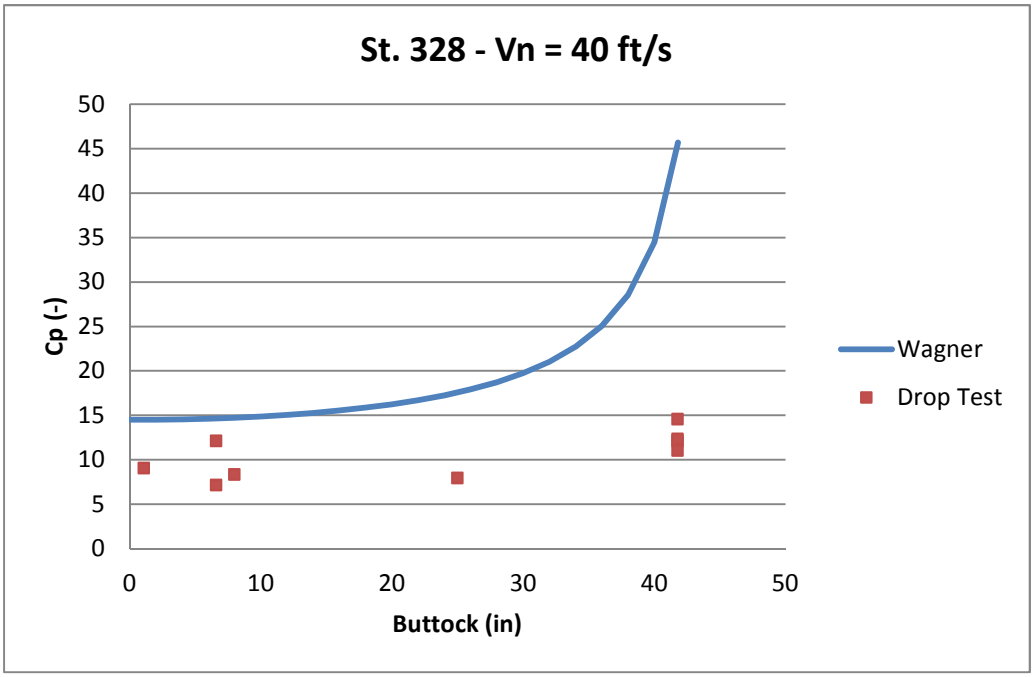

Figure 40. Wagner's pressure distribution compared with zero degree trim drop tests at 40 ft/s impact speed.

It is assumed that the accurate correlation between actual impact test data and Wagner's theory for other stations is valid. As previously stated, flight test data is not used in this study. This is due to the restrictions of Wagner's theory, since it can only be applied to vertical drops, and not oblique impact. However, to show the inaccuracy which Wagner's theory captures oblique impact, flight 29 – landing 3 and 7, in Figures 41 and 42 are provided. The location for the flight test data is at station 331, which has almost the same geometry as station 328 used in the drop test specimen

It is seen that Wagner's theory greatly over-estimates oblique impact pressures. The main discrepancy with applying Wagner's theory to an oblique impact case is that Wagner's theory does not consider the momentum imparted to downwash. Also, another discrepancy with the data is due to that fact that chine immersion had most likely not occurred during oblique impact at station 331. This is indicated by the low coefficient of pressures and the drop of pressures at buttock locations midway between the keel and chine. In comparison, Wagner's theory used in this study, calculated pressures for the onset of chine immersion.

Since pressure data is not given for the entire hull, Wagner's theory provides a good method to determine the transverse pressure distribution at each station. The pressures determined from theory were applied to the entire Maestro model since these pressures were justified with the drop test data.

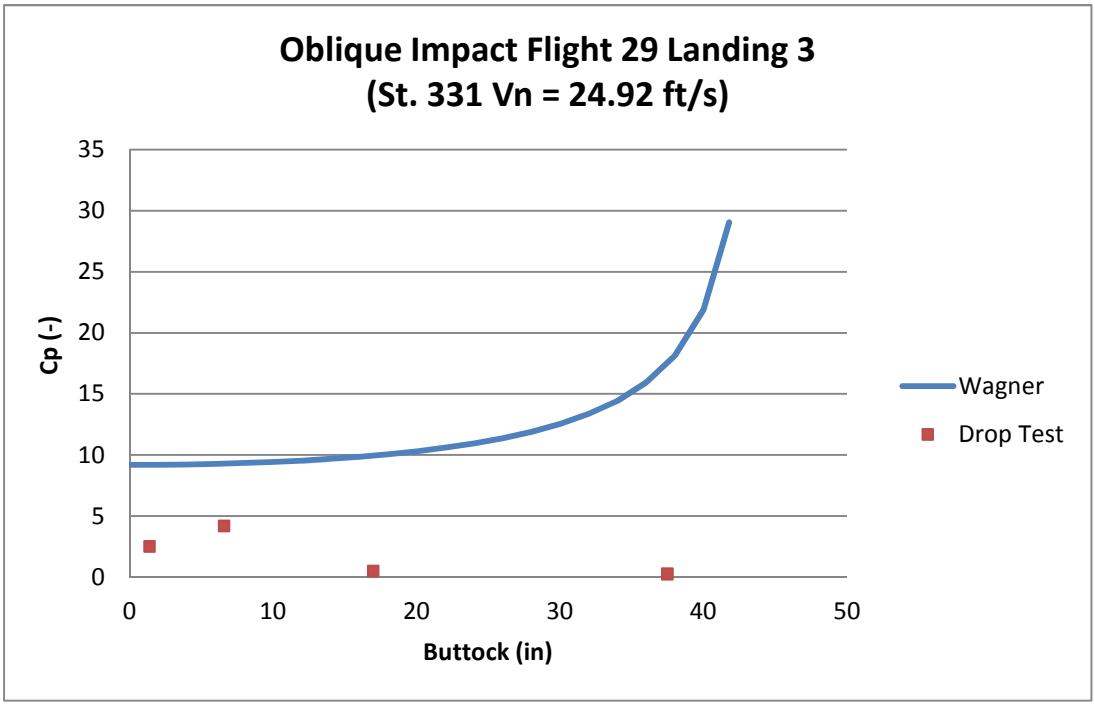

Figure 41. Wagner's pressure distribution compared with flight 29 landing 3 with oblique impact at speed Vn = 24.92 ft/s.

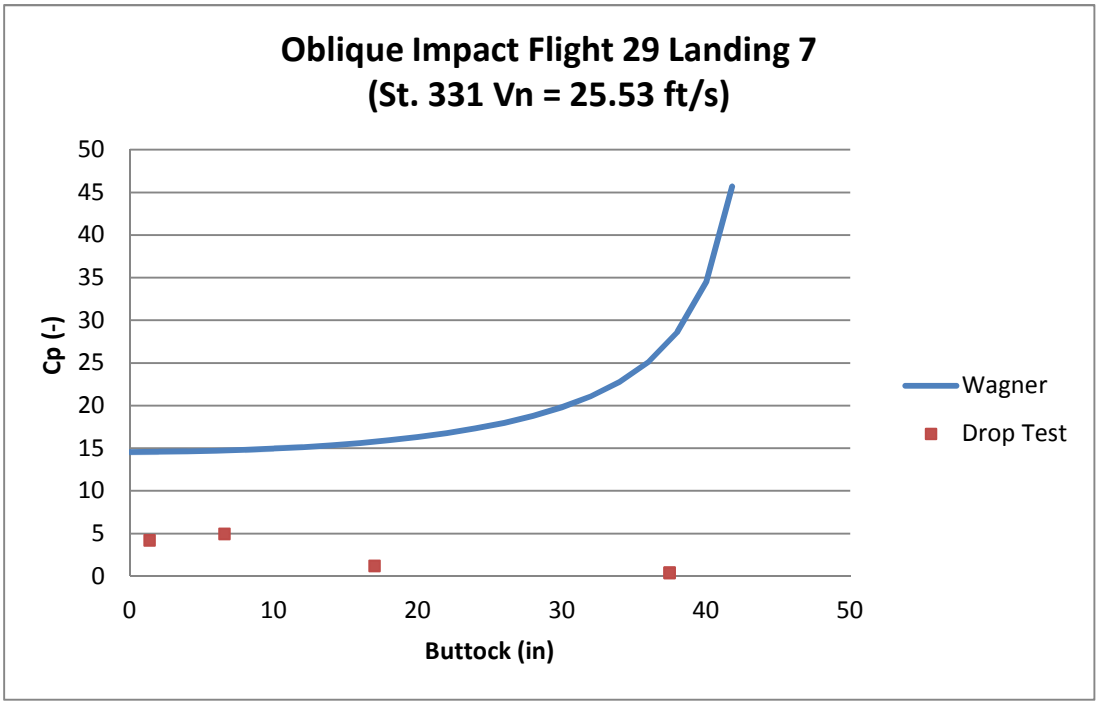

Figure 42. Wagner's pressure distribution compared with flight 29 landing 7 with oblique impact at speed Vn = 25.53 ft/s.

To compare current design specification pressures calculated from the CFR to pressures predicted by Wagner's theory, the actual pressure as opposed to the coefficient of pressure is used for comparison. This was done because the velocity used in the CFR is at stall speed with high forward velocity and Wagner's theory uses the velocity normal to the keel which is the vertical velocity in the drop test cases.

The transverse pressure distribution comparison is shown in Figure 43 for station 328. As to not be repetitive and show each station's CFR pressure data compared to Wagner's theoretical pressures, the station with the lowest overall pressure distribution using Wagner's theory, which is station 244, is compared with all CFR pressure distribution data for each station in Figure 44. In order to not compress the CFR data, the pressure at the chine for Wagner's theory is not included in both figures.

All CFR pressure distributions at each station are considerably lower than the lowest pressure distribution for the 40 ft/s drop case. This shows that the model was tested in loading conditions that a seaplane is not normally subjected to. The CFR data does however correspond with the oblique impact flight test data as seen in Figure 45. The CFR overestimates pressure for majority of the flight test data; however, some of the pressures are located in the band between the maximum and minimum pressures determined by the CFR calculations.

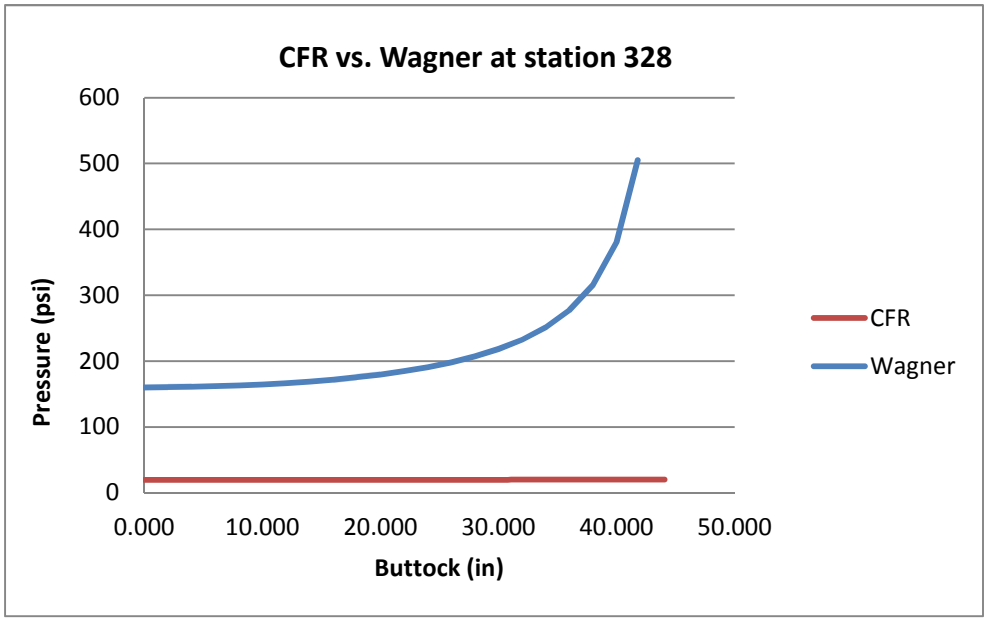

Figure 43. Transverse pressure distribution comparison at station 328 using Wagner's theory and the CFR.

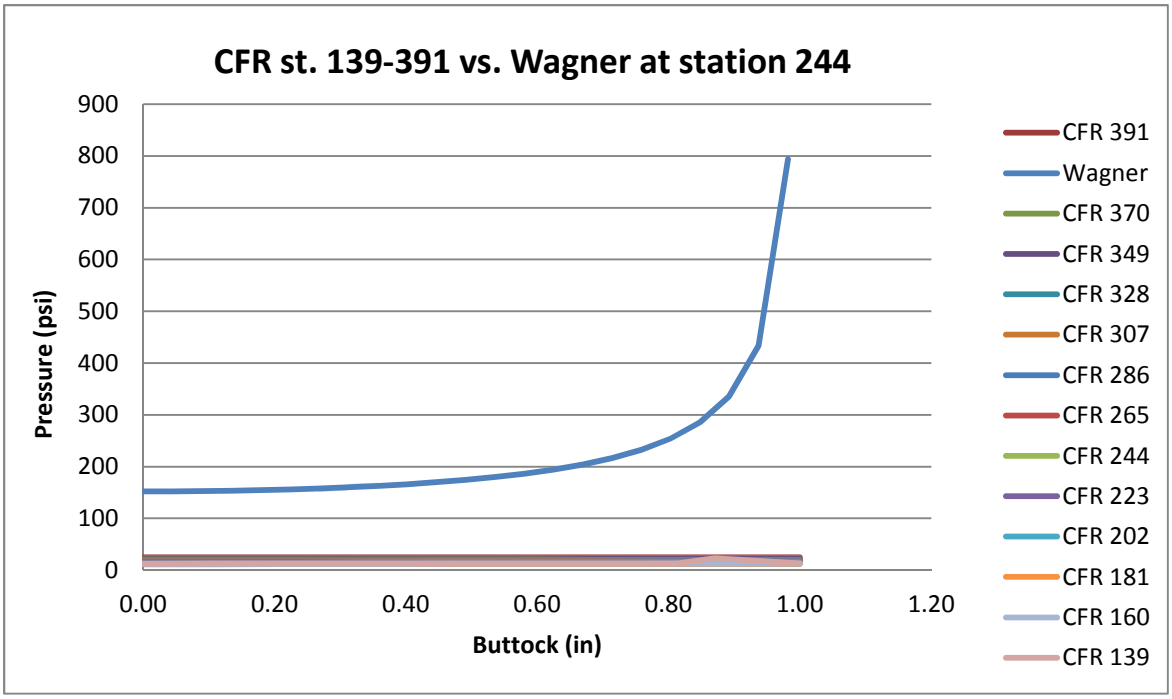

Figure 44. Transverse pressure distribution comparison for the lowest pressure distribution using Wagner's theory and all pressure distributions for CFR stations.

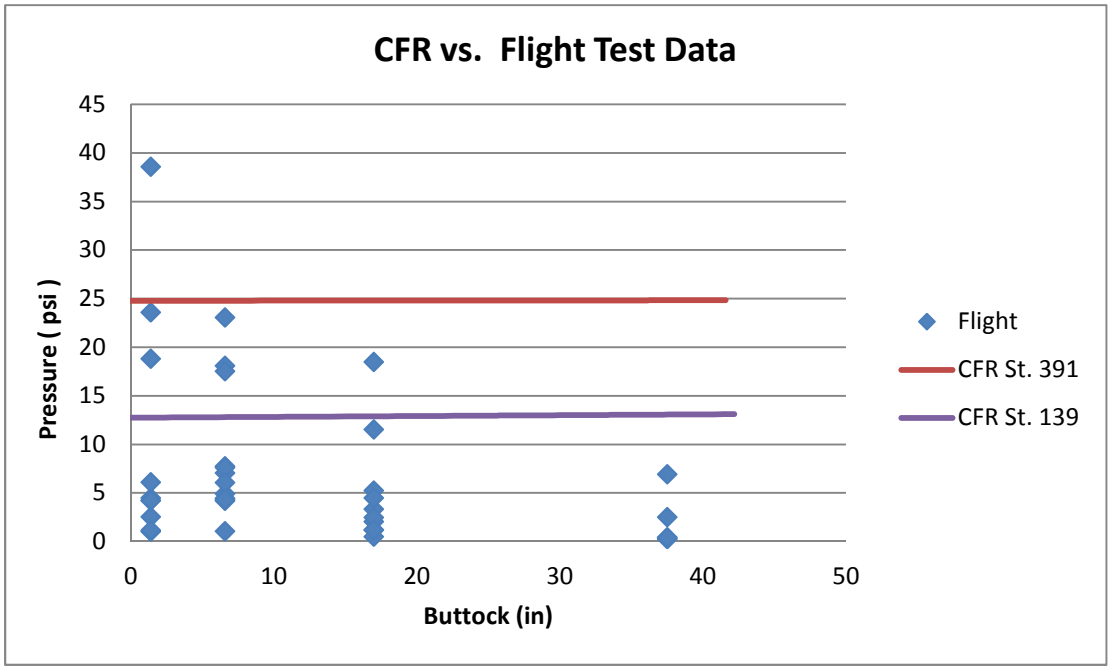

Figure 45. CFR pressure data in comparison with oblique flight test data.

B. MODELING STRUCTURAL COMPONENTS

The seaplane structure was modeled in Maestro version 9.1.098, a coarse mesh finite element analysis tool, in order to analyze how the impact pressures affect the structural reaction. Both the CFR and Wagner pressure distribution were applied to the Maestro model to determine if the structure meets current design standards.

Several assumptions were made due to either a lack of information on the structure and also the modeling capabilities of Maestro. As previously stated, the M270 structure is assumed to be a rigid structure, where the rivets are closely spaced and tightly fastened.

The other assumptions are a resultant in lack of knowledge of the structure. The thickness of the steel deck stiffener channel was assumed along with the web height of the deep side transverse floor frame. The floor frame web height was defined as varying and having a maximum height from the middle of the frame to the deck transverse floor frame and then a decreasing height to where the frame connects to the bottom plating. It was assumed to be the same web height of six inches as the deck transverse floor frame. In regards to the steel deck stiffener channel thickness, after several different inputs of thicknesses into Maestro, it was concluded that this thickness had negligible effect on the stresses experienced in the bottom plating and its support along with the web structure.

Several connectivity supports outlined in in the Martin (1955) report, were also ignored due to a lack of information on the connection points, material, and dimensions. The ignored connection supports include shallow former plates located at the intermediate frame sections which are attached to the five stringers outboard of centerline and the chine knees which are attached to the three stringers inboard of the side shell.

As well as assumptions and disregarding various structural sections, it was necessary to modify beam sections due to Maestro's modeling capabilities. Maestro could not handle the complex sections that the M270 was designed with for riveting purposes. All zee, capped zee, and channel sections required modeling the structural element twice, with two different shapes, as seen in Table 12 which shows the modified sectional inputs for Maestro. For example, the side transverse floor frame was modeled with two angles, with webs oriented perpendicular to each other and connected at the toe of each angle.

In addition to modeling the sections in separate parts, the top deck frames, the deep side shell frame, and longitudinal stiffeners S6A through S3 were resized to compensate for the truncation of the capped flange that could not be included in the sections. Reasons for the incapability to capture the capped flange in the model were due to the

inability to maintain connectivity in the total structural beam element while retaining total sectional inertia. Thus, flanges were resized to incorporate the inertia of the truncated cap flange, while still maintaining the total sectional inertia of the entire beam element. The changes in element sizes from the original M270 section to the modified Maestro section are noted in Table 12.

Table 12. Modified structural members for Maestro model.

	Item	Web (in)	Flange (in)	Thickness (in)
Stiffener Profiles	Deck Stiffener (6 x 0.25)			
	Angle	6	6	0.25
	Beam	6	-	0.25
	Centerline Stiffener (2-1/2 x 2 x 0.156)			
	T	2 1/2	2	0.156
	Web Topper Stiffener (2 x 1-3/4 x 0.125)			
	T	2	1 3/4	0.125
	Web Blhd Stiffener (1-7/32 x 1-9/16 x 1-1/32 x 0.064)			
	Angle	1 9/16	1 7/32	0.064
	Beam	-	1 1/32	0.064
	S0 and S1 (1-1/2 x 1-3/16 x 0.125)			
	Angle	1 1/2	1 3/16	0.125
	S2 (1-1/8 x 3-1/2 x 2 x 0.125)			
	Angle	3 1/2	1 1/8	0.125
	Beam	2	-	0.125
	S6A - S3 (9/16 x 1-1/4 x 2-1/2 x 0.072)			
	Angle 1	2 1/2	1 7/9 ***	0.072
	Angle 2	1 1/4	9/16	0.072
	Web Bottom stiffener (2 x 2 x 0.25)			
	Angle	2	2	0.25
Frames	Deck Transverse Floor Frame (5/8 x 1-1/4 x 6 x 0.064)			
	Angle 1	6	1 6/7 ***	0.064
	Angle 2	1 1/4	5/8	0.064
	Deep Side Transverse Floor Frame (3/8 x 1 x 6 x 1-1/4 x 1/2 x 0.0912)			
	Angle 1	5	1 2/3 ***	0.0912
	Angle 2	0.5	1	
	Intermediate Transverse Side Frame (1 x 2 -1/2 x 1 x 0.072)			
	Angle	1	2 1/2	0.072
	Beam	-	1	0.072

***structural members redesigned from original structure

A half model of the M270 is shown in Figures 46, 47, 48, and 49. Figure 46 shows a perspective view of the internal members and structure, whereas Figure 47 shows the perspective view of the external structure. Web plating was created using triangle and quad elements which are displayed with green and cyan respectively. The intermediate transverse side frames, centerline line stiffener, web bottom stiffener, web topper stiffener, and deck stiffener were all modeled with beam elements displayed in orange. The deep side transverse frames are displayed in red, except at station 139 which was modeled separately by beam elements. Longitudinal stiffeners are displayed in yellow with its corresponding bottom and keel plating shown in blue, except between station 202 and 223 where part of the side plate had to be modeled with quads and triangles.

Floor frame 328 which the entire hull structure was based on is shown in Figures 48 and 49. From these views the longitudinal stringers, transverse frames, and web stiffeners, which required two elements to model the structure, can be seen.

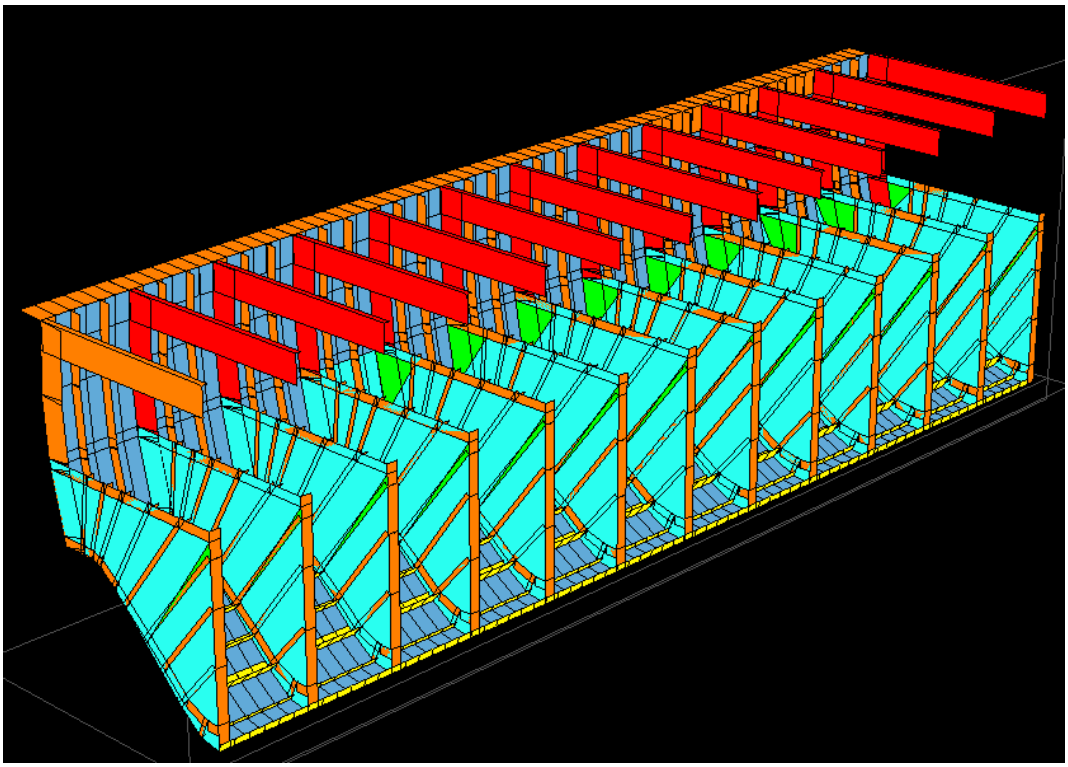

Figure 46. Perspective view of the internal structure, modeled in Maestro.

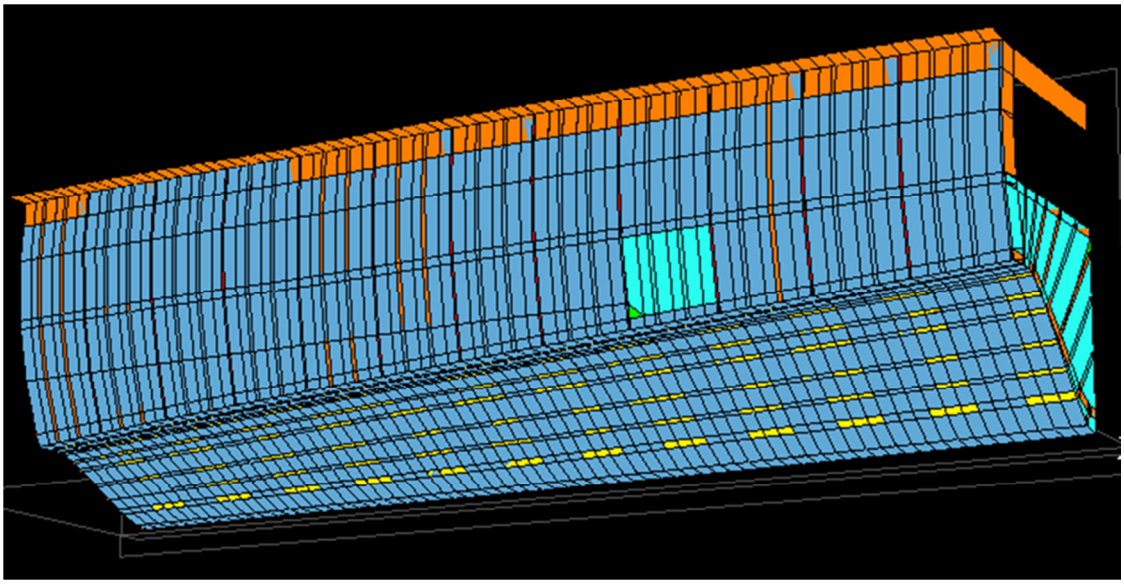

Figure 47. Perspective view of the external structure, modeled in Maestro.

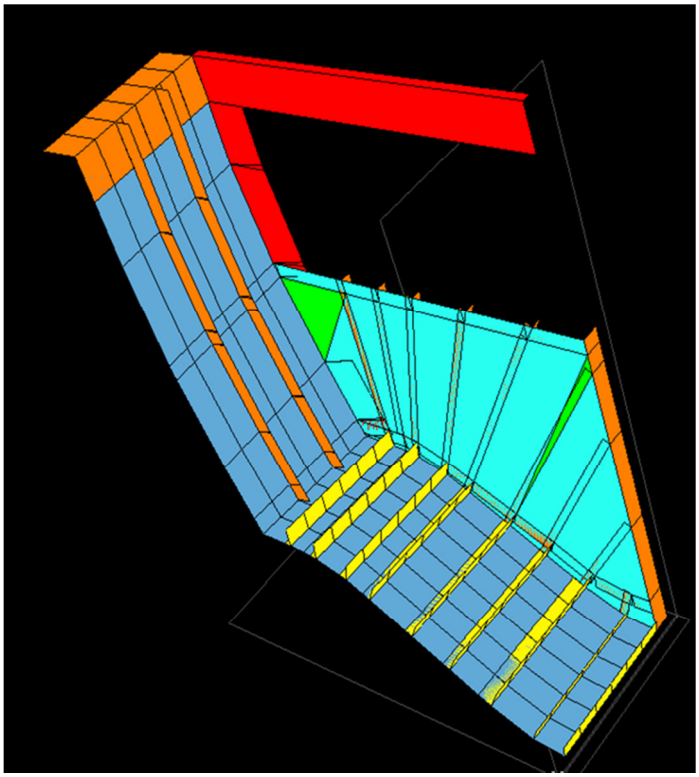

Figure 48. Maestro model of internal structure at Station 328 showing longitudinal stringers and transverse frames.

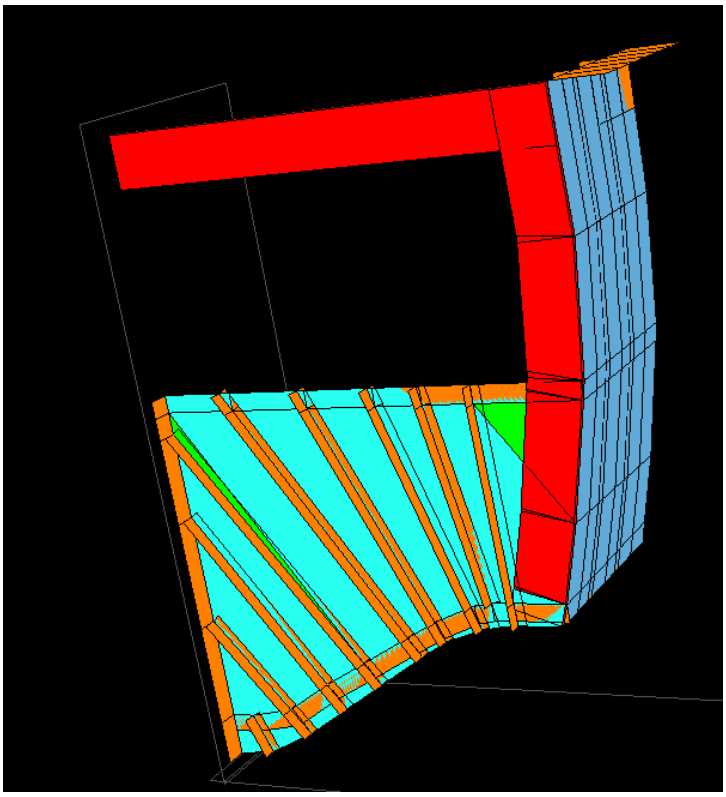

Figure 49. Maestro model of internal structure at Station 328 showing web stiffeners.

C. LOADING THE MODEL

The pressure distribution results from the CFR and Wagner's theory at the 40 ft/s drop case were applied to the Maestro model. The pressure was applied to each panel edge where the pressures were transversely linearly distributed on the plate and between panels. The pressures for each panel were kept constant longitudinally for each station and transferred to the consecutive stations pressures midway between the intermediate transverse frames. The structural mass and acceleration of the hull section was not included in the loading of the Maestro model, since most seaplane analysis assumes that the lift on the wings is roughly the same as the weight of the seaplane.

Figures 50 and 51 displays a colored scale of the pressure distributions on the deformed model after loading the bottom plating with the pressures calculated from the CFR and Wagner's theory respectively.

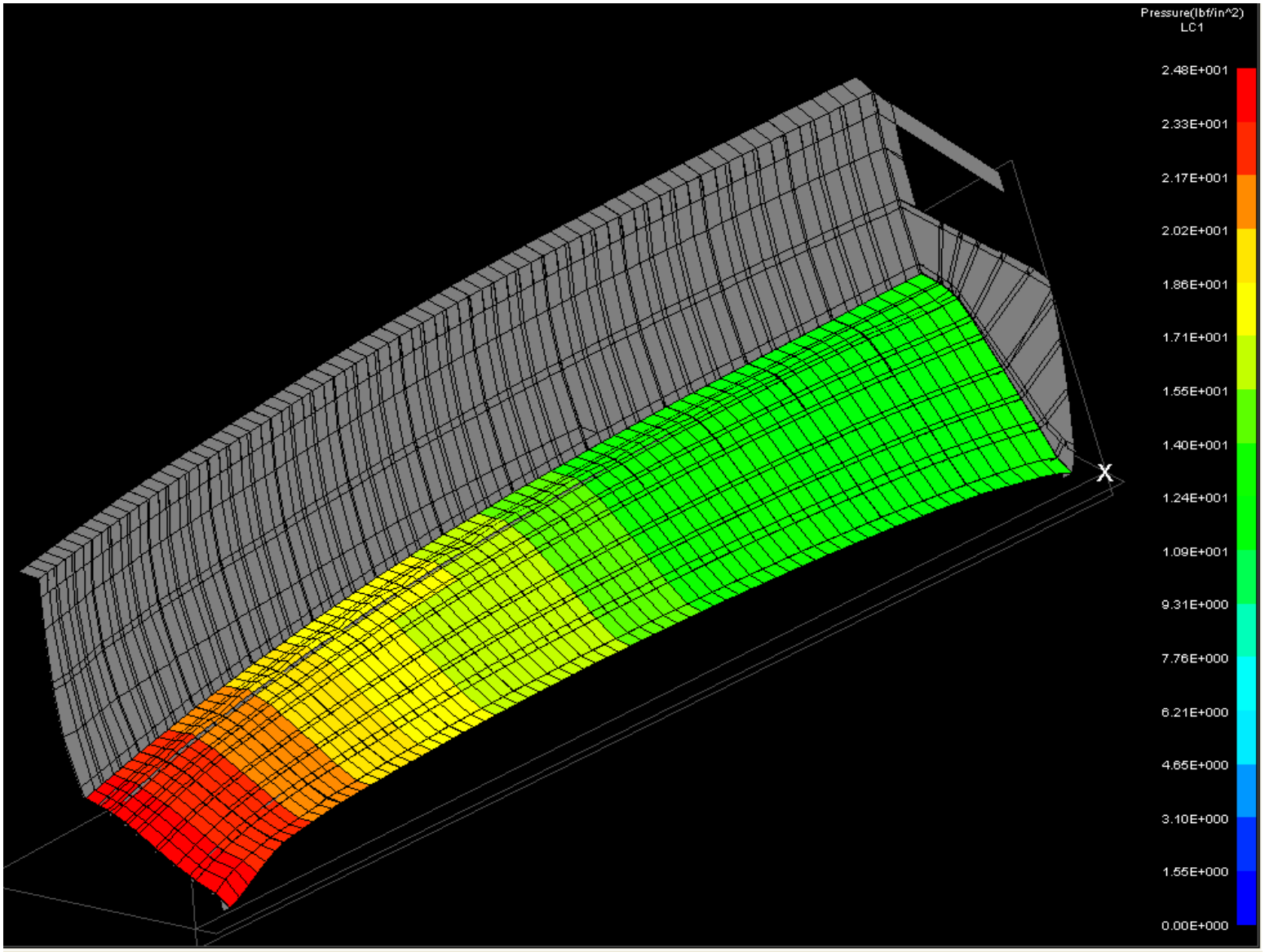

Figure 50. Maestro pressure distribution on hull using CFR data.

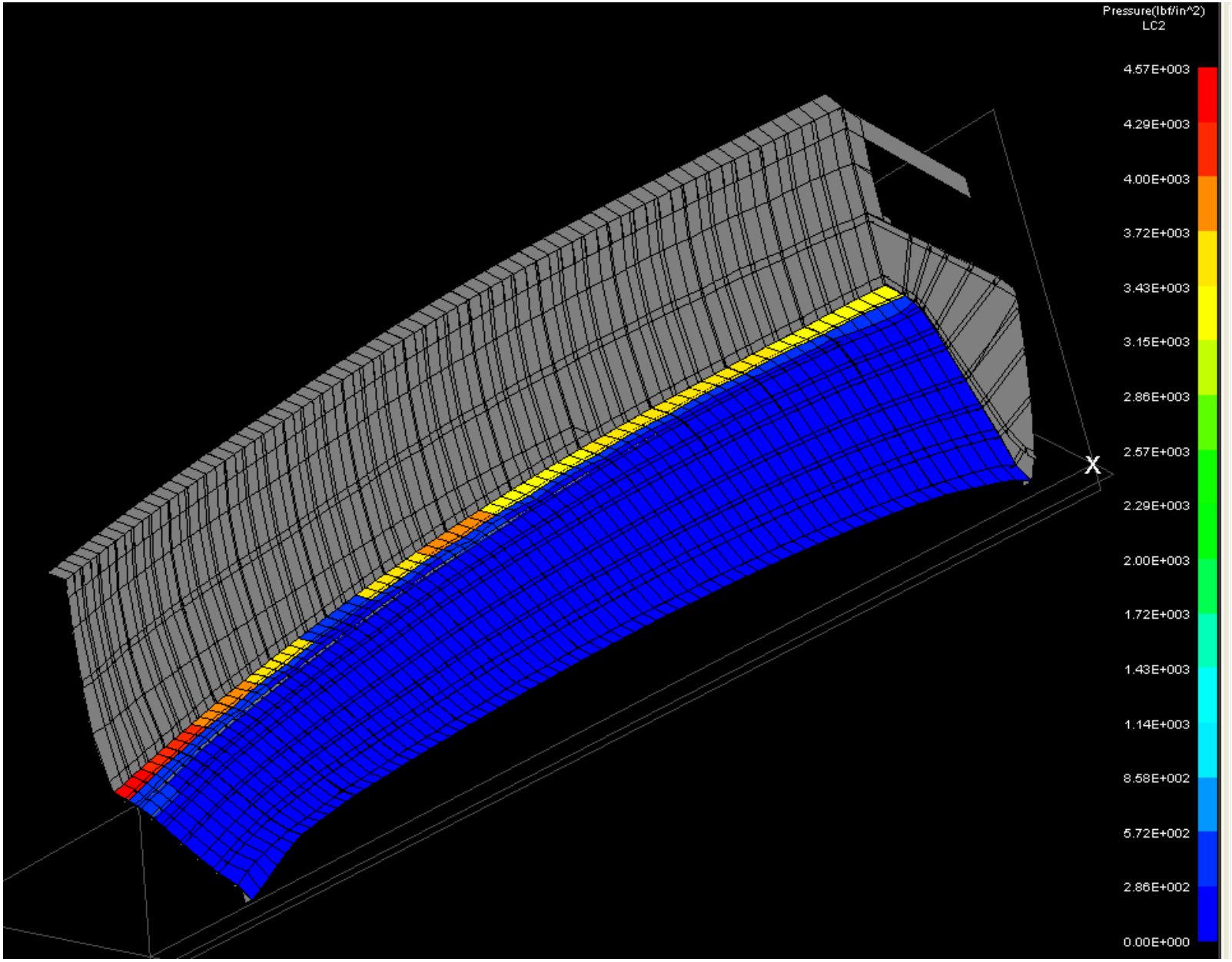

Figure 51. Maestro pressure distribution on hull using Wagner's data.

The highest pressure from the CFR loading is roughly 24 psi and is located at station 391. The longitudinal pressure distribution decreases moving forward to frame 139 where the maximum pressure is roughly 12 psi.

The pressure distribution for Wagner's case shows the concentration and peak pressure at the chine. The pressure distribution on the rest of the hull is considerably smaller than in the chine region and therefore is shown in blue with all pressures less than roughly 572 pounds per square inch. As stated previously, the chine region of station 307 was calculated by Wagner's theory and does not follow the same trend of a pressure peak at the spray root.

D. STRUCTURAL REACTIONS

To conclude with the Maestro analysis, stresses in the mid-x direction were determined and are displayed for both the CFR and Wagner's theory loading cases. The range of the plot legend for stress for both loading conditions was restricted to the yield stress extremities of ±70,000 psi for tension and compression. Figure 52 shows the stresses in the structure for Wagner's loading case and likewise Figure 53 shows the stresses in the structure for the CFR loading.

Wagner's case shows that the majority of the bottom plating and side plating have stresses greater than that of yield, which are shown in gray. From the drop test report, structural failures at station 328 were as follows: slight buckling of the centerline stiffener where it attaches to longitudinal stringer 2, buckling of longitudinal stringer 6A, and a considerable wrinkling of the test specimen's bottom (Martin 1955).

Maestro's output shows that centerline stiffener in station 328 is under tension at a maximum stress of 5.19×10^4 psi. All longitudinal stringers from floor frame 328 to the web connections at the floor frames on each side of station 328 are past yield stress. The maximum stress in stringer 6A is -2.49×10^5 psi in compression. The stress at which buckling occurs with an applied critical load for the longitudinal stringer 6A with the conservative approach of pinned-pinned boundary conditions is 2.30×10^5 psi. The actual stress from the Maestro model is greater than the calculated critical stress, thus the member buckled.

As previously stated, the stresses in the plating and longitudinal stringers in the majority of the hull are past yield stress. However, as seen in Table 13 which summarizes the stresses in the stringers and plating for the specimen in the Martin (1955) report dropped with an impact velocity of 40 ft/s, the stresses are much smaller than yield. The discontinuity of results between the experimental results and the Maestro model can be

accounted to the fact that Wagner's theory over predicted the pressures on the hull. However the severe wrinkling of the specimen's plating and permanent sets in the plating shows that the material surpassed the yield stress and went into the plastic regime for the drop test in some elements of the specimen.

Table 13. Drop test stresses in stringers and plating.

Stresses in Stringers and Plating (psi)				
S-0	S-1	S-2	S-5	Keel Plating Between S0-S1
-13,000	-20,500	-5,000	-13,000	-2,000

As stated previously the chine knee gussets were not modeled due to the lack of information on the properties, sizes, and the connection points of the structure to the side shell. Since the vast majority of the structure's stresses in the plating and longitudinal stringers for Wagner's loading condition went past yield, buckling was checked for the members which failed at the 40 ft/s drop test with the stresses from the CFR loading.

The maximum stress taken from Maestro in the centerline stiffener and web stringer 6A are 2.67×10^3 psi in tension and -6.25×10^3 psi in compression respectively. The results show that the stress in stringer 6A is less than the critical stress of -2.30×10^5 psi, and this critical stress is also less than the yield stress. Therefore, the members which failed in the 40 ft/s experimental drop case do not fail with the design pressures from current industry standards taken from the CFR.

Overall, the hull stresses for the CFR case are less than yield stress, however, the floor frame 391 showed stresses over yield in the web plating in the vicinity of the keel. The deformations in this section were unusually distorted. The deflection in the x-direction of the top of the web frame near centerline is 2.80 inches, which is much higher than defections seen in other floor frames with similar loading. Connectivity between element nodes in the FEA model was checked and the reasons for the behavior of this distortion are unknown. Thus, the stresses in this frame may be inaccurate.

Overall, the maximum stress that exists in the hull, not including floor frame 391, when loaded with results taken from the CFR is roughly -1.70×10^4 psi in compression. This is located in the vicinity of the keel plate, and is considerably less than the yield stress of the aluminum.

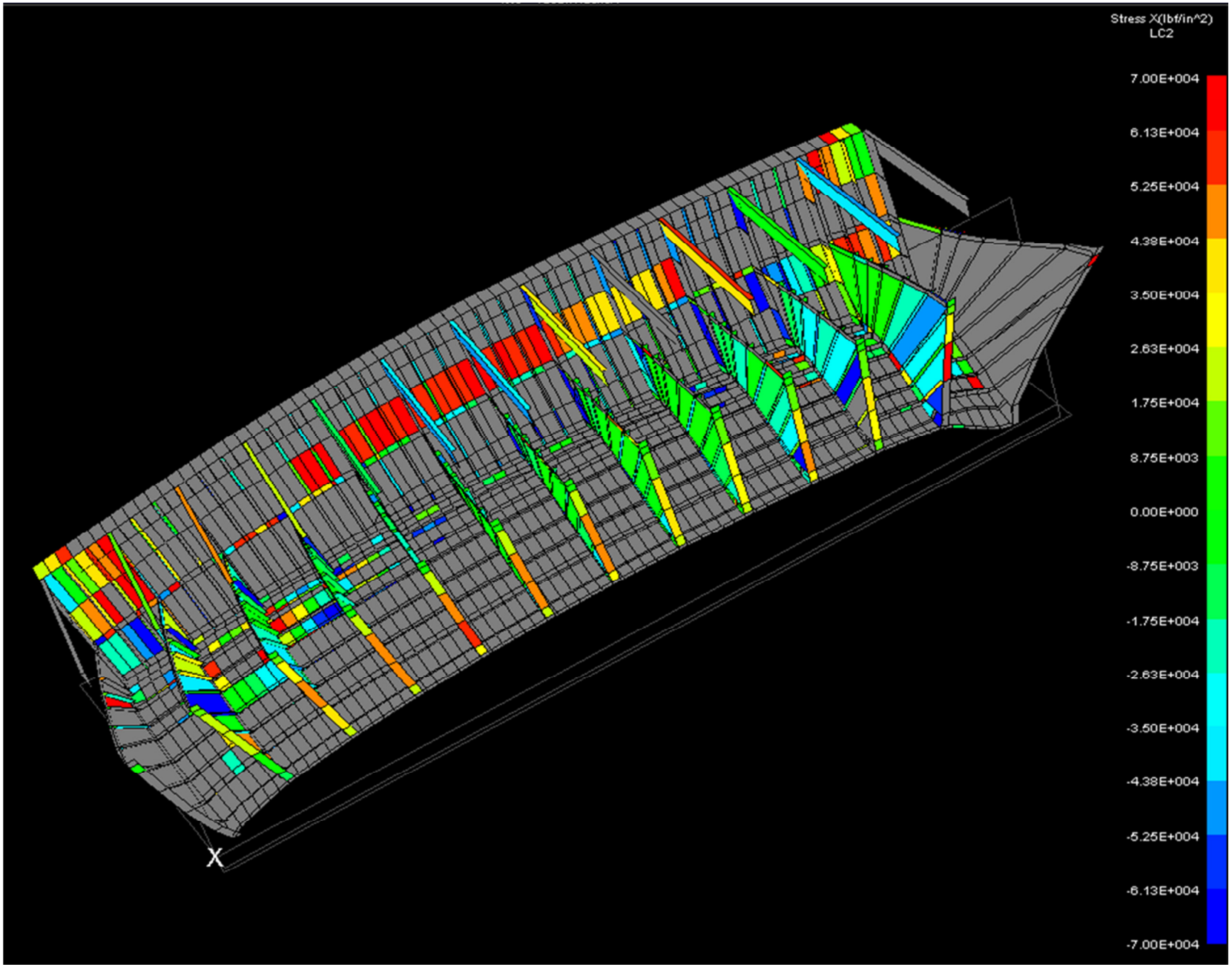

Figure 52. Stress in structure in the x-direction from Wagner's theory, color scaled showing members with stress less than yield stress and structural members greater than yield stress in gray.

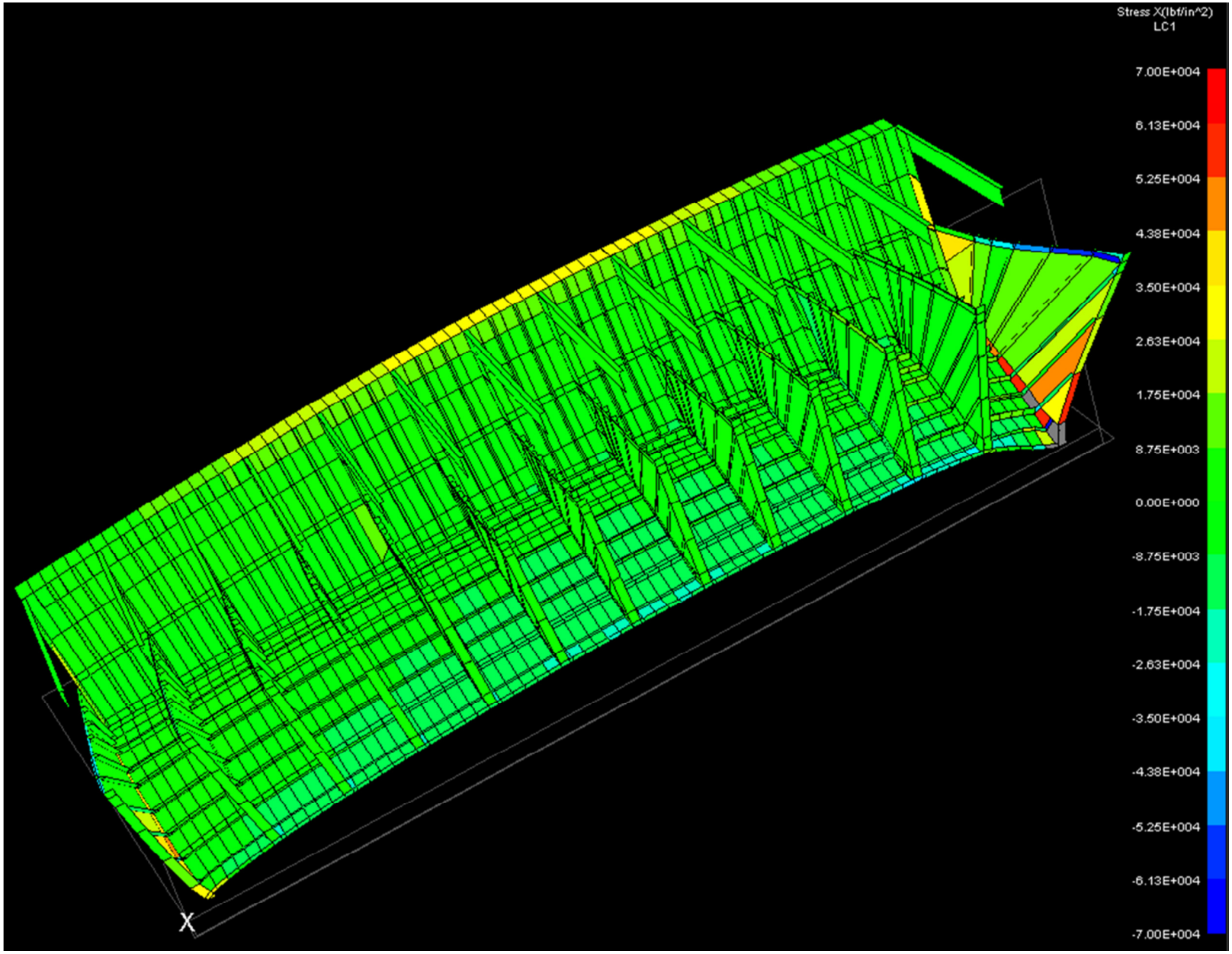

Figure 53. Stress in structure in the x-direction from CFR, color scaled showing members with stress less than yield stress.

IX. CONCLUSIONS

The M270 impact theory review and the preliminary global structural review proved to capture the impact problem fairly accurately. Using model test data and flight test data was useful in comparing and validating impact theory and suggesting improvements. Several conclusions were determined from the research conducted for the master's thesis.

Drop test data shows an overall trend of increasing pressure with the normal velocity squared. This trend is validated with a linear correlation between pressure and normal velocity squared for buttock locations inboard of the chine region. Near the chine flare region, the ratio of pressure to the squared contact speed is lower at high speeds and greater at lower speeds. This relationship could not be validated for oblique impact due to a lack of data. This relationship is useful in utilizing drop test data with only a limited set of tested impact velocities.

Oblique impact relationships for the pressures of varying buttock lines along the beam of the hull showed a linear correlation with the resultant angle. In cases inboard the chine the pressure increased as the resultant angle increased. This trend could not be verified in chine flare regions since there was a lack of data. Overall, this trend shows that the angle at which oblique impact occurs is an important factor on impact loads.

Wagner's theory was chosen because of the availability of required information needed for the theory, the validation with experimental tests, its ability to be applied to non-prismatic hullforms, and the theory's ability to capture a good portion of the impact process. The parameters previously stated were also dependent on the semester timeline in order to complete the project.

To validate Wagner's theory only the drop test cases were used, which showed a fairly accurate correlation of pressure trends in regions inboard of the chine. Wagner's theory predicted pressures greater than recorded in regions starting midway between to keel and chine and extending out to the chine.

It would have been beneficial to compare pressure data from the drop test at the onset of chine immersion in order to compare the magnitude of the pressure peaks against Wagner's prediction. Since the drop test pressures are peak pressures and not a time history of pressure and draft, it cannot be determined if the transducers were able to measure the magnitudes of the peak pressures of short duration at chine immersion, or if they only measured the pressures of smaller magnitude before or after chine immersion occurred.

Overall, for this level of detail in analysis of the impact problem, Wagner's theory did depict the impact problem reasonably, thus it was justified for use in applying to the Maestro model. If the

timeline had been longer, a theory should have been used that captured both the momentum imparted to the water mass as well as to the downwash. Thus cases with a horizontal velocity component in oblique impact could have been compared with pressure data from the flight tests.

As previously stated, Wagner's theory was justified for use for the drop test case. However, the overestimation of pressures in the theory was apparent in deformation and stresses in the Maestro model. However, both drop test and Maestro output did show that the model surpassed yield stress and went into the plastic regime with permanent sets in the stringers in plating.

The CFR pressure results showed that a seaplane today would not be designed to take the pressures that resulted from the drop test conditions of 40 ft/s at which that the specimen was tested. The CFR pressures more precisely correlate with the magnitudes of pressure of the oblique flight test data. However, the pressures from the CFR are greater than the majority of the recorded pressures from the flight test data. The pressures that resulted from the CFR prove that the structure is adequately designed to take the resulting loads. Stresses in the plating and members do not reach yield and the members that buckled in the 40 ft/s drop test case did not buckle with CFR loading according to the maestro model.

If the study was continued from a model test perspective as well as from an analytical perspective several recommendations are suggested. In testing, a seaplane time history of the pressures as well as the immersion depth should be recorded. This would indicate the pressure distribution during immersion and the change in pressure distribution on the onset and after chine immersion occurs. A greater number of pressure transducers should be fitted to the hull at more longitudinal and transverse locations along the hull bottom. The pressure transducers should also be capable of recording short duration/high magnitude pressures, especially in regions where chine wetting does occur.

Further impact estimation models should be studied that can handle oblique impact cases as well as chine immersion cases. It was assumed that the wetted half-beam for drop tests impact was at the chine width, thus simulating the case right before chine immersion and the peak and concentrated pressure at the spray root. Using theory that is designed to handle chine immersion would determine if the peak pressures seen at the spray root are accurate.

Overall, Wagner's theory and Maestro output proved to be good tools to do first order design impact estimations as well as a global structural analysis. Continued work on oblique impact cases is necessary in order to properly capture the impact at which a seaplane normally lands.

WORKS CITED

Benscoter, S.U. *Impact Theory for Seaplane Landings.* NACA Technical Note 1437, 1947.

Beukelman, W. *Slamming on Forced Oscillating Wedges at Forward Speed, Part I: Test Results*. Report No. 888. Delft University of Technology, Ship Hydromechanics Laboratory, Netherlands, 1991.

Blundell, R.W, and Jones, E.T. *Force and Pressure Measurements on V-Shapes on Impact with Water Compared with Theory and Seaplane Alighting Results.* R & M No. 1932, 1938.

Code of Federal Regulations. "Water Loads" Title 14 Ch. I Subpart C. Sec. 25.533, 1 January 2010. pp. 422-424 and 542.

Crewe, P. R. *A Proposed Theory to Cover Water Impacts of Seaplanes in which the Craft has Constant Attitude and a Tangential-to-Keel Velocity Relative to the Water.* R & M No. 2513, 1946.

Crewe, P.R., and Gerry, D. *Proposal C-Seaplane Design Problems.* Contract No. N68171-77-C-8345, 1977.

Faltinsen, O. M. "Slamming on Rigid Bodies." *Hydrodynamics of High-speed Marine Vehicles.* Cambridge: Cambridge UP, 2005. Print.

Glenn L. Martin Company. *U.S. Navy P5M Marline Seaplanes: Design Digest.* Glenn Martin Company: Maryland, 1951.

Green, A. E. The Gliding of a Plate on a Stream of Finite Depth Part II. Proc Cambridge Phil Soc Vol 32, May 1935

Hamilton, J.A. *Full Scale Measurements of Impact Loads on a Large flying Boat and Part II-Results for Impacts on Main Step.* A.R.C. Technical Report No. 205, 1955.

Martin. *Martin Model 270: Water Loads Investigation Hull Bottom Pressures and Impact Loads.* 1955.

Mayo, W.L. *Analysis and Modification of Theory for Impact of Seaplanes on Water.* NACA Report No. 810, 1945.

Niu, M. C.Y. *Airframe Structural Design: Practical Design Information and Data on Aircraft Structures.* Lockheed Aeronautical Systems Company. Burbank, California: Conmilit Press Ltd., 1988.

Von Karman, T., and Wattendorf, F.L. *The Impact on Seaplane Floats During Impact.* NACA Technical Note No. 321, 1929.

Wagner, H. *Phenomena Associated with Impacts and Sliding on Liquid Surfaces.* No. 4, Vol. 12, August 1932.

Yenne, B. *Seaplanes & Flying Boats.* New York, N.Y.: BCL Press, 1997.

VITA

Carrie Sell was born in Crystal Lake, Illinois to Anthony Sell and Kimberly Johnson. She received her undergraduate degree in Naval Architecture and Marine Engineering at the University of New Orleans in May 2010. She will be receiving her graduate degree December 2011. She has worked as a graduate research and teaching assistant for the School of Naval Architecture and Marine Engineering for the past year. Carrie has interned previously at Bollinger Shipyards and has participated in the Naval Research Enterprise Intern Program at the Center for Innovation in Ship Design at NAVSEA NSWC Carderock Division for the past two summers.